DEPARTMENT OF ONCOLOGY
Medical Sciences Division

UNIVERSITY OF OXFORD
Department of Chemistry

Multiple Strategies to Enhance Efficacy of Oligonucleotide Therapeutics

Thesis Presented for the Degree of Doctor in Philosophy

By

Siqi Li

Kellogg college

Supervisors:

Professor Katherine A. Vallis (Department of Oncology)

Professor Tom Brown (Department of Chemistry)

A thesis submitted to the University of Oxford in partial fulfilment of the requirement for the degree of Doctor of Philosophy

ABSTRACT

Background

Nucleic acids (NAs) such as plasmid DNA, messenger RNA (mRNA), and small interfering RNA (siRNA) are a group of gene therapy agents that hold enormous clinical potential in cancer medicine. Despite their undoubted potential, clinical translation of these molecules, however, has been largely held back by their limited bioavailability in target tissues/cells. To overcome this, many drug delivery systems and strategies have been devised.

Aim

This research aims to introduce a recently developed cell-penetrating peptide (CPP)-based delivery platform to enhance the internalisation of nucleic acid therapeutics (NATs) into tumour cells. It also aims to explore strategies to trigger the escape of NAs from endosomes to facilitate intracytoplasmic target engagement and controlled release, thereby improving the efficacy and precision of NA-based cancer therapies.

Results

The recently developed CPP, tri-cTatB, combines the advantages of multimerisation and cyclisation of the archetypal TAT peptide and shows highly efficient tumour cell internalisation capability. In this study, a self-assembling stable complex composed of tri-cTatB and NAs was developed. The complex showed efficient and evident cellular uptake within 1 hour at a low carrier concentration of 1 μM. In a study to identify the mechanism of internalisation, it was found that the siRNA/tri-cTatB complexes enter cells via clathrin-mediated endocytosis and that the NA cargoes become trapped in endosomes and lysosomes.

To trigger NA release from intracellular vesicles, various endosome escape strategies were investigated. It was found that photochemical internalisation (PCI) was an effective additional component to the tri-cTatB-mediated NA complex delivery platform. PCI-controlled delivery of GAPDH siRNA caused marked GAPDH enzyme activity downregulation by 91, 51 and 44%

in HeLa, MDA-MB-231 and HEK293T cells compared to untreated groups, respectively. In another application, significant polo-kinase-1 (PLK1) knockdown in cancer cell lines was demonstrated following their exposure to siPLK/tri-cTatB complexes. This PCI-controlled tri-cTatB delivery platform was also applied to other types of nucleic acids including mRNA and plasmid DNA with efficient delivery demonstrated in both cases.

Conclusion

In summary, this research describes the use of a tricyclic Tat construct that enables intracellular delivery of nucleic acid at effective concentrations as low as 1 μM and is the first report of the combination of a Tat-derived peptide and PCI to achieve highly efficient and controlled release of NATs.

ACKNOWLEDGEMENT

After ten years in higher education, writing this piece as the last part of my thesis feels like the end of an era. I am writing this acknowledgement to thank everybody who has been so important and supportive in my academic study and life and will still be impactful in my whole life.

First and foremost, I would like to express my heartfelt gratitude to my supervisor, Prof. Kate Vallis, for granting me the privilege of working with her research group. Her exceptional scientific expertise, kind encouragement, and unwavering patience with my independent approach have been invaluable in shaping this thesis. I am grateful to my co-supervisor, Prof. Tom Brown, for having me in his outstanding chemistry lab, offering generous support, and sharing his profound knowledge and insights.

I also extend my gratitude to my DPhil examiners, as well as my transfer and confirmation assessors Prof Robert Carlisle, Prof Andrew Kellett, Prof Len Seymour, Prof Bart Cornelissen and Prof Shisong Jiang, for bearing my writings, and for the opportunity to learn from the best.

It has been an honour to have worked alongside intelligent people in Kate's and Tom's group, who budded a culture of support, friendliness, and hard work devoid of competition. Especially Dr. Irini Skaripa-Koukelli and Dr. Fernando Cortezon Tamarit, thanks for being the best postdoc and my best friends in Oxford, for bearing all my negative emotions and stupid questions, and for sharing all those happy moments. Dr Jin Chen, I can't express more gratitude for not just your academic insights but also for being like a family member in this foreign country. Sebastian, thanks for all your help with chemistry and for being a great friend, I enjoyed all our talks, coffee and the White Rabbit. I am also grateful to Prof Afaf EI-Sagheer, Jerry, Anna, Sarah, Diallo and any other lab members who kindly helped me, thanks for making this DPhil easier.

I’d like to express my gratitude to Dr. Ole Tietz for synthesising tri-cTat peptides and for all his inspiring ideas about this project. I also want to thank Joel Balkaran from IBME for helping me with the DLS, Yuewen for helping me with the Cryo-EM, and Yi Yuan for helping me with the TEM.

I dedicate this thesis to my beloved parents, who gave me this strong soul and always stood by my side in every step of my life. To my grandmother, who never had any degree, but raised me and made me to this stage, I know she would be proud of me even if she had never seen this. Dr. Liquan Pi, I wouldn’t have gone this far without you. Over the last ten years in the UK, thank you for always having my back and sharing my best and tough times.

My last tribute to the strength, resilience, and growth I've found within myself.

凡是过往，皆为序章

DECLARATION

I declare that this thesis has been written solely by myself and that it has not been submitted, in whole or in part, in any previous application for a degree. Except where stated otherwise by reference or acknowledgement, the work presented is a true and honest account of my own research, which was conducted ethically, and the results obtained are genuine.

Siqi Li

List of publication

Li, S., Tietz, O., Golojuch, S.,Blades, R., Ei-Sagheer, Brown, T. Vallis, K. A., Photochemically enhanced cellular delivery of siRNA/multimeric cell-penetrating peptide complexes results in PLK1 silencing and apoptosis in cancer cells. [Manuscript ready to submit].

Jin, C., Ei-Sagheer, A. H., **Li, S**., Vallis, K. A., Tan, W., & Brown, T. (2022). Engineering Enzyme-Cleavable Oligonucleotides by Automated Solid-Phase Incorporation of Cathepsin B Sensitive Dipeptide Linkers. *Angewandte Chemie*, *61*(13), e202114016. https://doi.org/10.1002/anie.202114016

Jin C, **Li S**, Vallis KA, El-Sagheer AH, Brown T. Modular and automated synthesis of oligonucleotide-small molecule conjugates for cathepsin B mediated traceless release of payloads. RSC Chem Biol. 2024 May 29;5(8):738-744. doi: 10.1039/d4cb00112e. PMID: 39092443; PMCID: PMC11289880.

Conference

AACR 2024

Siqi Li, Ole Tietz, Afaf H. El-Sagheer, Tom Brown, Katherine A. Vallis; Abstract 5816: An effective delivery platform for nucleic acid therapeutics: Enhanced cancer cell internalization and endosomal escape. Cancer Res 15 March 2024; 84 (6_Supplement): 5816. https://doi.org/10.1158/1538-7445.AM2024-5816

Table of Contents

Table of Figures

LIST OF ABBREVIATIONS

ASO: antisense oligonucleotides

APC: Allophycocyanin

AF488: Alexa Fluor 488 dye

BCA: bicinchoninic acid

BSA: bovine serum albumin

CCK8: Cell Counting Kit - 8

CME: clathrin-mediated endocytosis

CPP: cell-penetrating peptide

Cryo-EM: cryogenic electron microscopy

cTat: cyclic form of Tat peptide

CuAAC: copper-catalysed azide-alkyne cycloaddition reactions

CvME: caveolae-mediated endocytosis

DBCO: dibenzocyclooctyne

DLS: dynamic light scattering

DMEM: Dulbecco's Modified Eagle's Medium

DMSO: Dimethyl sulfoxide

dsRNA: double-stranded RNA

EDTA: ethylenediaminetetraacetic acid

EED: endosomal escape domains

EGFP: enhanced green fluorescent protein

EMSA: electrophoretic mobility shift assay

FDA: Food and Drug Administration

LNP: Lipid nanoparticle

miRNA: microRNA

mRNA: messenger RNA

MW: molecular weight

N/P: nitrogen/phosphate

NaAsc: sodium ascorbate

NATs: nucleic acid therapeutics

NHS: N-hydroxysuccinimide

NT: no treatment

PCI: photochemical internalisation

PDI: polydispersity index

pDNA: plasmid DNA

PDT: photodynamic therapy

PI: Propidium Iodide

PLK1: polio-like kinase 1

PTD: protein transduction domain

PS: photosensitizer

PI: propidium iodide

RISC: RNA-induced silencing complex

RNA: ribonucleic acid

RNAi: RNA interference

ROS: reactive oxygen species

scrRNA: scramble double-strand RNA

SD: standard deviation

GAPDH: Glyceraldehyde-3-phosphate dehydrogenase

gRNA: guide RNA

GalNac: N-acetylgalactosamine

HIV-1: Human immunodeficiency virus 1

HPLC: high performance liquid chromatography

IVT: In vitro transcription

Lipo: lipofectamine

siGAPDH: siRNA targeting GAPDH

siPLK: siRNA targeting PLK1

siRNA: small interfering RNA

siRNA/tri-cTatB: siRNA complex with tri-cTatB

TAT: Cell penetrating peptide trans-activator of transcription

THPTA: tris((1-hydroxy-propyl-1H-1,2,3-triazol-4-yl)methyl)amine

tri-cTatB: cyclic TAT peptide trimer scaffoldB

Chapter 1

General Introduction

1.1 Cancer and cancer therapy

Cancer is a global health problem responsible for one in six deaths worldwide. In 2022, there were an estimated 20 million new cancer cases and about 9.7 million cancer deaths globally[1]. Cancer is a very complicated sequence of disease conditions, which is caused by a series of genomic/molecular alterations, leading to uncontrolled growth and proliferation of cells, causing a rapid increase in tissue mass in the affected parts of the body[2]. Cancer represents a heterogeneous array of diseases and has been defined using a series of distinct characteristics or "hallmarks"[3]. These essential characteristics include self-sufficiency in growth signals, insensitivity to anti-growth signals, evasion of apoptosis, evasion of immune destruction，limitless replicative potential, sustained angiogenesis, and some new dimensions including unlocking phenotypic plasticity and nonmutational epigenetic reprogramming[3]. The hallmark characteristics can be viewed as therapeutic targets, as their reversal would be expected to reduce cancer growth.

For many decades, there were only a few options for cancer treatment including surgery, chemotherapy, and radiation therapy as a single treatment or in combination[4]. But in recent years, many pathways involved in cancer therapy progression have been elucidated and the approaches to how they can be targeted have improved. New approaches, including drugs, biological molecules, and immune-mediated therapies, are being utilised in cancer treatment. However, these therapies have yet to reach the expected level of effectiveness needed to significantly reduce mortality rates and extend survival times for metastatic cancer[5]. Among those new approaches, nucleic acid therapeutics (NATs) hold great potential.

1.2 Nucleic acid therapeutics

Nucleic acid therapy is a burgeoning field at the intersection of molecular biology and medicine which holds immense promise for treating a wide range of diseases, from genetic disorders to cancer. NATs are a diverse class of DNA or RNA molecules such as plasmids, messenger RNA

(mRNA), antisense oligonucleotides (ASO), small interfering RNA (siRNA), microRNA (miRNA), aptamers and gene-editing guide RNA (gRNA). NATs are versatile pharmacons with applications ranging from altering gene expression through up-or down-regulation to modulating immune responses[6,7]. Since the first gene therapy to treat disease was proposed half a century ago, many technological and biological breakthroughs have led to safe, effective nucleic acid drugs (Figure 1.1). The successful clinical application of these technologies has sparked great interest in improving tissue specificity, for example, ASO and siRNA N-acetylgalactosamine (GalNAc) conjugates targeting the asialoglycoprotein receptor (ASGPR) on hepatocytes in the liver. Up to now, several FDA approved NATs have emerged as noteworthy advancements, particularly the rapid development of mRNA and gene-editing therapies, which are either in clinical trials or have already been approved for treating infectious diseases and cancer (Figure 1.1).

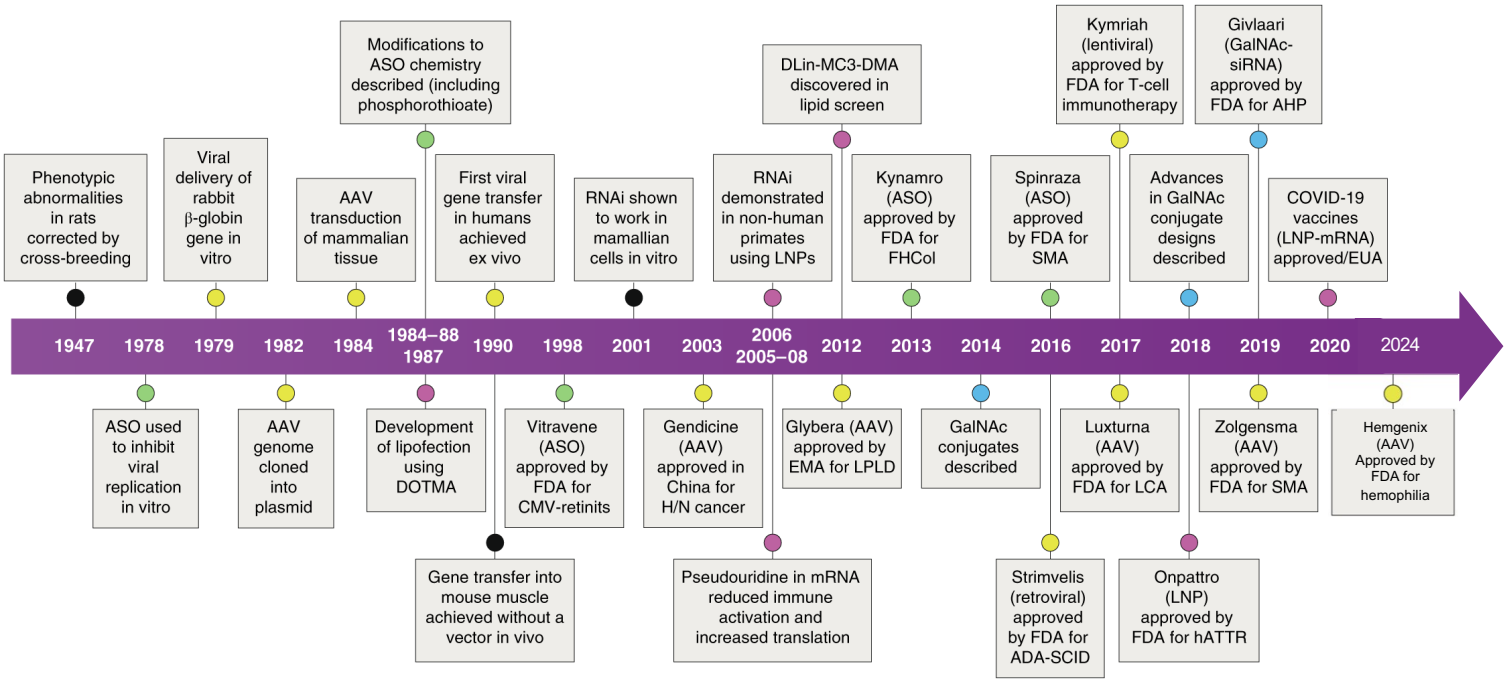

Figure 1.1 Timeline of the development of NATs. Each timeline point has a colour-coded circle: major developments (black), ASO (green), GalNAc–siRNA (blue), lipid (purple) and viral (yellow). AHP, acute hepatic porphyria; CMV, cytomegalovirus; H/N, head and neck cancer; FHChol (familial hypercholesterolemia); LCA (Leber congenital amaurosis). Figure adapted from Kulkarni *et al*. (2021)[8]. Copyright by Springer Nature.

1.2.1 Nucleic acid therapeutics in oncology

The high specificity, functional versatility, reproducible batch-to-batch manufacture, and tuneable immunogenicity of NATs make them good candidates for cancer therapy. There are five main categories of NAT for cancer therapy. Gene-regulating nucleic acid drugs such as ASO and siRNA can regulate post-transcriptional gene expression and silence targeted mRNA, subsequently regulating intracellular signalling pathways involved in cancer progression[9]. mRNA therapeutics and plasmid DNA (pDNA) can be tailor-designed to express proteins or peptides of interest, such as antigens or cancer immunotherapeutic proteins[10]. Aptamers, which are short single-stranded nucleic acids, have been studied as nucleic acid mimics of antibodies for cancer immunotherapy[11]. Genome editing-related nucleic acids, such as guide RNA (gRNA), can precisely modify target genes in coordination with Cas nucleases, thereby enabling the regulation of gene expression for cancer immunotherapy[12]. Moreover, nucleic acids immunostimulants such as unmethylated cytosine-guanosine deoxynucleotides (CpG), poly I:C and 5'-triphosphate RNA can induce or augment anticancer immune activation[13]. The focus of this thesis is the application of siRNA and mRNA oligonucleotides in cancer.

1.2.2 Small interfering RNA (siRNA)

RNA interference (RNAi) was first discovered in 1998 by Fire, Mello *et al*. and gained international attention for the ability of double-stranded RNA to silence gene expression in the nematode worm *C. elegans*[14]. Mello and Fire were subsequently awarded the Nobel Prize in Medicine in 2006 for their seminal work in unravelling the biological role of RNAi, which highlighted an endogenous, evolutionarily conserved mechanism, that involves sequence-specific post-transcriptional gene silencing with double-stranded RNA (dsRNA) as a trigger. In 2001, Tuschl and co-workers published their proof-of-principle experiment demonstrating that synthetic siRNA duplexes specifically suppress the expression of endogenous and heterologous genes in different mammalian cell lines[15]. Since the first report of successful

siRNA gene silencing in mice, the life science sector has made considerable efforts to develop siRNA therapeutics for the treatment of various diseases including cancer and viral infections. As of 2024, six siRNA drugs have been approved by the US FDA: Patisiran (Onpattro), Givosiran (Givlaari), Lumasiran (Oxlumo), Inclisiran (Leqvio), Vutrisiran (Amvutta) and Nedosiran (Rivfloza)[16].

siRNA is a double-stranded molecule composed of 21-23 nucleotides. It can be designed and synthesised as complementary sequences to a target mRNA. The two main stages involved in siRNA mediated gene silencing are transcriptional gene silencing (TGS) and post-transcriptional gene silencing (PTGS). PTGS can be further classified into two mechanisms called direct sequence-specific cleavage-led translation repression and consequent degradation[17]. Once siRNA is delivered into cells and present in the cytoplasm, it is incorporated into a protein complex called the RNA-induced silencing complex (RISC) (Figure 1.2A)[18]. Argonaute 2 (AGO2) is a protein in RISC that mediates cleavage of the passenger strand of double-stranded siRNA. Then the activated RISC containing the siRNA antisense strand selectively seeks and degrades the mRNA that is complementary to the siRNA antisense strand[19]. The cleavage of mRNA occurs between bases 10 and 11 on the complementary strand relative to the 5' end of the siRNA guide strand, thereafter leading to the subsequent degradation of the cleaved mRNA transcript by cellular exonucleases[20,21]. siRNA mediated gene silencing has shown selective mRNA inhibition with low cytotoxicity.

Table 1.1. Some selected RNAi therapeutics have entered clinical trial phase for cancer treatment.

siRNA name	Target	Indication	Current development
CALAA-01	RRM 2	Cancer, Solid Tumour	Phase I/Terminated
ALN-VSP02	VEGF, KSP	Solid Tumours	Phase I
siRNA-EphA2-DOPC	EphA2	Advanced Cancers	Phase I
TKM- PLK1 (TKM-080301)	PLK-1	Adrenal Cortical Carcinoma(II), Hepatocellular Carcinoma(II), Neuroendocrine Tumour(II)	Phase II/Completed
siG12D LODER	KRAS G12D mutation	Pancreatic Ductal Adenocarcinoma, Pancreatic Cancer	Phase II
NBF-006	GSTP	Non-Small-Cell Lung, Colorectal, Pancreatic Cancer	Phase I

1.2.3 Messenger RNA (mRNA)

Messenger RNA (mRNA) is a type of single-stranded ribonucleic acid that is transcribed from a strand of DNA, which carries the coding information for protein synthesis to be further transcribed and processed into functional proteins (Figure 1.2B). *In vitro* transcription (IVT) mRNA consists of a 5' cap, 5' and 3' untranslated regions (UTRs), an open reading frame, and a 3' poly(A) tail [22]. mRNA-based vaccines were proposed following the successful transfection of mRNA and subsequent production of an immune response in a dose-dependent manner by direct injection into mice to express therapeutic proteins[23]. Theoretically, a mRNA-based *in vitro* or *in vivo* approach can produce any protein/peptide via the protein synthesis machinery in the transfected cell[22].

Recent advances in mRNA technology, spurred by the success of mRNA vaccines during the COVID-19 pandemic, have accelerated research in this field. Compared to other functional biomolecules such as DNA, mRNA-based drugs have higher transfection efficiencies and lower toxicities than DNA-based drugs, and they do not require translocation into the nucleus

to function[22]. Importantly, mRNA has broad potential for treating diseases requiring protein expression and high therapeutic efficacy due to its continuous translation into encoded proteins/peptides to trigger long-lasting expression compared to transient conventional protein/peptide drugs[24,25]. mRNA can now be reproducibly synthesised by IVT using DNA templates, and RNA polymerases (T7, T3 or Sp6 phage) with additional capping[26]. These unique properties make mRNA a highly promising and versatile class of NAT, with applications ranging from cancer vaccines to therapies. Versatile approaches include *ex vivo* mRNA transfer for therapeutic adoptive cell engineering and the direct use of cancer-specific antigen-encoding mRNA as cancer therapeutic vaccines[26].

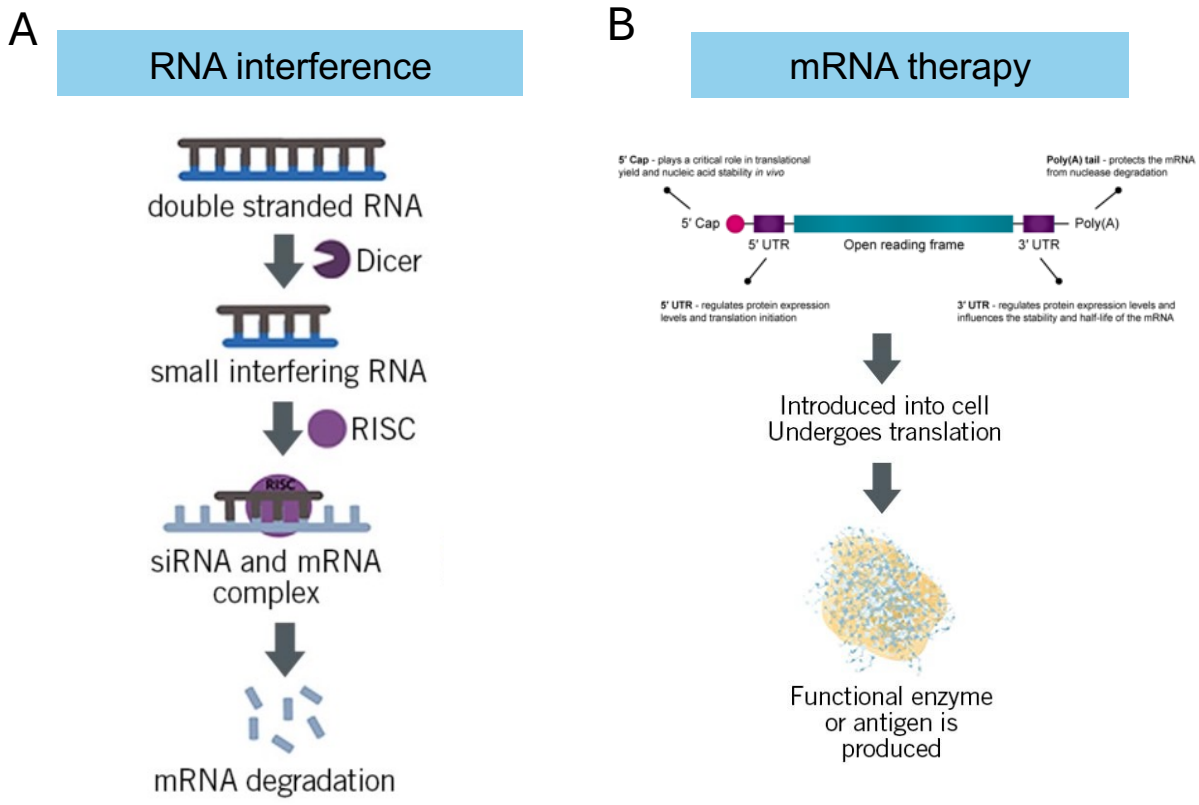

Figure 1.2 Working mechanism of siRNA and mRNA. (A) siRNAs can reduce gene expression via RNA-induced silencing complex (RISC) – mediated mRNA degradation**. (B)** *In vitro* transcribed mRNA consists of a 5' cap, 5' and 3' untranslated regions (UTRs), an open reading frame encoding antigen(s), and a 3' poly (A) tail. Figure adapted from Eurofins genomic (2021)[27].

1.3 Delivery of nucleic acids therapeutics

Despite enormous potential, employing nucleic acids as therapeutics is challenging because they are susceptible to degradation by nucleases in the circulation, contribute to immune activation and have unfavourable physicochemical characteristics that prevent efficient access to the site of action. Unlike traditional small molecule medicines or antibodies, the delivery of NATs can be adversely impacted by their properties such as negative charges, hydrophilicity, susceptibility to enzyme degradation, immunogenicity, and off-target effects[28,29]. Therefore, the challenge is to develop tailored systems that can facilitate nucleic acid uptake into target cells. The carrier itself must overcome extracellular and intracellular barriers, provide protection from nuclease activity in the bloodstream, enhance and assist with cellular uptake, and promote endosomal escape once cell entry has been accomplished.

1.3.1 Physical methods for NAT delivery

Strategies for NAT internalisation include viral vectors, non-viral vectors and physical vectors. The physical vectors such as electroporation, microinjection magnetofection and gene gun allow the direct penetration into the cytosol of both small and large nucleic acid molecules. Electroporation is a widely used technique that applies short, high-voltage electrical pulses to create transient pores in the cell membrane, allowing nucleic acids to enter the cytoplasm[30]. Microinjection involves the direct injection of nucleic acids into individual cells using a fine glass micropipette. This technique ensures precise delivery but is labor-intensive and limited to small-scale applications[31]. Magnetofection employs magnetic nanoparticles conjugated with nucleic acids, which are guided into target cells using an external magnetic field. This method enhances transfection efficiency while reducing cytotoxicity and has shown promise for both in vitro and in vivo applications[32]. Gene gun (biolistic delivery) propels nucleic acids coated onto gold or tungsten particles into target cells using a high-pressure gas pulse. This method is especially effective for transfecting hard-to-transfect cells but the air pressure may damage the cell[33].

Although these systems have achieved considerable transfection efficiency or even therapeutic effects in vivo in some cases, they have some drawbacks. For instance, electroporation is generally associated with low cell viability and its transfection efficiency varies in different types of tumours and tissues[33].

1.3.2 Viral vectors for NAT delivery

NAT delivery systems that have been investigated fall into two groups: viral and non-viral vectors. A viral vector can deliver a gene of interest by using a mechanism for transfecting genes into virus-infected cells. Viral vectors are especially effective for DNA delivery since viruses have evolved to exhibit tropism for specific cell types. They are among the few delivery systems capable of actively transporting their payload to the nucleus, where the DNA can function[8]. Viruses with high DNA transfection efficiency including parvoviruses, adenoviruses and adeno-associated viruses, have been used to treat diseases like muscular dystrophy, HIV and cancer[34].

Figure 1.3A illustrates the most popular viral vector, adeno-associated virus (AAV). Wild-type AAV is a small, non-enveloped parvovirus (~25 nm) with a ~4.7 kb single-stranded DNA (ssDNA) genome. Recombinant AAV vectors exploited as delivery vehicles generally contain the same capsid components and structure as wild-type AAV but all viral coding sequences are replaced by therapeutic gene expression cassettes, reducing immunogenicity and maximising packing capacity[35]. Notably, oncolytic viruses (OVs) have emerged as promising vectors for nucleic acid delivery in cancer therapy. By leveraging their tumour-selective replication and ability to penetrate the tumour microenvironment, OVs can be engineered to deliver NATs directly into cancer cells[36].

Although viral gene delivery systems show high transfection efficiency, their limitations include rapid clearance of the virus due to pre-existing antibodies, generation of neutralising antibodies against the vector, limited vector size capacity (usually below 7 kb) and possible

side effects[37]. Thus, efforts have been made to design non-viral gene delivery systems, based on lipids, polymers and peptides.

1.3.3 Non-viral vectors for NAT delivery

The most commonly used non-viral vectors include conjugated and non-conjugated forms of lipoplex (complexes of plasmid DNA and cationic lipids), dendrimers, polyplex (complexes of polymers and nucleic acids), and various nanoparticles[38,39].

1.3.3.1 Lipid nanoparticle delivery

Lipid nanoparticle (LNP)-mediated nucleic acid delivery has gained attention following the success of the COVID-19 mRNA vaccine. The landmark work in cationic lipids-mediated delivery was first reported by Felgner *et al*[40]. The discovery of ionisable cationic lipids was essential for LNP-based RNA therapeutics because they are positively charged at a low pH to enhance the encapsulation of negatively charged RNA. LNPs are now a key class for drug delivery platforms, approved by the FDA for delivering liver-targeted siRNA therapeutics and mRNA vaccines.

Lipid-based structures usually consist of a core-shell arrangement and ligands can be conjugated to their surface for active targeting (Figure 1.3B) which can protect from serum nuclease activity and immunogenicity[41]. FDA-approved LNPs are typically composed of four components: phospholipids, ionisable cationic lipids, cholesterol and polyethylene glycol (PEG). Scientists have investigated the structure of lipid-based delivery systems for nucleic acids[42] and demonstrated that lipid structure can alter how LNPs interact with cells[43]. Given that lipid structure influences delivery and that lipids can be easily synthesised using different approaches including Michael addition-based, epoxide-based and alcohol-based reactions, thousands of chemically distinct lipid delivery systems have been created[44]. Ionisable lipids present a positive charge under acidic pH conditions to complex with nucleic acids. Ideally,

these lipids should have a near-neutral surface charge to prevent rapid sequestration by the mononuclear phagocyte system and toxic effects upon *in vivo* intravenous administration[45]. Despite their advance, LNP drug delivery systems have significant limitations such as lack of targeting selectivity, short blood circulation time, and instability *in vivo*. For instance, the FDA-approved LNP-based siRNA drug, Patisiran is short-lived in circulation, with a plasma half-life of only 2–10 minutes[46].

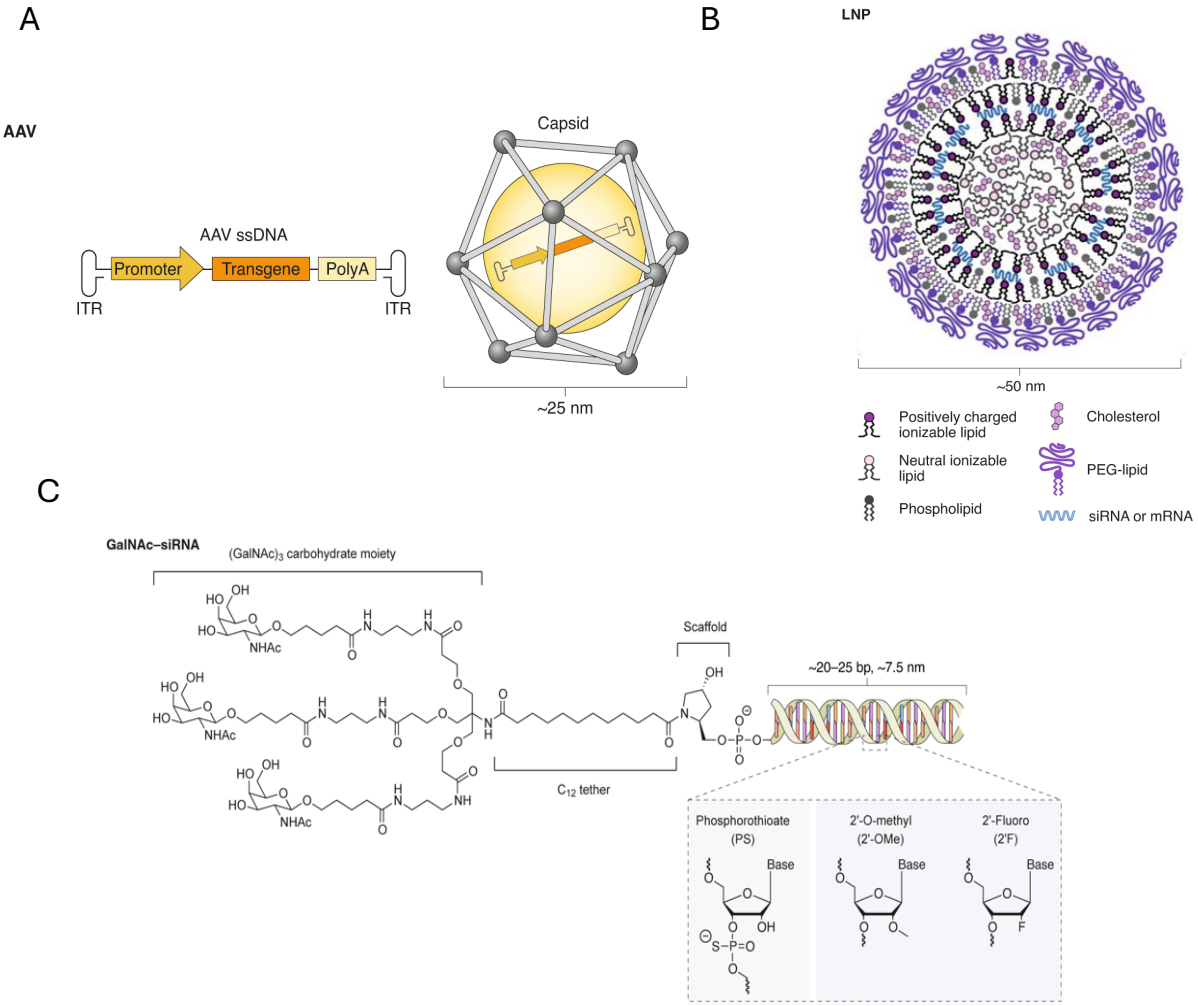

Figure1.3. Approved delivery platforms enabling *in vivo* NATs in the clinic. (A) Schematic representation of an AAV vector containing a 4.7-kb ssDNA with inverted terminal repeats (ITR). **(B)** In addition to the RNA payload, LNPs often consist of cholesterol, an ionisable lipid, a PEG-lipid, and a cationic or ionisable lipid as the shell and siRNA or mRNA nucleic acids as the payloads. **(C)** GalNAc-siRNA conjugation illustration. The siRNA backbone is chemically modified with phosporothioate, 2'-O-methyl or 2'-fluoro. Figure adapted

from Kulkarni *et al.* (2022)[8] and Guo *et al.* (2024)[47]. Copyright by Springer Nature and Cell Press.

1.3.3.2 Conjugation delivery: active targeting

RNAs can be transfected into target cells by "active targeting". In this delivery strategy, a ligand that can bind to a specific cell surface molecule is added to the delivery system (Figure 1.3C)[48]. The most successful and clinically validated example is N-acetylgalactosamine (GalNAc) conjugated siRNA or ASOs. For this class of drugs, siRNA or ASO is conjugated to a triantennary GalNAc moiety targeting the ASGPR. This receptor is predominantly expressed by hepatocytes and therefore provides access to a specific cell type within the liver. ASGPR specifically binds carbohydrates with terminal galactose or GalNAc residues[49]. After ligand binding, the receptor−ligand complex is internalised by a clathrin-dependent endocytosis pathway. Because of its abundant expression on the hepatocyte sinusoidal membrane (>95% of total expression), ASGPR is an ideal receptor for hepatic siRNA delivery[8].

For chemical conjugation of ligands and nucleic acids, RNAs have to be chemically modified to ensure their stability in the cell circulation after parenteral administration[50]. All clinically approved ASO/siRNA drugs are chemically modified. Three FDA approved GalNAc–siRNA drugs are Givosiran (acute hepatic porphyria), Lumasiran (primary hyperoxaluria type 1) and Inclisiran (hypercholesterolaemia or mixed dyslipidaemia)[51]. Moreover, a robust pipeline of GalNAc-conjugated therapeutics is progressing into the clinic for liver diseases including hepatitis B virus infection, transthyretin-mediated amyloidosis and α1-antitrypsin deficiency[37]. The greatest barrier to the clinical translation of this platform is that the ligand is liver-specific, which limits its application to other tissues. Therefore, the development of ligands based on other tissue receptors is needed.

1.3.3.3 Peptide delivery

A recently introduced delivery platform is a peptide-based formulation which consists of 5-30 amino acids typically as cell-penetrating peptides (CPP) or targeting/homing peptides. Both can interact with nucleic acids in a covalent or non-covalent manner[52] thereby facilitating cell internalisation. Figure 1.4 shows how CPPs, receptor-targeting peptides and stimuli-responsive peptides can mediate delivery via different internalisation pathways. CPPs are often derived from natural protein transduction domains and can also be artificially designed. Thus, amino acids within the CPPs can be conjugated with oligonucleotide bases through covalent linkage. Moreover, CPPs typically consist of many positively charged amino acids and electrostatic interactions can be exploited in the formation of complexes between the peptide carriers and oligonucleotides which are typically negatively charged[52].

One drawback of peptide-mediated nucleic acids delivery is the entrapment of the cargo in endosomes as they are usually internalised by endocytosis. CPPs also often lack specificity for a single cell type, which can be addressed through the use of targeting moieties, such as peptide ligands that bind to specific receptors[37]. Although clinical progress in the application of peptides, alone or combined with nano-assemblies, is moving forward slowly, large investments and wide-ranging research efforts are being made, confirming their promising potential as a delivery platform for therapeutic systems. Based on the great potential of peptide-mediated nucleic acid delivery, the focus of this thesis is on harnessing the capabilities of CPPs to develop an efficient delivery platform.

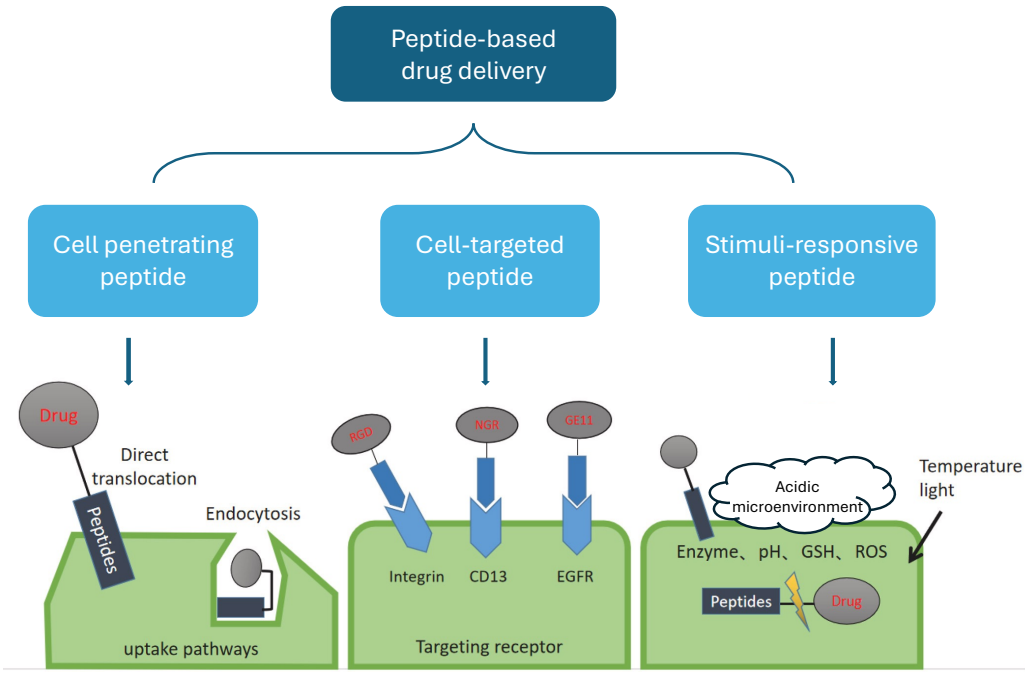

Figure 1.4. Three types of peptide-based drug delivery. The peptides-based drug delivery systems include cell-penetrating peptides, cell-targeting peptides (homing peptides), or stimuli-responsive peptides alone or in combination. Different peptide delivery systems could internalize into the cell by different mechanisms.

1.4 Cell-penetrating peptides

1.4.1 Introduction to cell-penetrating peptides

CPPs represent a class of therapeutically interesting vectors for drug delivery, derived from naturally occurring proteins, designed *de novo* or in combination[53]. The classical definition of CPPs, or protein transduction domains (PTDs), is that they consist of short cationic sequences (less than 30 amino acids long), and are rich in arginine (Arg, R), histidine (His, H), and lysine (Lys, K) residues. Their highly polar amino acid sequence allows them to cross the negatively charged lipid bilayer of the cell membrane, a key hurdle in the delivery of a wide range of molecules including proteins, pharmaceuticals and nucleic acids into cells[54]. Since the initial discovery of the HIV-1 derived trans-activator of transcription (TAT)[55], or drosophila-derived antennapedia homeodomain protein-derived peptide (Antp)[56], research characterising

mechanisms of action and identification of novel CPPs has rapidly expanded, with over 1,800 unique CPPs currently listed on the online database CPPsite[57].

Given the large repertoire of available CPPs, several approaches are used for their classification, including origin, sequence and application[58]. The most used classification system is based on chemical properties and consists of three groups: cationic, amphipathic and hydrophobic (Table 1.2). Cationic CPPs were the first to be characterised and typically incorporate a succession of positively charged amino acids, notably arginine and lysine. Typical examples include the TAT peptide (GRKKRRQRRRPPQC), Antp (RQIKIWFQNRRMKWKK) and nona-arginine (R9). Another group, the amphiphilic CPPs, contain both charged, mostly lysine and arginine, and non-charged amino acids. They share similar amphiphilic properties with phospholipids, can insert into the lipid bilayer and cross the cell membrane by formation of lipid rafts. MPG (GLAFLGFLGAAGSTMGAWSQPKKKRKV) and Pep-1 (KETWWETWWTEWSQPKKRKV) represent two examples of the amphiphilic CPP[59]. Hydrophobic CPPs represent a smaller group of CPPs and typically contain mostly non-polar residues and a low net charge. The presence of hydrophobic motifs increases the affinity of these CPPs for the hydrophobic domains of the cellular membrane, thus promoting membrane insertion. Examples include Pep-7 (SDLWEMMMVSLACQY) and the fibroblast growth factor 12 (FGF-12) derived CPP-C (PIEVCMYREP)[60]. A few more examples of commonly used CPPs and their classification have been listed in Table 1.2. Considering the wide spectrum of applications of CPPs, many CPPs are now under clinical investigation. For example, a TAT-delivered subunit delta Protein Kinase C (δPKC), inhibitor has been applied to treat myocardial infarction and spinal cord injury[61].

Table 1.2. Examples of CPP-based therapeutics under clinical development

CPPs	Cargos	Recruitment status	Application	Year
TAT	Botulinum toxin A	Phase IIIb (completed)	Cervical dystonia	2012
TAT	JNKI-1	Phase III (completed)	Postoperative ocular inflammation	2015 2017
TAT	D-JNKI-1 gel	Phase III (completed)	Hearing loss, idiopathic sudden sensorineural	2016 2015
TAT	Botulinum toxin A	Phase II (completed)	Cervical dystonia	2016
ATX-101	N/A	Phase Ib/Iia (recruiting)	Several cancers	2021
(R-AHX-R)4	PMO	Phase III (terminated)	Cardiovascular disease, coronary artery bypass	2007
R7	Cyclosporin A	Phase II	Psoriasis	2003
ALRN-6924	Topotecan	Phase 1a (terminated)	Small cell lung cancer	2019

1.4.2 A typical cell-penetrating peptide: TAT

HIV-1 Tat was, in 1988, the first cell-penetrating peptide to be discovered. Frankel and Pabo observed that exogenously added Tat protein could enter HeLa cells unaided and localise in the nucleus. Tat has several domains involved in the recognition of the transactivator response element (TAR), an HIV-1 specific secondary mRNA structure, and the recruitment of elongation factor complexes, such as the positive transcription elongation factor (P-TEFb). Further research with truncated variants of Tat identified the basic domain (GRKKRRQRRRPPQC) was essential for cell membrane translocation[62]. This breakthrough ultimately led to the development of the cationic CPP Tat (GRKKRRQRRRPPQC). In addition to its cell-penetrating ability, Tat is also able to localise into the cell nucleus via a nuclear localisation sequence (GRKKR). In vitro analysis has shown that Tat is capable of binding both

importin-α[63] and importin-β[64], which are principally involved in classical energy-dependent nuclear import pathways.

The combination of both cell-penetrating and nuclear localisation characteristics makes Tat an ideal CPP for targeting macromolecular cargo proteins to the cell nucleus. Subsequently, Tat and Tat-bound bioconjugates have undergone extensive research investigating potential applications for intranuclear therapeutic delivery, including enhanced delivery of small molecule inhibitors, nucleic acids and full size proteins[62].

1.4.3 Cell-penetrating peptide delivery of nucleic acid

CPPs have garnered widespread attention as delivery vehicles due to their capability of autonomous and receptor-independent intracellular translocation with low cytotoxicity and risk for immunogenicity compared to other carriers such as viral vectors. Cytotoxic effects are only observed at elevated peptide concentrations that are often not needed for efficient internalisation. Accordingly, CPPs have been exploited for *in vitro* and *in vivo* delivery of therapeutic cargos including nucleic acids.

Typically, the conjugation of CPPs to nucleic acids is mainly by non-covalent complex formation or by covalent bonds (Figure 1.5). CPPs can be covalently conjugated with nucleic acids via different stable linkers such as thiazolidine, amide and oxime bonds or cleavable chemical linkers such as hydrazine linkage and disulfide bond formation[65]. Cleavable bonding such as hydrazine linkage and disulfide bonds are easily dissociated under certain environmental conditions, with subsequent release of the nucleic acid cargo from the CPP and delivery of genes to targeted sites. For covalent conjugation, PEG polymer linkers are often introduced as a crosslinker to increase delivery efficiency since this modification can reduce electrostatic interactions between positively charged peptides and negatively charged nucleic acids[66]. Chemical covalent linkers such as thiazolidine, amide, and oxime bonds can provide stable conjugation between the peptide and oligonucleotide, enabling the conjugates to cross

the cell membrane and enter the cytoplasm or nucleus. Although covalent conjugation is most suitable for uncharged oligonucleotide analogues such as morpholino oligomers (PMO) and peptide nucleic acids (PNA), this method is limited because of difficulties in the purification of chemical conjugates and there is concern that the biological activity of the nucleic acid cargo may be altered after conjugation [66].

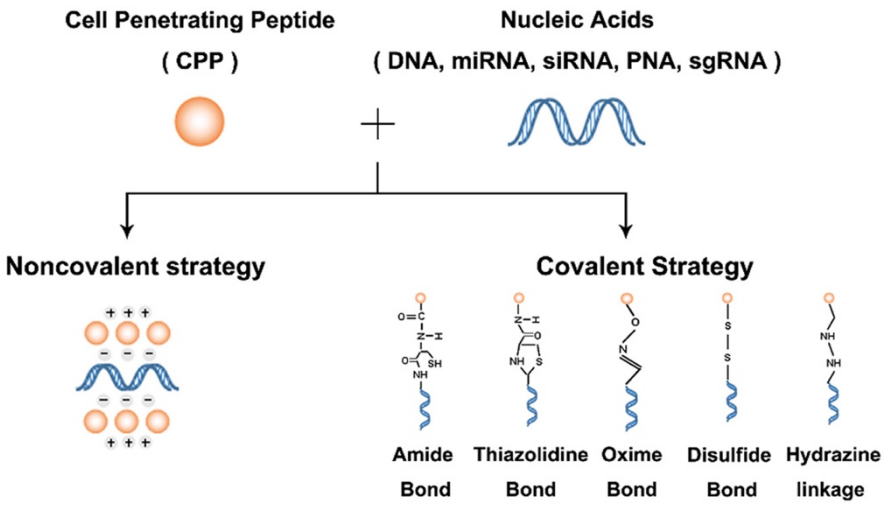

Figure 1.5. Two main strategies of CPP-mediated delivery of nucleic acids. The covalent conjugation and non-covalent strategies of CPP mediated nucleic acids delivery. Figure adapted from Geng *et al* (2022)[67]. Copyright by Elsevier.

Non-covalent conjugation, which is based on electrostatic interactions between peptides and nucleic acids, is considered more suitable for the delivery of negatively charged nucleic acids such as siRNA, mRNA, and plasmid DNA. Two methods of CPP-mediated non-covalent conjugation have been reported: direct interaction with nucleic acids by simple co-incubation under appropriate conditions[68], and incorporation of nucleic acids in CPP-nanoparticle (NP) conjugates[69]. The direct interaction method is straightforward, as it relies on the complexation of peptides with nucleic acids without complicated chemical modification or cross-linking. For nanoparticulate delivery, peptides are functionalised to interact with nanoparticles such as liposomes, lipids, dendrimers, micelles, or quantum dots, and nucleic acids are incorporated into the nanoparticles via electrostatic interactions.

1.4.4 Exemplar applications of CPP-based nucleic acid delivery

Numerous studies on the use of CPPs for the delivery of nucleic acids into mammalian cells have been published. The majority report *in vitro* experiments because the application of CPPs for nucleic acid delivery is associated with several difficulties, mostly related to a relatively short circulating half-life and lack of tissue and organ specificity of CPPs. However, reports on the use of CPPs for the delivery of therapeutic nucleic acids in animal models of various diseases (tumours, inflammation, or infections) are published regularly. Table 1.3 summarises some *in vivo* studies on CPP-mediated NATs.

Table 1.3. Examples of CPP-mediated nucleic acid therapeutic *in vivo* studies.

Peptides	Transported nucleic acid	Disease model	References
MPG-8	siRNA	xenografted tumours in mice	Crombez *et al*., 2009
TAT–DRBD	siRNA	mouse models of intracranial glioblastoma	Michiue *et al*., 2009
TAT	peptide nucleic acid	mouse model of acute hepatitis B (HBV)	Zeng *et al*., 2016
(RXR)4XB	PMO	mouse model of HSV-1 infection	Moerdyk-Schauwecker *et al*., 2009
KK-46	plasmid DNA, siRNA	model of SARS-CoV-2 infection in Syrian hamsters	Khaitov *et al*., 2021
T9(dR), TP	siRNA	mice models infected with influenza virus	Zhang *et al*., 2019
B-mR9	siVEGF	NCI-H460 tumor bearing mice	Yoo *et al*., 2017
PepFect6 (PF6)	siEGFP, siHPRT1, siOct4, siluc	primary mouse ESCs and bioluminescence model in mice	Andaloussi *et al*., 2011
Tat-A1E28, Tat-A4V48	siRNA	murine breast carcinoma 4T1 allograft mice model.	Yi *et al*., 2020
TAT-NBs with ultrasound irradiation	siEGFR	nude mice bearing xenograft tumour	Jing *et al*., 2016

CPP-based platforms for the delivery of siRNA therapeutics have shown great potential. The first CPP-siRNA delivery was reported in 2003, MPG condensed siRNA into complexes via electrostatic interaction and mediated siGAPDH delivery, resulting in downregulation of the target mRNA by 60%[70]. MPG-8 is a truncated version of the amphipathic peptide MPG, which was used to deliver siRNAs against the cell division regulatory protein cyclin B1, whose expression is upregulated in various forms of cancer. MPG-8 was used to form nano-complexes with siRNA molecules. Intravenous administration of these complexes to mice bearing xenografted tumours caused a significant reduction in tumour growth[71].

In addition to non-nonvalent complexes, the conjugation of the Tat carrier peptide and PNA directed against the genome of the hepatitis B virus (HBV) inhibited HBV replication in HepG2.2.15 cells, TAT–PNA-DR was developed. In the mouse model of HBV infection, administration of TAT–PNA-DR decreased the viral load by 80%. Moreover, TAT–PNA-DR showed low acute toxicity in mice, as well as high stability in the serum[68].

Peptide-based delivery of nucleic acids also played a role in fighting COVID-19 infection. The world's first etiotropic drug MIR 19 is a complex of locked nucleic acid (LNA)-modified siRNA and KK-46 peptides. In phase II clinical trials, the complexes were administrated by inhalation to hospitalised patients with severe COVID-19 infection. 52 patients in the test group received MIR 19 by inhalation at a dose of 3.7 and 11.1 mg per day and 52 patients in the control group received standard therapy. The clinical results have shown that MIR 19 was well tolerated and resulted in a significant reduction of cough, fever relief and restoration of oxygen saturation compared to the control group[72].

While mRNA is emerging as a powerful format for vaccine and nucleic acid therapeutics, efficient and safe delivery systems are required for mRNA to be delivered into the correct cellular compartments to achieve proper presentation and function. Cationic CPPs can be an excellent vehicle for mRNA delivery as they can combine low charge densities and condense

mRNA into stable nanocomplexes with strong membrane-penetrating capabilities. For example, the cationic CPP, PepFect is developed to efficiently deliver mRNA encoding reporter by forming the CPP-mRNA nanoparticle. Successful delivery led to high expression of a reporter protein in two-dimensional tissue cultures and three-dimensional cancer cell spheroids. Notably, the PepFect14-mRNA nanoparticles showed better expression in various tumour cell types than a lipid-based transfection platform[62].

1.4.5 Challenges of systemic delivery to tumour

Although various delivery strategies have been extensively studied and developed to overcome extracellular barriers, systemic delivery of nucleic acids to tumours remains challenging in achieving effective functionality in humans. Once injected into the body, delivery particles (vectors carrying cargo) encounter various physical and biological barriers, such as diffusion limitations, shear forces, aggregation, protein adsorption, phagocytic sequestration, and renal clearance. These factors significantly impact the proportion of administered particles that successfully reach the target diseased tissues and cells[73].

One of the challenges of nanoparticle delivery of nucleic acids is organ selectivity and/or cell selectivity, mainly owing to the numerous factors that affect the biodistribution of nanoparticles[74]. Renal and hepatic clearance is a crucial step since the liver and spleen likely capture most particles with sizes ranging from 50 nm to 200 nm. Thus, the current clinical success of nucleic acid nanotherapeutics has been limited to either liver targeting or local administration. Unlike normal tissues, tumours have twisted, chaotic, and leaky vessels and poor lymphatic drainage[75]. Consequently, therapeutic particles accumulate in a molecular weight-dependent manner in tumours. Small nucleic acid molecules (<10 kDa) are rapidly excreted via the kidneys, while larger particles (>200 nm) will activate the complement system and be quickly removed from the blood stream, accumulating in the liver and spleen[76].

Moreover, when nanoparticles are administered into the body, their physicochemical properties change. The nanoparticles interact with serum proteins to form a 'protein corona' and may aggregate. The corona is diverse and consists of ions, opsonins and other serum proteins[77]. The adsorption of proteins can cause nanoparticle aggregation, leading to larger particle sizes that may be more susceptible to clearance by the mononuclear phagocyte system (MPS) in the liver and spleen[73].

1.5 Overcoming endosome entrapment

1.5.1 Endosome entrapment remains a challenge for nucleic acid therapy.

Small molecule therapeutics are able to cross the cell membrane via passive diffusion because they are less than 500 Da in size and have no net charge. Macromolecular NATs, however, are too large, highly charged, and too hydrophilic to passively diffuse across the cell membrane[78]. A typical siRNA size is >12 kDa with more than 40 anionic charged phosphodiester linkage and a hydrophilic log P value >1. Consequently, NATs normally internalise into cells by endocytosis and the endosomal membrane constitutes a barrier for the release of nucleic acids from vectors into the cytosol.

Endocytosis is subdivided into phagocytosis and pinocytosis, where pinocytosis includes caveolae-mediated endocytosis, clathrin-mediated endocytosis (CME), fluid phase endocytosis, and micropinocytosis. How these different pathways are regulated is largely unclear, and is dependent on cell type and the characteristics of specific delivery vectors[79]. Under normal circumstances, vesicles formed by endocytosis are trafficked to an early endosome, which has a slightly acidic lumen (pH ~6.5)[80]. The early endosome then undergoes maturation to a late endosome, becoming more acidic in the process (pH ~5.5), before finally fusing with a lysosome (pH ~4.7). At this stage oligonucleotides trapped in the lysosome are susceptible to rapid degradation by hydrolytic enzymes. Endosomal release, or escape, before lysosomal degradation presents a critical bottleneck for effective cytoplasmic nucleic acid delivery, and

is highly inefficient[81]. In the recent work by Jiang *et al*., who used a highly quantitative NanoSIMS microscopy found that only 1%–2% of the endocytosed non-modified ASO escape from endosomes *in vivo*[82].

Thus, the lack of endosomal escape is one of the biggest problems preventing the widespread use of nucleic acid therapeutics for treating cancer and a multitude of other diseases.

1.5.2 Strategies to trigger endosome escape

Oligonucleotides in endocytic vesicles are either recycled back to the extracellular space through exocytosis or progress to lysosomes, the degradative compartment of the cell and only a very small number of oligonucleotides enter the cytoplasm. Through slow leakage from endo-lysosomes. When endosomes mature, they fuse to form multivesicular bodies (MVBs) and then fuse with lysosomes, during the fusion process[83]. At this time there is a breach of the lipid bilayer, which could allow localised nucleic acids to escape. Less than 1% of nucleic acids spontaneously exit the endo-lysosome to enter the cytoplasm, and it is extremely difficult to ascertain where and when the escape occurred. A wide variety of approaches over decades have been developed to enhance endosomal escape and thereby improve nucleic acid therapy.

As mentioned, siRNA and ASOs may be slowly released from endosomes and lysosomes, but during this process, it is crucial that they retain stability and bioactivity since they are vulnerable to the action of nucleases. Certain modifications incorporated into the oligonucleotide's backbone and ribose have been developed to render oligonucleotides resistant to lysosomal nucleases and many of them have been clinically approved. As illustrated in Figure 1.6, chemical modification steps can be applied to (i) the ribose sugar, (ii) the phosphodiester backbone, (iii) the nucleoside base, or (iv) the nucleotide structure itself. Modifications of the furanose ring at the 2' position involve substitution of the 2'-OH group with either 2'-O-Methyl (2'-OMe) or 2'-fluoro (2'-F) structure which can confer potency, specificity and reduced immunogenicity[84]. Common backbone modifications include

phosphorothioate (PS) and boranophosphate modifications, which improve biodistribution, nuclease resistance and uptake by cells[85]. Moreover, modifications of the nucleoside bases, mostly uracil, are used to increase base-pairing properties either alone or in combination with other stabilising modifications[86]. These chemical modifications can reduce the negative charge of nucleic acids, increasing their chance of endosomal release and extending their lifetime until they gradually escape from endo-lysosomes.

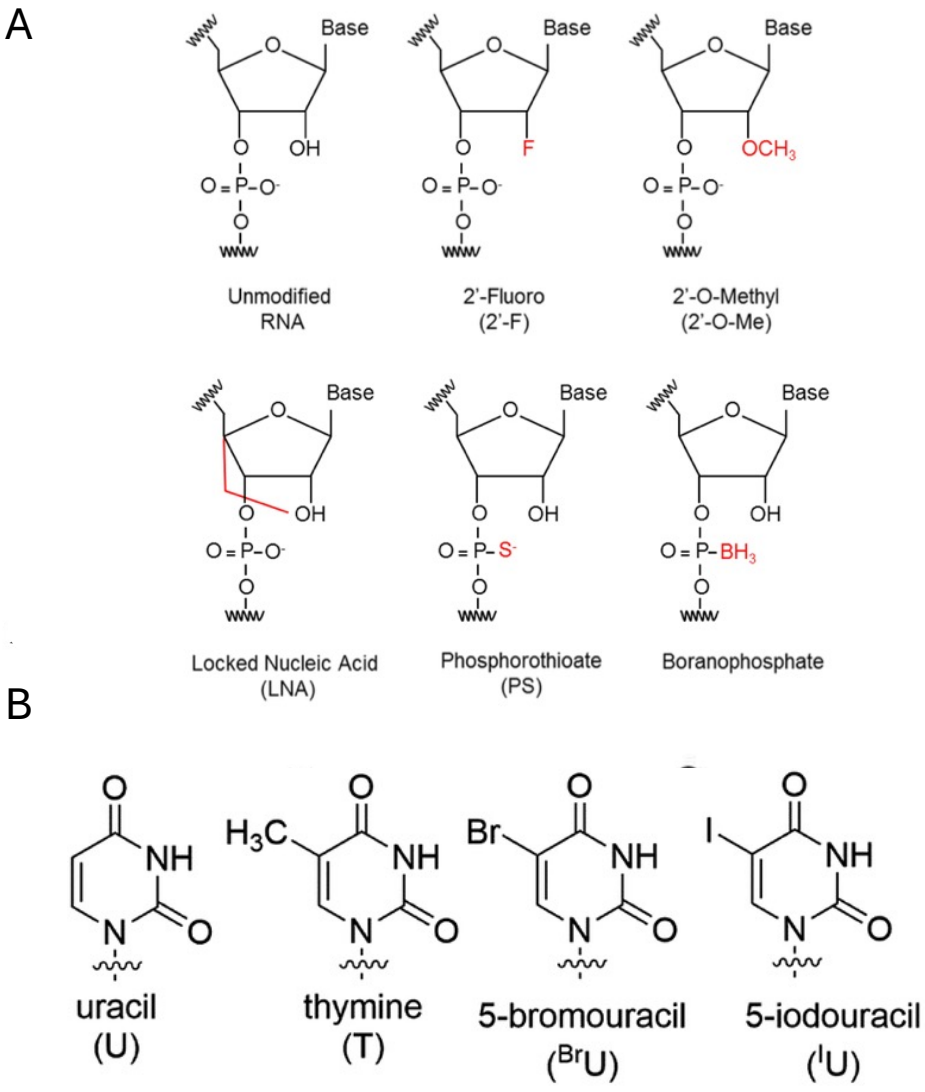

Figure 1.6. Examples of chemical modifications used to improve the therapeutic activity of oligonucleotides. **(A)** Stabilising modifications in the ribose furanose ring (top panel) or in the phosphodiester backbone (lower panel). **(B)** Side chain substitutions in uracil, the most common stabilised base.

Figure 1.7. lists some approaches relying on external mechanisms to disrupt the endosome membrane. The addition of small endolytic molecules such as chloroquine, an antimalarial drug has shown the ability to enhance endosomal escape[87]. Chloroquine has two ionisable nitrogen atoms, preferentially concentrating 1000-fold or more in a low pH environment of endosomes, followed by insertion of its hydrophobic bicyclic aromatic rings into the lipid bilayer, resulting in endosomal disruption[87]. Multiple viral peptides and insect toxins have been found with capability of enhancing membrane disruption. For example, melittin, the active peptide in bee venom, comprises C-terminal cationic and N-terminal hydrophobic residues, forms a pore through the cell membrane and has been studied as an endosomal enhancer[88]. Another endolytic peptide for endosome escape is a derivative of the influenza fusogenic hemagglutinin-2 (HA2) peptides, called INF7. It was shown that the GalNAc-INF7 endolytic peptide could enhance the endosomal escape of a co-administered GalNAc-siRNA 20-fold *in vivo*[82]. Photochemical internalisation is a novel technology based on light-triggered endo-lysosomal escape developed at the Norwegian Radium Hospital[89]. This unique mechanism relies on the activation of light to disturb endocytic structure usually exploiting a small molecule (normally photosensitizer) that is susceptible to light and can help to produce a large amount of oxidising active substances after illumination to disrupt the endosomal membrane.

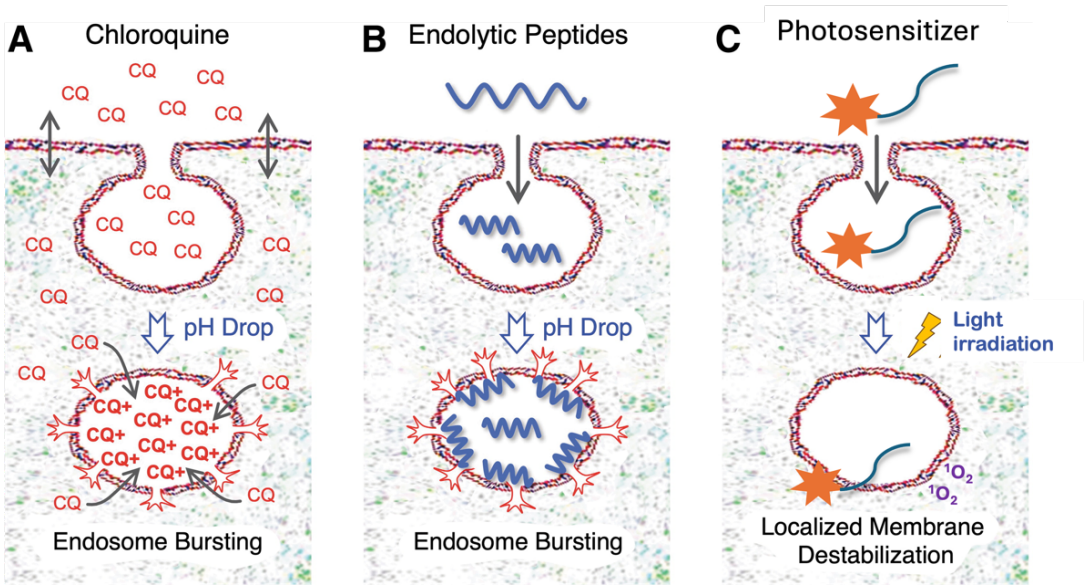

Figure 1.7. Examples of endosomal escape approaches. (A) Small molecules, such as chloroquine (CQ), accumulate preferentially in the low pH environment of endosomes, resulting in a 1000-fold increase in concentration leading the endosome to burst. **(B)** Endolytic peptides or polymers with endosomolytic properties may be co-delivered with nucleic acids to disrupt the endosomal lipid bilayer. **(C)** Photosensitizers accumulate in endosomes/lysosomes and produce reactive oxygen species (ROS) upon light excitation to achieve endosomal release.

1.6 Aims and Objectives

Nucleic acids such as plasmid DNA, mRNA, and siRNA are a group of ribonucleic acid-based therapeutic compounds with enormous clinical potential. Despite their undoubted potential, the clinical translation of these molecules has been largely held back by their limited bioavailability in the target tissues/cells and limited endosomal escape. To overcome this, many drug delivery systems and strategies have been devised.

The aim of this research was to introduce a novel CPP-based delivery platform to enhance the internalisation of NAT into tumour cells. This novel CPP which was developed by our group[90], exploits the advantages of multimerisation and cyclisation of the prototypic CPP, Tat peptide, and shows highly efficient tumour cell internalisation capability. The research presented in this thesis is the application of this novel peptide to the delivery of nucleic acid agents, particularly siRNA and mRNA. To further enhance the delivery efficiency and targeting, strategies to trigger nucleic acid escape from endosomes were investigated. In addition, preliminary research was conducted to explore the potential of this new platform to be a universal carrier for a range of NATs.

Accordingly, the project was structured around the following objectives:

The aims of the research reported in Chapter 3 were to:

1) Synthesise and purify the novel cell-penetrating peptide: cyclic Tat peptide trimer (tri-cTatB).

2) Investigate whether the novel CPP, tri-cTatB, shows higher efficiency than monomeric Tat in delivering siRNA into cancer cells by tracking fluorophore-labelled siRNA.
3) Develop an appropriate strategy for the delivery of nucleic acids either through co-incubation delivery or self-assembling complexes.
4) Characterise the physical properties of tri-cTatB/siRNA complexes (size, charge, morphology, stability).

The aims of the research reported in Chapter 4 were to:

1) Investigate the intracellular localisation of nucleic acid cargoes delivered by siRNA/tri-cTatB complexes through subcellular trafficking studies.
2) Study the mechanism of tri-cTatB/siRNA internalisation, to identify the endocytosis pathway used.
3) Investigate the bioactivity of delivered siRNA by using siRNA targeting GAPDH, and to evaluate siRNA downregulation by means of the GAPDH activity assay.
4) Develop strategies to trigger the endosome escape of endocytosed siRNA: endolytic peptides or photo-activation.

The aims of the research reported in Chapter 5 were to:

The aims of the research presented in this Chapter were to:

1) Investigate the safety and bioactivity of the newly developed light-controlled siRNA/tri-cTatB delivery platform.
2) Evaluate a therapeutic application of the delivery platform: downregulation of the oncogene, polo kinase-1.
3) Test the versatility of the delivery platform by extending the application to another nucleic acid format, mRNA.

Chapter 2

Method and Materials

2.1 Tissue Culture

The following cell lines were obtained from the American Type Tissue Culture Collection (ATCC): HeLa (human cervical carcinoma), MDA-MB-231 (breast adenocarcinoma), MCF-7 (breast adenocarcinoma) and HEK293T (human embryonic kidney derived). Cells were maintained at 37 ^{o}C at 5% CO_2 in a humidified incubator (HeraCell^{TM} 150 incubator, Thermo Fisher Scientific, Waltham, USA). Cells were grown in Dulbecco's Modified Eagle's Medium (DMEM; Sigma-Aldrich #D5796) with 10% foetal bovine serum (FBS; Gibco #10270) and 1% penicillin/streptomycin/glutamate (PSG; Sigma-Aldrich #G1146). Cells were regularly passaged when they reached 70-90% confluency by using 0.05% trypsin-EDTA (Gibson #25300-054) for 3 minutes to detach the cells. Cells were checked monthly for mycoplasma contamination (MycoAlert testing kit; Lonza #LT07). Subsequently, frozen stock vials were prepared with complete DMEM containing approximately 4 x 10^6 cells further supplemented with 10% v/v dimethyl sulfoxide (DMSO) and 40% FBS (final concentration 50% v/v in freezing media) in 1.5 mL cryovials. The vials were transferred into a freezing container (Mr Frosty^{TM}, Thermo Fisher Scientific, Waltham, USA) kept at -80^{o}C, and then stored in liquid nitrogen.

2.2 Nucleic acids

siRNAs used in this study were obtained from Thermo Fisher Scientific. These were non-targeting siRNA (negative siRNA control), siRNA targeting glyceraldehyde 3-phosphate dehydrogenase (siGAPDH), siRNA targeting polo-like kinase-1 (siPLK), scrambled RNA (scrRNA). Fluorophores such as Cy5 and FAM were used to label non-targeting siRNAs.

The mRNA encoding eGFP was made by Sebastian Gołojuch. Cy5-labelled EGFP mRNA was prepared via primed in vitro transcription followed by oxidation and reductive amination. To generate the DNA template, pmRNA-EGFP-A120 (Addgene plasmid # 225903) was linearised with AarI and purified using ion-pairing reversed-phase HPLC. The primed in vitro

transcription reaction was performed using HiScribe® T7 High Yield RNA Synthesis Kit (#E2040S, New England Biolabs) according to the manufacturer's protocol.

Table 2.1 RNAs used in this study (EED represents endosome escape domain).

Sequence	Sense (5' – 3') Antisense (3' – 5')	Source
GAPDH	CCAUGAGAAGUAUGACAACAG UUGGUACUCUUCAUACUGUUG	Thermo Fisher Scientific
PLK1	GGAUCACACCAAGCUCAUCTT GTCCUAGUGUGGUUCGAGUAG	Thermo Fisher Scientific
Scramble	UUGGGAAAAAGUUGAGUGGUU AACCCUUUUUCAACUCACCAA	Integrated DNA Technologies
Negative siRNA	proprietary	Thermo Fisher Scientific
EED labelled siGAPDH	CCAUGAGAAGUAUGACAACAG-PEG$_6$-EED UUGGUACUCUUCAUACUGUUG	In-house synthesised

2.3 Chemical Syntheses

2.3.1 Synthesis of the novel trimeric cyclic Tat peptide

Synthesis of the CPP cyclic Tat trimer (tri-cTatB) followed the protocol by Tietz O. *et al.*[27]. All reagents and solvents were obtained from Sigma-Aldrich, unless otherwise stated. The starting material of azidolysine-cyclicTat-NH_2 (cTat-azide (49-57)) was provided by Cambridge Peptides (UK). Peptide and fluorophores were conjugated to a tetrakis scaffold using a copper-catalysed azide alkyne cycloaddition reaction (CuAAC). Molar ratios of reagents were normalised to the number of CuAAC per molecule and were quoted for each reaction specifically. For the reaction shown in Figure 2.1, 4 eq. $CuSO_4$ and 20 eq. tris((1-hydroxy-propyl-1H-1,2,3-triazol-4-yl)methyl)amine (THPTA) were dissolved and mixed in

water for 5 minutes, 1 eq tetrakis and 4 eq cTat-azide were dissolved in DMSO and water respectively and reacted for 5 minutes. The mixture of cTat-azide and tetrakis was then added with 8 eq. sodium ascorbate (NaAsc) and 12 eq. aminoguanidine hydrochloride (AminoGuan) followed by adding the $CuSO_4$ and THPTA mixture. The mixture solution was dissolved in 30% DMSO/ phosphate-buffered saline (PBS) and heated at 70 °C for 20 minutes. Then the reaction product was purified by HPLC (Agilent Technology, US) and characterised by mass spectrometry (MS QTOF [ES+]: 5100.32, MW calculated: 5100.14 for $C_{209}H_{386}N_{108}O_{43}$).

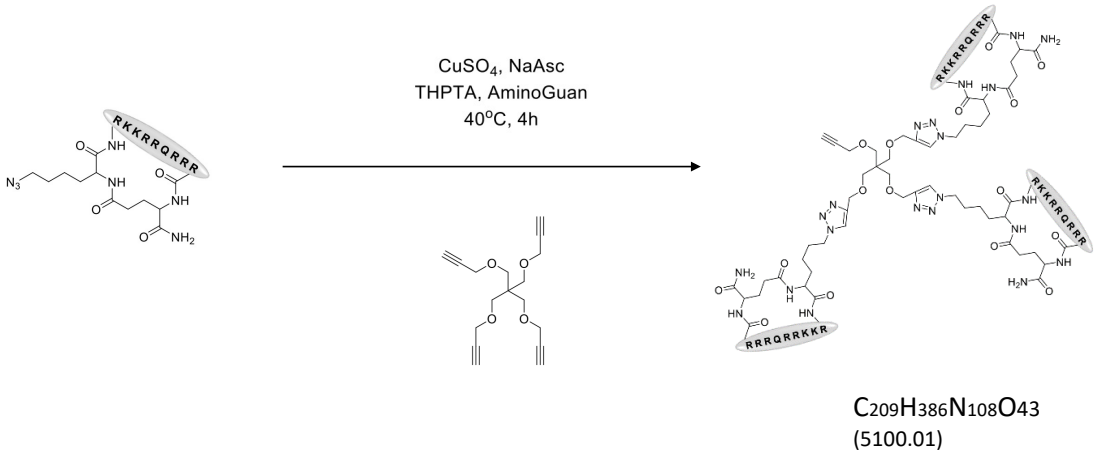

Figure 2.1. The reaction scheme of tri-cTatB synthesis. 3 cTat-azide was added on the tetrakis via CuAAc based click reaction at 40°C for 4 hours.

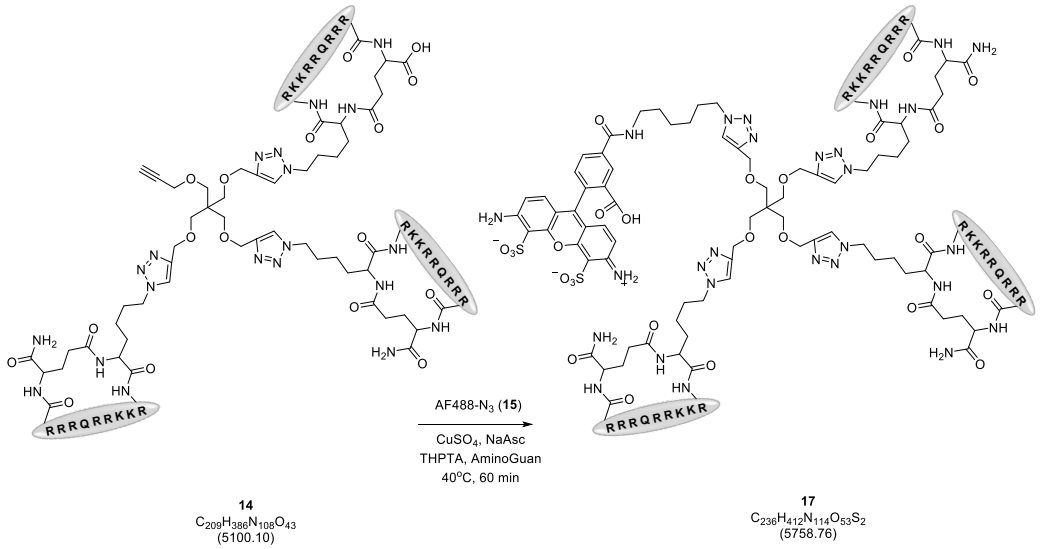

Figure 2.2. The reaction scheme of AlexaFluor(AF) 488 labelling to tri-cTatB. The fluorophore AF488 with azide functionality reacted with tri-cTatB (alkyne on the 4th arm) by CuAAc based click reaction.

To label tri-cTatB with a fluorophore, 2 eq. Alexa Fluor™ 488 5-carboxamido-(6-Azidohexanyl), bis-(Triethylammonium Salt), 5-isomer (AF488-azide) (Thermo Fisher Scientific, USA) were dissolved in H_2O and reacted with 1 eq. tri-cTatB tetrakis scaffolds on the 4th arm for 5 minutes. As well as CuAAC reagents (1 eq. CuSO4, 5 eq.THPTA, 2 eq. sodium ascorbate and 3 eq. aminoguanidine hydrochloride) were dissolved in 30 % DMSO/PBS and heated at 40°C for 60 min. The reaction mixture was then purified by HPLC. MS QTOF [ES+]: 5759.09 (MW calculated: 5758.76 for $C_{236}H_{412}N_{114}O_{53}S_2$).

2.3.2 Endolytic peptide conjugation to oligonucleotides

To promote endosomal release, an endosome escape domain (EED) was covalently conjugated to the 3' end of the sense strand of the siRNA-GAPDH. The sequence of the EED was GFWFG with a six PEG unit (PEG_6) spacer and an azide functional group at the end of the PEG sequence (N_3-PEG6-GFWFG). This customised sequence was synthesised by Biomatik (Cambridge, Canada). The sense strand of siRNA-GAPDH with an amine group labelled at the 3' end was synthesised by 394 Automated DNA/RNA synthesiser (Applied Biosystems, US). To enable strain-promoted alkyne azide cycloaddition (SPAAC) reaction, the amine labelled strand was coupled with DBCO-NHS Ester (6-oxo-6-(dibenzo[b,f]azacyclooct-4-yn-1-yl)-caproic acid sulfo-N-hydroxysuccinimide ester) (GLEN Research, UK) in $NaCO_3$ buffer to provide DBCO-labeled siRNA. For the click reaction, 1 eq. of DBCO-RNA click reaction with 25 eq. of N_3-PEG_6-GFWFG without copper catalyst (pH ~7 environment). Following incubation for 3 hours, the mixture was characterised by mass spectrometry (XEVO G2-QTOF MS instrument) and purified by HPLC (MW calculated: 8206 for $C_{224}H_{270}N_{62}O_{92}P_9$).

2.4 Preparation and characterisation of peptide and siRNA complexes

2.4.1 Complexation of siRNA and peptides

siRNA stock was dissolved in nuclease-free water to a concentration of 50 μM and then diluted in PBS buffer or cell culture medium to a concentration 10 μM for use in experiments. All peptides were dissolved in distilled water to a concentration of 50 μM. To allow self-assembly, peptides and siRNA in PBS or medium were incubated together at room temperature (25°C) for 20 mins at the desired nitrogen/phosphate (N/P) ratio. The N/P ratio was derived from the molar ratio of amine groups in cationic peptides and phosphate groups in the RNA.

2.4.2 Electrophoretic mobility shift assay

The electrophoretic mobility shift assay (EMSA) is affinity electrophoresis used to study the interaction of nucleic acids and peptides. The rate of RNA migration to the positive end of the gel is shifted or retarded when complexed with peptide. This assay was conducted to confirm the formation of siRNA/peptide complexes formation. A mixture containing 5 pmol of siRNA and 5/10/25/50 or 100 pmol of tri-cTatB peptides were self-assembled in a range of N/P ratios (1:1, 1:2, 1:5, 1:10, 1:20 and free siRNA included). siRNA was also complexed with monomeric Tat peptide at different N/P ratios for comparison to tri-cTatB. After adding 6×loading dye (2 μL), the siRNA/peptide complex mixture (12 μL) was loaded onto a 2% (w/v) agarose gel prepared in 1×TAE buffer (40 mM tris, 20 mM acetic acid, 1 mM EDTA, pH 8.6). 10000X SYBR Gold Nucleic Acid Gel Stain (5 μL; Thermo Fisher, MA USA) was added for visualisation. Gels were run at 130 V for 40 min using a Horizontal Electrophoresis System (VWR, US). Gels were visualised under UV transillumination, and images were acquired using an Odyssey® Imager system (LI-COR, Nebraska USA). A 1:10 N/P ratio resulted in stable siRNA and tri-cTatB complexes, and so this ratio was used for all subsequent experiments.

2.4.3 Characterisation: Size, charge and shape

The size and morphology of siRNA/peptide complexes were characterised by dynamic light scattering (DLS) and cryogenic electron microscopy (Cryo-EM). To measure the size and zeta potential of the complex, siRNA and tri-cTatB peptide were allowed to self-assemble at a 1:10 ratio in PBS buffer for 20 min, then diluted in 1 mL PBS for the measurement of hydrodynamic diameter. The siRNA/tri-cTatB complex solution was loaded into a cuvette and analysed using a Zetasizer Nano ZS (Malvern Instruments Ltd., Worcestershire, UK) according to the manufacturer's instructions. Zeta potential was measured using a disposable folded capillary Zeta cell filled with the siRNA/tri-cTatB complex solution in Milli-Q water. Mean particle size (Z-average), polydispersity index (PDI) and zeta potential were derived from three replicate measurements per sample.

The morphology of the siRNA/tri-cTatB complex was further characterised by cryogenic electron microscopy (Cryo-EM). siRNA and tri-cTatB peptide were allowed to self-assemble at a 1:10 ratio in PBS buffer for 20 mins. The complex was applied to copper grids which were then plunge frozen in liquid ethane, following the manufacturer's instructions. Grids were kept in liquid nitrogen before imaging. Cryo-EM images were acquired using a Glacios Cryo-EM (Thermo Fisher Scientific)

2.4.4 Serum stability test

To test the stability of siRNA alone and within siRNA/tri-cTatB complexes, samples were incubated in 10% and 50% FBS at 37 °C. Aliquots were collected after incubation for 2, 6, 24 and 48 hours. siRNA was dissociated from the complexes by incubation with 1 mg/mL heparin (Sigma Aldrich, UK) at 37 °C for 30 min. Samples were then analysed on a 20% non-denaturing polyacrylamide gel electrophoresis (PAGE) (Thermo Fisher Scientific) to monitor the release or degradation of siRNA. The gel was run at 120 V for 60 min using a PowerPac™ High Current power supply (Bio-Rad Laboratories Ltd., UK) and subsequently imaged using an Odyssey® Imager.

2.5 Live-cell confocal microscopy

Cells were seeded onto a Greiner 75/25 mm glass bottom CELLview™ cell culture slide (Greiner Bio-One, UK), allowed to adhere for 24 hours and washed with serum-free medium (3x) before treatment.

Cells were visualised using a Zeiss 880 NLO Inverted Confocal Microscope fitted with a Plan-Apochromat 63x / 1.40 Oil DIC M27 objective (Zeiss, Germany). Different lasers and colour channels were applied depending on the aim of individual experiments. Images were analysed using Fiji ImageJ 2.1.0 software[91].

2.5.1 Cell internalisation analysis

For the co-delivery of siRNA and tri-cTatB, Cy5-labelled siRNA (200 nM) was added to cells followed by Alexa488 labelled peptide (1 μM) in 100 μL Opti-MEM serum-free medium. After incubation for 1 hour, cells were washed 3 times with serum supplemented DMEM and the nuclei were stained using 1 μg/mL Hoechst 33342 (Abcam, UK) for 10 min. For the delivery of siRNA/tri-cTatB self-assembled complexes at different N/P ratios, samples were added to HeLa cells for 1 hour of incubation. The cells were then washed 3 times with serum supplemented medium post internalisation. Hoechst 33342 was used to stain nuclei in the final step. Lipofectamine iMax (Thermo Fisher, MA USA) mediated siRNA transfection was included in internalisation experiments, and for this the manufacturer's instruction was followed. Cells treated with siRNA without any carrier agent were included as a negative control.

2.5.2 Intracellular trafficking

For intracellular trafficking, HeLa cells were transduced with CellLight™ Rab5a-Red Fluorescent Protein (RFP) and Lamp1-Green Fluorescent Protein (GFP) which were used as endosome and lysosome trackers, respectively, according to the manufacturer's instructions

(BacMam 2.0 kit, Thermo Fisher Scientific). After 24 hours of incubation in medium, cells were transfected with FAM or Cy5 labelled siRNA and tri-cTatB complexes in serum-free medium. Confocal microscopy images were captured at different time points to evaluate the co-localisation of siRNA with endosomes and lysosomes (Zeiss LSM 880 microscope) and the quantification of fluorescence from FAM-siRNA was analysed using Fiji ImageJ.

2.5.3 Mechanism of cell internalisation

To assess the endocytosis pathway through which the complexes enter cells, HeLa cells were incubated with endocytosis inhibitors methyl-b-cyclodextrin (2.5 mM), chlorpromazine (10 μg/ml), NaN_3 (100 mM) or amiloride (20 μM) for 30 mins. All endocytosis inhibitors were purchased from Sigma-Aldrich (UK). After treatments, cells were washed with PBS three times. The complex consisting of FAM-labelled siRNA (100 nM) and tri-cTatB (1 μM) was allowed to self-assemble as described and then added to inhibitor-treated cells. Cells were incubated with complexes in serum-free medium for 1 hour at 37°C in a 5% CO_2 incubator. Hoechst 33342 was used to stain the nuclei. Then cells were washed with medium and imaged by confocal microscope.

2.6 GAPDH enzymatic activity assay

GAPDH activity was used as a rapid and sensitive method to investigate whether the internalised siRNA could function as predicted. GAPDH enzymatic activity was determined using the GAPDH Activity Assay Kit (Abcam #204732, UK). GAPDH catalyses the conversion of glyceraldehyde-3-phosphate (GAP) to 1,3-bisphosphate glycerate (BPG) and the intermediate, NADH, which reacts with a developer to form a coloured product that absorbs maximally at 450 nm. GAPDH activity is indicated by measuring NADH production at 450 nm using a fluorescence spectrophotometer.

In brief, cells were seeded in 12-well plates at 5×10^4 per well and allowed to adhere overnight. On the following day, cells were washed with PBS for 3 times and then treated according to the experimental design in serum-free medium and incubated in full medium for 48 hours in 37 °C, 5% CO_2. Cells were washed with cold PBS and resuspended in 100 µL of ice-cold GAPDH assay buffer and incubated on ice for 10 mins for lysis. Cell lysates were scraped and transferred to Eppendorf tubes and centrifuged at 14,000 x g for 5 minutes at 4 °C. The supernatants were harvested, and the protein concentration of each sample was determined using the Bicinchoninic Acid (BCA) Protein Assay Kit (Thermo Fischer Scientific, UK). All samples were equilibrated to load the same amount of lysate and assayed according to the manufacturer's protocol in a 96-well plate. The output was measured by the fluorescence spectrophotometer (Tecan, Germany). The concentration of GAPDH in the test samples was calculated as follows:

$$GAPDH\ Activity = \left(\frac{B}{\Delta T x\ V}\right) * D = nmol/min/\mu L = mU/\mu L = U/mL$$

Where:

B = Amount of NADH from standard curve (nmol).

ΔT = Reaction time (minutes). D = Sample dilution factor.

V = Original sample volume added into the reaction well (µL).

2.7 Western blot analysis

Cells were seeded in a 6-well plate at 1×10^5 cells per well and the following day were washed 3 times with PBS and then transfected with various conditions in in serum-free medium and incubated at 37 °C, 5% CO_2 according to experimental design. Cells were washed with PBS and lysed with RIPA buffer (Sigma Aldrich, UK) containing a protease and phosphatase inhibitor cocktail (Abcam, UK) on ice for 5 minutes. Cell lysates were scraped and transferred to Eppendorf tubes and centrifuged at 14,000 x g for 10 minutes at 4 °C. The supernatants were harvested, and the protein concentration of each sample was determined using a BCA Assay

Kit. The resulting absorbance was measured by an Infinite 200 Pro Platereader (Tecan, Germany). Samples were prepared in lithium dodecyl sulfate (LDS) loading buffer supplemented with sample reducing agent NuPAGE™ (Thermo Fisher Scientific, USA) and were then heated at 80 °C for 10 minutes.

Cell lysates (20 µg protein) were loaded into wells of a 4-12% Bis-Tris Gel (12-well, NuPage™ Novex™, Thermo Fischer, UK). Gels were run on a XCell SureLock™ Mini-cell system (Thermo Fisher Scientific, UK) in MOPS running buffer supplemented with antioxidants to maintain the reduced state of the proteins. SeeBlue™ Plus2 Pre-stained Protein Standard (Thermo Fischer Scientific, UK) and MagicMark™ XP Western (Thermo Fischer Scientific, UK) were used as standard markers. Gels were allowed to run for 60 min at 160 V at room temperature, using a PowerPac™ High Current power supply (Bio-Rad Laboratories Ltd., UK). Protein transfer was performed using an Invitrogen iBlot™ 2 Dry Blotting system (Thermo Fisher Scientific, UK). Protein was transferred from gels to 0.2 µm nitrocellulose membranes (BioRad) using an iBlot™ mini Transfer Stack (Thermo Fisher Scientific, UK).

Membranes were blocked in 5% bovine serum albumin (BSA) blocking buffer (Sigma Aldrich, UK) in TBS-T (0.1% Tween20) for 1 hour and then incubated overnight with primary antibodies diluted in blocking buffer at 4°C (see Table 2.2 for details). The β-Actin primary antibody was used as a loading control for all western blots. Membranes were washed for 5 minutes with TBST for 3 times and incubated with fluorophore labelled secondary antibodies for 1 hour at room temperature, immunoblots were visualized using the Odyssey imager (LI-COR Biosciences, USA) (see Table 2.2 for details).

Table 2.2 Antibodies used in western blot analysis.

Antibody	Species	Cat. Number	Manufacturer	Dilution
PLK 1	Rabbit mAb	4513	Cell Signalling	1:1000
β -Actin	Mouse mAb	3700	Cell Signalling	1:1000
IRDye 800CW anti-Rabbit IgG	Goat	925-32211	LI-COR Bio	1:20,000
IRDye 600RD anti-Mouse IgG	Goat	925-68070	LI-COR Bio	1:20,000

2.8 Photo-irradiation:

The photosensitiser, meso-tetraphenyl chlorine disulfonate (TPCS2a /fimaporfin) was obtained from BOC Science. Fimaporfin was diluted in 3% polysorbate 80, 2.8% mannitol and 50 nM Tris (pH 8.5) to a final concentration of 0.35 mg/mL and kept at 4 °C protected from light. Except during irradiation, all work with fimaporfin was performed under light protection. For experiments involving photo-irradiation, cells were pre-treated with 0.35 µg/mL fimaporfin in the culture medium during the cell seeding step and incubated at 37 °C, 5% CO_2 for 18 hours. The following day, cells were washed three times in a culture medium and incubated for another 4 hours in drug-free medium, to ensure the removal of fimaporfin from the plasma membrane prior to light exposure.

For monitoring of endosomal release, cells were treated with Cy5-siRNA/tri-cTatB complexes or Cy5-siRNA. After 1 hour of delivery, cells were washed with medium 3 times. Live cell confocal images were acquired prior to light exposure and cells were subsequently exposed to the LED light (ThorLab) at 415 nm, using a current adjusted to 20 mA[92] and the final irradiation energy corresponded to 11 J/cm^2.

$J/cm^2 = (Amp \times Voltage \times Time) / Area$

To investigate the biological effect of siRNA activated by irradiation, cells were treated with siRNA/tri-cTatB complexes, scrRNA/tri-cTatB complexes or lipofectamine transfected siRNA for 1 hour. Cells were then washed with medium 3 times and subsequently exposed to LED light at 415 nm as described above. Following incubation for 48 hours, cells were collected for GAPDH activity assays or western blot analysis.

2.9 Annexin-V to detect early apoptosis

An Annexin V-APC/Propidium Iodide (PI) Apoptosis Detection Kit (Abcam, US) was used for the detection of siPLK/tri-cTatB plus light mediated cell apoptosis. Briefly, MCF-7 and MDA-MB-231 cells were seeded onto 6-well plates and fimaporfin was treated at the same time. After overnight incubation followed by 4 hours of chasing, cells were treated with siPLK/tri-cTatB and scrRNA/tri-cTatB in Opti-MEM at an siRNA concentration of 100 nM for 1 hour. Lipofectamine transfected siPLK was included as the positive control. Cells were washed with medium for 3 times. Cells were then exposed to light (415 nm, 10 J/cm^2) for desired groups. Cells were incubated for 24 hours at 37 ºC before harvest to allow the PLK1 regulation and completion of cell cycles. Cells were centrifuged at 1300 rpm for 5 min and resuspended in Annexin V binding buffer (10 mM HEPES, 150 mM NaCl, 5 mM KCl, 1 mM $MgCl_2$, 1.8 mM $CaCl_2$). Then cells were stained with Annexin V-APC/PI Apoptosis Detection Kit according to the manual. Finally, cells were analysed on a flow cytometer.

2.10 Flow Cytometry

For flow cytometry, 5 x 10^5 cells were plated in a 12-well plate with complete culture medium and incubated overnight at 37°C with 5% CO_2. Following treatment (as defined for individual experiments), cells were washed twice with PBS and collected using trypsin EDTA (Thermo Fisher Scientific). Cells were collected in a Greiner round bottom tube and spun down at 400 x g for 5 min. Following 2 washes with PBS, cells were suspended in ice-cold FACS buffer

(PBS, 5% FBS, 0.1% NaN_3 sodium azide). Samples were then tested using CytoFlex (Beckman, USA). Data analysis was carried out using FlowJo™ v10.6.2 software (FlowJo LLC, USA).

2.11 Peptide delivery and transfection of mRNA

The reporter gene, enhanced green fluorescence protein (eGFP) was used to evaluate the efficiency of mRNA transfection of mRNA/tri-cTatB complexes. HeLa or HEK29T cells were seeded in CELLview™ cell culture slides at a density of 1×10^4 cells per well for live cell imaging or in 12-well plates at a density of 5×10^4 cells per well for flow cytometry. Fimaporfin (0.35 μg/mL) was added after cell seeding. After 24 hours, fimaporfin-containing medium was replaced with fresh culture medium and cells were incubated for a further 4 hours. The medium was then replaced with Opti-MEM (90 μL), followed by the addition of 10 μL of freshly prepared mRNA/tri-cTatB complexes. The final concentration of eGFP mRNA and tri-cTatB was 40 nM and 2 μM respectively (mRNA: CPP ≈ 1:50). Lipofectamine iMAX was used as a positive control. After incubation for 2 hours, the medium was removed, and the cells were washed twice with PBS before the addition of 100 μL of medium per well. After incubation for 20 hours, eGFP expression was assessed by live cell confocal imaging and flow cytometry.

2.12 Cell viability assay

A colourimetric assay, the Cell Counting Kit 8 (CCK-8), was used to measure cell viability in this study. The CCK-8 assay utilises the water-soluble tetrazolium salt WST-8 which produces a water-soluble formazan dye on reduction in the presence of an electron carrier. The amount of the formazan dye generated by the activity of dehydrogenases in cells is directly proportional to the number of living cells.

For the CCK-8 assay, cells were seeded in 96-well flat-bottom clear plates at a density of 10,000 cells per well. Following treatment, as defined for individual experiments, cells were incubated for another 24 hours at 37 °C, 5% CO_2. 10 μL of CCK-8 solution was added to each

well to make a total volume of 100 µL. Cells were incubated with CCK-8 solution for 2 hours. Blank wells were included to provide a background reading. Colour intensity was measured at OD 460 nm using an Infinite 200 Pro Platereader (Tecan, Germany).

2.13 Statistical analysis

Processing of raw data was performed using Microsoft Excel (Microsoft, WA, USA) and then imported to Prism 7 (GraphPad Software, USA) for statistical analysis and to plot graphs. Data were obtained from a minimum of three technical replicates unless otherwise stated. Data were plotted using means and error bars representing the standard deviation. For the assessment of statistical significance, the *p* value was set at 0.05 and the data was analysed by the Holm-Sidak method. Statistically significant results are indicated with asterisk symbols (*) where: * $P<0.05$, ** $P<0.01$, *** $P<0.001$, and **** $P<0.0001$, while non-significant results are not labelled on graphs.

Chapter 3

The novel peptide tri-cTatB synthesis and delivery of siRNA

3.1 Introduction

3.1.1 Cell-penetrating peptides: Tat and its derivatives.

The intracellular delivery of macromolecules such as antibodies and nucleic acids remains a significant biomedical challenge due to the limited efficacy and toxicity of currently available methods. As introduced in Chapter 1.4, CPPs have shown initial promise in overcoming the barriers of cell permeability. One of the frequently explored CPPs is the cationic, arginine-rich peptide known as Tat, obtained from the HIV-1 virus. The archetypal CPP Tat has been used extensively in the design of intracellularly targeted therapeutics. However, inefficient cell membrane permeability and endocytic entrapment are recognized as a hindrance to intracellular delivery. The low-level leakage of Tat-delivered cargos from endosomes is typically too inefficient to lend itself to most intracellular targeting applications[93,94]. Therefore, several recent studies have attempted to address the problem of inefficient permeability and endosomal entrapment by modifying the structure of CPPs to develop Tat derivatives.

Some studies found that cyclisation of Tat peptide improves its access to the cytosol and nucleus by enhancement of direct translocation across the cell membrane. Lättig-Tünnemann *et al*. found that the cyclic form of Tat (cTat) at 20 μM was able to permeate into cells on average 15 min faster than other arginine-rich peptides, accumulated in cells in larger amounts, and exhibited enhanced transduction kinetics[95]. Nischan *et al*. modified Tat into a cyclic form (cTAT, N_3-PEG_2-[K(rRrGrKkRr)E]) using PEG as a spacer. They found that cyclic TAT was considerably more efficient than its linear counterpart at delivering protein (GFP) into cells (Figure 3.1A)[96]. The improved penetrability of cTAT may be because non-endocytic uptake is the predominant mechanism for their intracellular transport but not endocytosis[97]. However, these Tat modifications are not feasible *in vivo* due to the high concentrations needed to achieve a therapeutic effect *in vitro* (> 10 μM). The typical dosing of clinically used

immunotherapeutics is 10 mg/kg, emphasising the need for carriers that can transfect clinically relevant amounts of macromolecules at the lowest concentration possible[98].

Interestingly, recent insights into the relationship between the charge density of polycationic agents and their delivery efficiency, have provided clues about how to address the dosing issue. It was hypothesised that prearranging Tat peptides into multimeric clusters on a defined chemical scaffold would increase their internalisation efficacy [99,100]. This hypothesis is credible based on the observation that branched multimers of Tat, on peptide scaffolds or connected by disulfide bonds, result in increased intracellular delivery. Research efforts have been directed particularly at bridged dimers of Tat and oligoarginine[101,102]. Pellois' group (2010) has proved greater endosomolytic activity of the trimeric TAT than its monomeric and dimeric counterparts.

Combining the recent advances in Tat peptide development, Tietz *et al*. recently reported a novel Tat-derived CPP that combines the cyclisation of the archetypal Tat (cTat) with the formation of a multimer construct via the conjugation of three copies of cTat to a tetrakis core structure (Figure 3.1B)[90]. The synthesis of this new cyclic trimer peptide is based on an alkyne-functionalised scaffold, the peptide was therefore named as tri-cTatB.

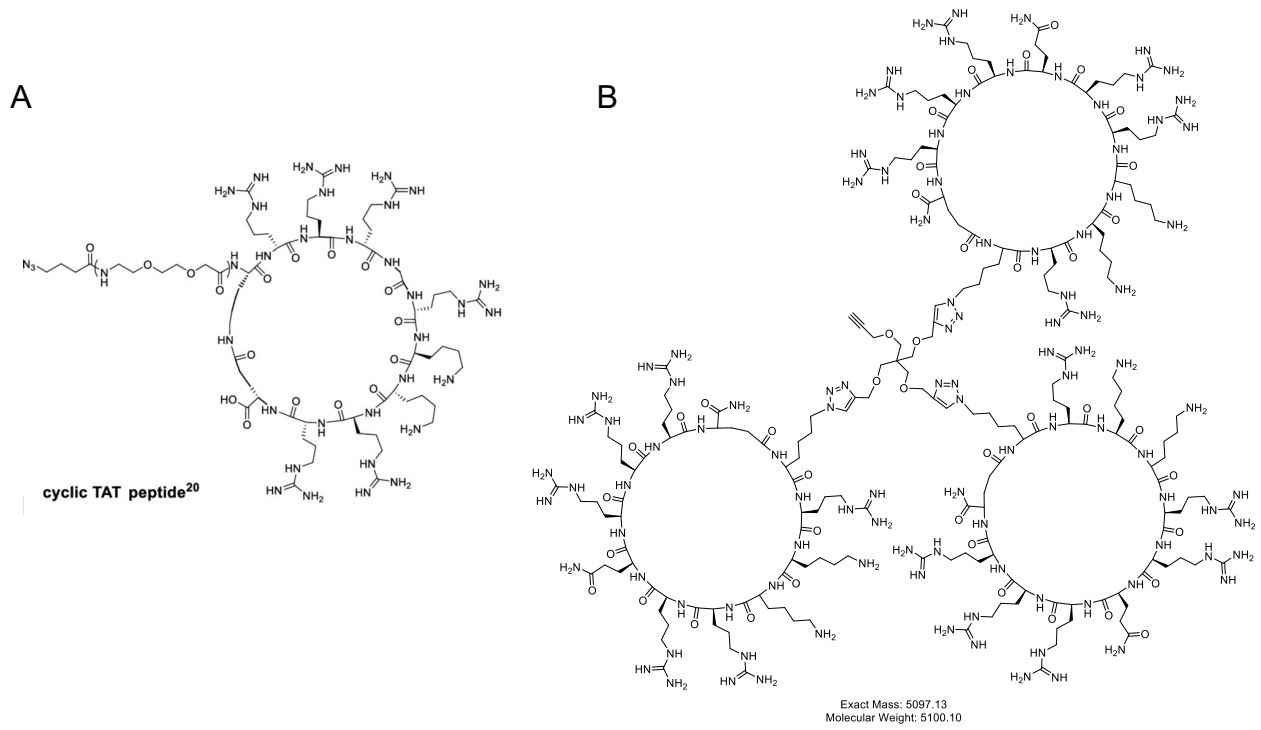

Figure 3.1. Derivatives of Tat peptides. (A) The chemical structure of cyclic Tat peptide conjugated to a spacer developed by Nischan *et al*[96]. **(B)** Chemical structure of tri-cTatB. The development of tri-cTatB combines the cyclisation of Tat (cTat) with the use of three copies of cTat attached to a tetrakis core structure, forming a trimeric CPP.

3.1.2 Tri-cTatB co-delivery of antibodies

In the study by Tietz *et al*., tri-cTatB was shown to provide more effective cellular transduction compared to monomeric cTat at a concentration of 1 μM (Figure 3.2A). In HeLa cells, from 1 min to 13 min after the addition of AF488 labelled tri-cTatB, the peptide displays little association with the plasma membrane but large vesicular bodies containing the CPP form in the cytosol. The fluorescence signals then spread from these vesicles into the cytosol which suggests that the route of cell entry of tri-cTatB is through the formation of vesicle-like bodies followed by vesicular escape.

The efficacy of tri-cTatB was assessed by evaluating its ability to co-deliver antibodies (whole IgGs) and antibody fragments. Exposure of HeLa cells to 500 nM AF647-labelled non-specific mouse Fab fragment plus 1 μM AF488-tri-cTatB for 30 min resulted in the successful delivery of Fab into the cytosol and nucleus of 50% of cells in a typical experiment. The time course of

Fab uptake by tri-cTatB follows a similar pattern as tri-cTatB itself: within 23 min significant antibody uptake was observed in the cytosol.

Although the tri-cTatB peptide could deliver a functional antibody into cells, it is not clear whether this peptide can mediate the delivery of other types of biomacromolecule cargo, such as nucleic acids. The aim of this study was to evaluate whether tri-cTatB promotes nucleic acid intracellular delivery.

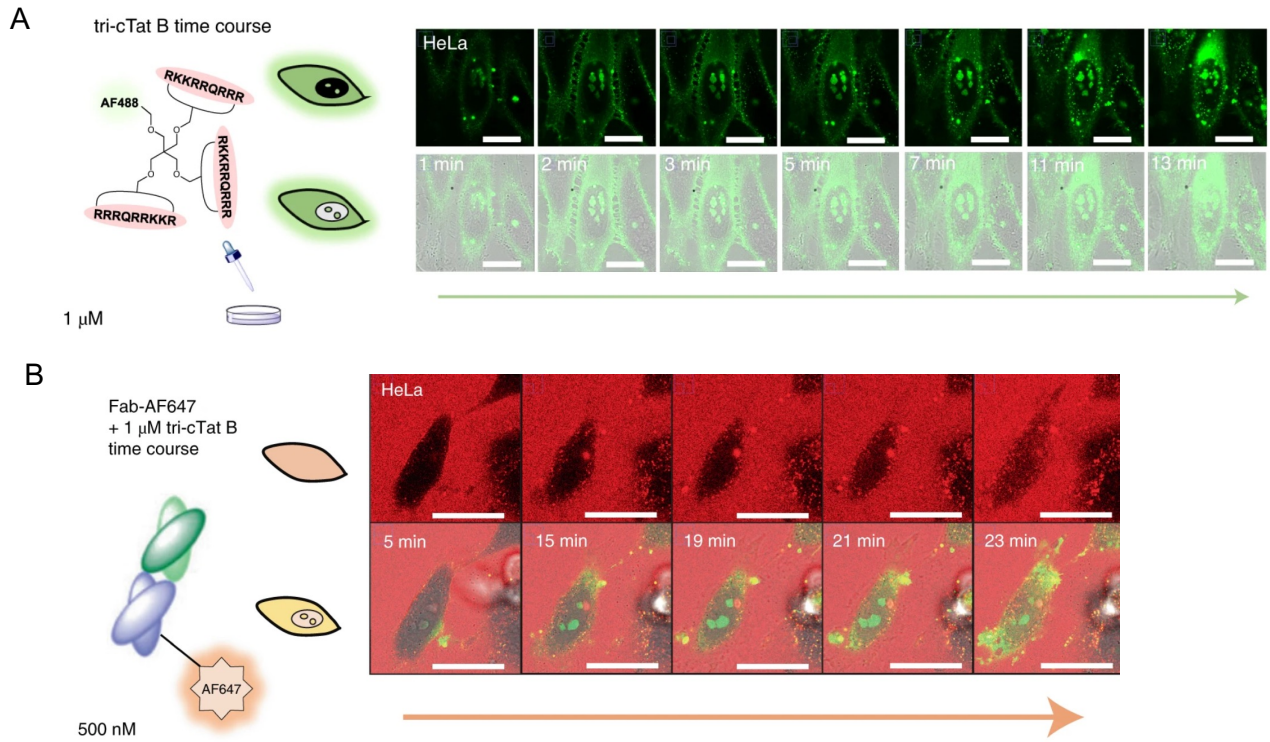

Figure 3.2. Internalisation of tri-cTatB and co-delivery of antibodies in live HeLa cells using tri-cTatB. (A) Time-course uptake of 1 µM AF488-tri-cTatB. **(B)** Continuous live-cell confocal microscopy of HeLa cells treated with 500 nM Fab-AF647 (red) and 1 µM AF488 labelled tri-cTatB (green).

3.1.3 Cell-penetrating peptide delivery of siRNA

As introduced in Chapter 1.4.4, CPPs have shown great potential in delivering a range of nucleic acids such as ASO, siRNA and mRNA. In terms of the delivery of nucleic acids, CPPs

demonstrate versatility through the wide range of strategies that can be employed. Figure 3.3 presents four strategies developed to deliver siRNAs.

In co-incubation protocols (Figure 3.3A), sample preparation is simple and the inherent properties of the CPPs and siRNA are preserved. While this method can be efficient using *in vitro* conditions it is associated with serious limitations. To be effective *in vivo*, the cargo and CPP must co-localise at the target site in sufficient concentration to cause the intended biological effect. However, it is unlikely that this can be accomplished when the CPP and nucleic acid cargoes are simply simultaneously co-administered[103]. Simple CPP-oligonucleotide conjugates use a covalent bond to ensure a stable linkage between the peptide and the cargo, which makes structure-activity relationships more straightforward to interpret (Figure 3.3B). CPPs and siRNAs may be attached via a cleavable linker that allows the separation of the peptide from the RNA in the cytoplasm. This facilitates the recruitment of the released siRNA by the RISC complex, avoiding its localisation in the nucleus. A popular type of cleavable linker includes a disulfide bond, which breaks in a reducing environment. Muratovska *et al*. conjugated Penetratin to siRNA against luciferase via a disulfide linkage and achieved effective downregulation of a luciferase reporter gene[104]. Notably, binding the Tat or Penetratin peptide to the 3' end instead of the 5' end of the siRNA strand increased the downregulation of the target gene[105].

Non-covalent complexation between cationic CPPs and anionic siRNAs is a commonly used strategy (Figure 3.3C). The complex formation of the two components is straightforward and cost-effective since it does not require any complicated reaction conditions or purification. The nature of the complex formation between CPPs and nucleic acids via electrostatic interactions allows a versatile complex formulation using a simple "mix and incubate" technique at room temperatures. A high density of positive charges on the peptides is necessary to avoid instability and premature release of nucleic acid cargoes[106]. Defining an optimal balance between peptide and siRNA is needed to avoid charge neutralisation and to preserve a positive overall charge is

mandatory for efficient uptake[106]. Moreover, the complexation may provide protection to siRNA, therefore chemical modifications on the oligonucleotides are not necessary for this strategy. Many studies have successfully delivered RNA to various cell lines *in vitro* using complexes. For example, Eguchi *et al*. developed PTD-DRBD, a Tat peptide fused to a single dsRNA binding domain, and succeeded in silencing reporter genes even in primary cell types (T cells, Human umbilical vein endothelial and embryonic stem cells)[107], which are known hard to be transfected due to their low proliferation rate and robust plasma membrane.

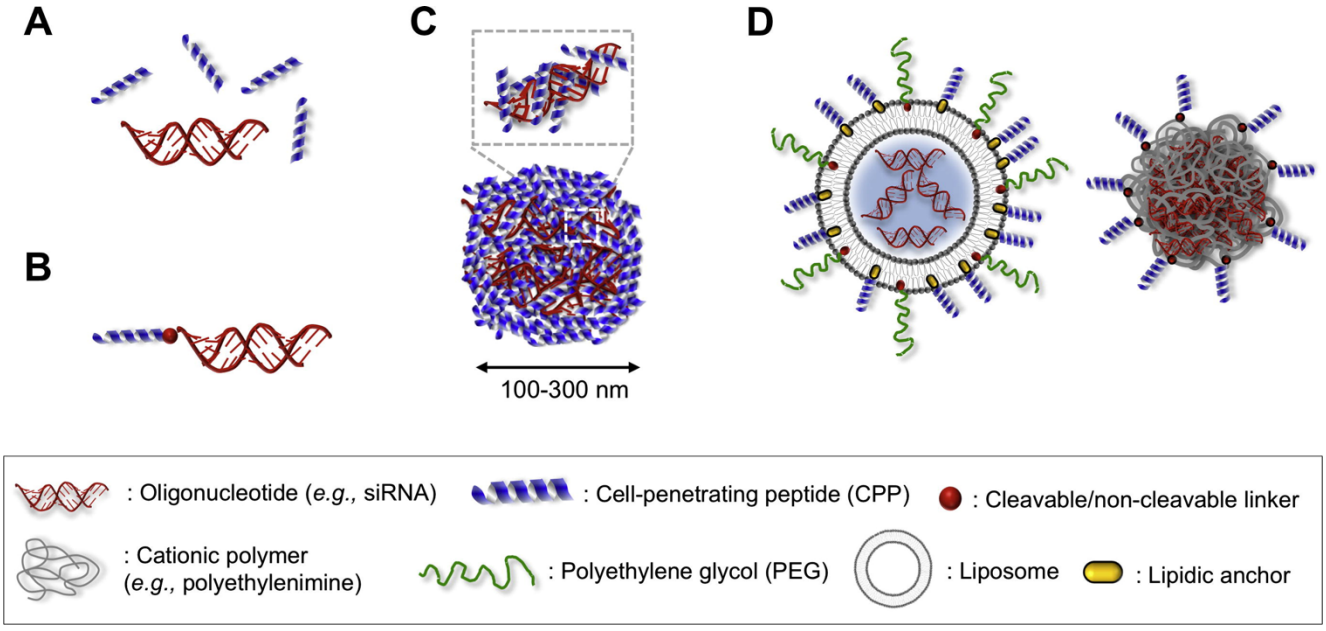

Figure 3.3. Schematic diagrams of oligonucleotide delivery strategies involving CPPs: **(A)** Co-incubation. **(B)** Direct conjugation. **(C)** Non-covalent complex. **(D)** CPP-functionalised liposome or polymer complexes. Figure adapted from Lee *et al*[103].

Finally, CPPs have been used as a transduction element in more complex nanoparticulate formulations such as polymeric nanoparticles or liposomes (Figure 3.3D). CPPs covalently modified to cationic polymers can complex oligonucleotides to form polymeric nanoparticles. Peptides can also be conjugated on the surface of preformed polymer/oligonucleotides polyplex[103]. For example, Mudhakir *et al*. injected octaarginine-grafted liposomes intravenously into mice and showed enhanced tissue distribution and better total clearance compared to neutral liposomes[107].

This thesis will focus on utilising the newly developed tri-cTatB to deliver siRNA and other nucleic acids via non-covalent strategies.

3.2 Aims

The aims of the research presented in this Chapter were:

1) To synthesise and purify the novel peptide cyclic TAT peptide trimer (tri-cTatB).
2) To investigate the efficiency of tri-cTatB-mediated delivery of siRNA into cancer cells by tracking fluorophore-labelled siRNA, in comparison to monomeric linear TAT.
3) To investigate different approaches to tri-cTatB delivery of siRNA: co-delivery versus complex formation.
4) To characterise the physical properties of tri-cTatB/siRNA complexes (size, charge, morphology, stability).

3.3 Results

3.3.1 Synthesis of the novel cell-penetrating peptide: tri-cTatB.

Tri-cTatB was synthesised by copper(I)-catalysed cycloaddition (CuAAC) reactions between azide- and alkyne-functionalised components. Following the published method, the cyclic Tat peptide was custom designed to match the linear sequence (RKKRRQRRR) and modified with addition of an azide-lysine (K(N_3)) residue at the N terminus (Figure 2.1). Then tri-cTatB was formed via CuAAC with an excess of cTat compared to the tetrakis alkyne functionalised scaffold B as described in Section 2.3.1. The reaction led to the formation of a mixture of by-products including cTat peptide starting materials, dimers, and trimers. HPLC purification was used to separate the cTat trimer (tri-cTatB) from the mixture. In Figure 3.4 A, Region 2 represents the collection of the target product, tri-cTatB, which has a retention time (rt) at 5:25 min while Region 1 represents the starting material, cTat, Region 3 represents cTat dimer by-product. The peak integration region of interest % (ROI) of the target product was 37%. The

peak of Region 2 solution was collected for confirmation of identity by liquid chromatography-mass spectrometry (LC-MS) (Figure 3.4B), and a molecular mass of 5100.0 Da was detected which matches the molecular weight of tri-cTatB (5100.10 g·mol^{-1} for $C_{209}H_{386}N_{108}O_{43}$).

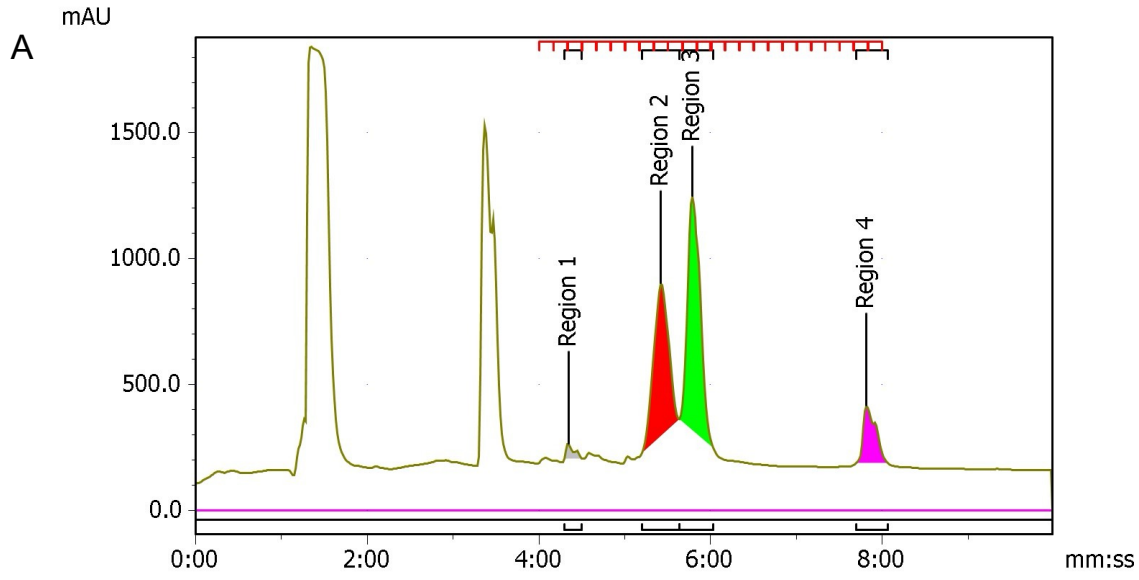

Name	Start (mm:ss)	End (mm:ss)	Retention (mm:ss)	Area (mAU·s)	%ROI
Region 1	4:18	4:30	4:21	326.1	1.68
Region 2	5:12	5:38	5:25	7186.3	37.00
Region 3	5:38	6:02	5:47	9674.1	49.81
Region 4	7:42	8:04	7:49	2233.9	11.50
4 Peaks				19420.5	100.00

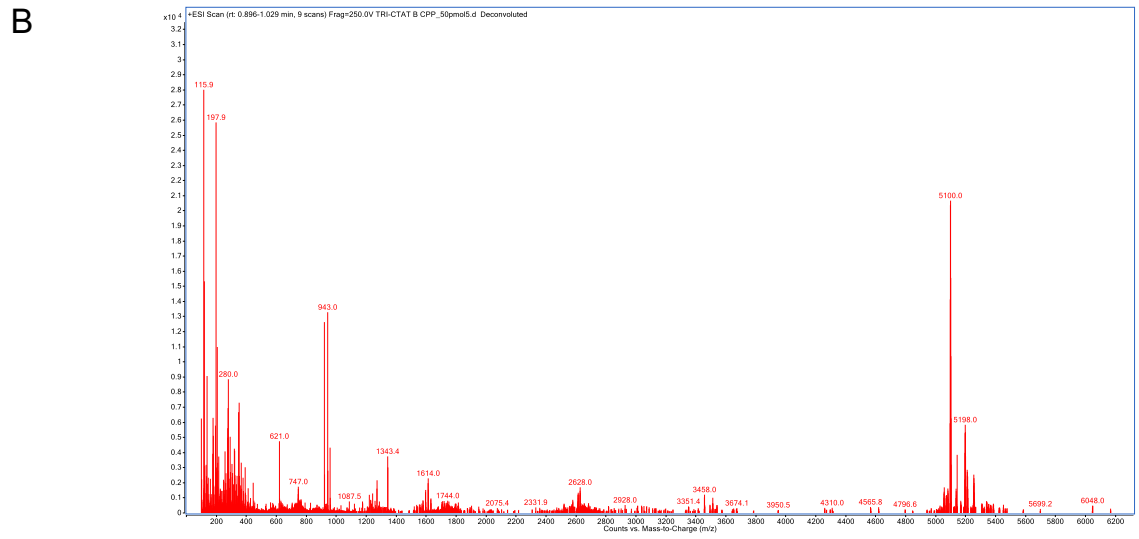

Figure 3.4. tri-cTatB synthesis characterisation. (A) High-pressure liquid chromatography (HPLC) chromatogram indicates the synthesis of Tri-cTatB (Region 2, red), cTatB dimer (region 3), cTat starting material (region 1). Quantification of each peak was done by integrating the peaks (%ROI). **(B)** Maximum entropy deconvoluted MS QTOF mass spectra of

tri-cTatB (theoretical molecular weight at 5100.10 g·mol^{-1} for $C_{209}H_{386}N_{108}O_{43}$) confirmed the right product at mass 5100.0 g·mol^{-1}.

3.3.2 Tri-cTatB mediated delivery of siRNA: Co-delivery

The potential of this newly developed tri-cTatB CPP to deliver nucleic acids was evaluated by using siRNA as the cargo. As introduced in Chapter 3.1.3, the strategies of co-incubation and complexation to mediate siRNA intracellular delivery were investigated.

The first siRNA delivery strategy attempted was based on peptide and siRNA co-incubation, which is also the method reported for tri-cTatB mediated antibody co-delivery. In this approach, tri-cTatB was added to cells prior to the nucleic acid cargo. AF488-tri-cTatB and Cy5-siRNA enabled the observation of tri-cTatB as green and siRNA as red in live cell imaging experiments. HeLa cells were treated with 1 μM tri-cTatB followed by the addition of 100 nM siRNA. After 1 hour of incubation, successful internalisation of tri-cTatB and siRNA was observed (Figure 3.5). The tri-cTatB (green) signal homogenously stained the cell cytoplasm and nucleus which is consistent with the previous report while siRNA (red) accumulated in foci distributed throughout cytosol. Co-localisation of the siRNA and tri-cTatB was minimal. In this experiment, the commercial transfection reagent, lipofectamine transfection for 1 hour, was included for comparison. At 1 hour, lipofectamine mediated very limited siRNA cellular uptake.

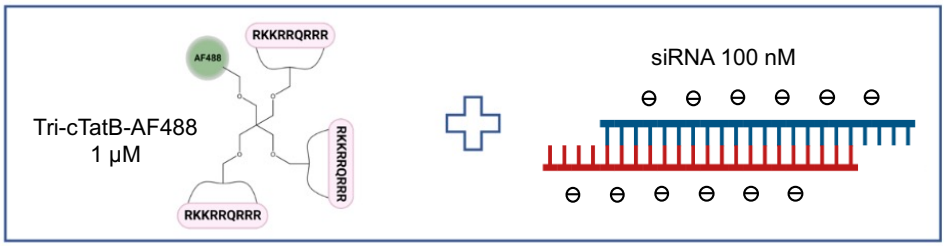

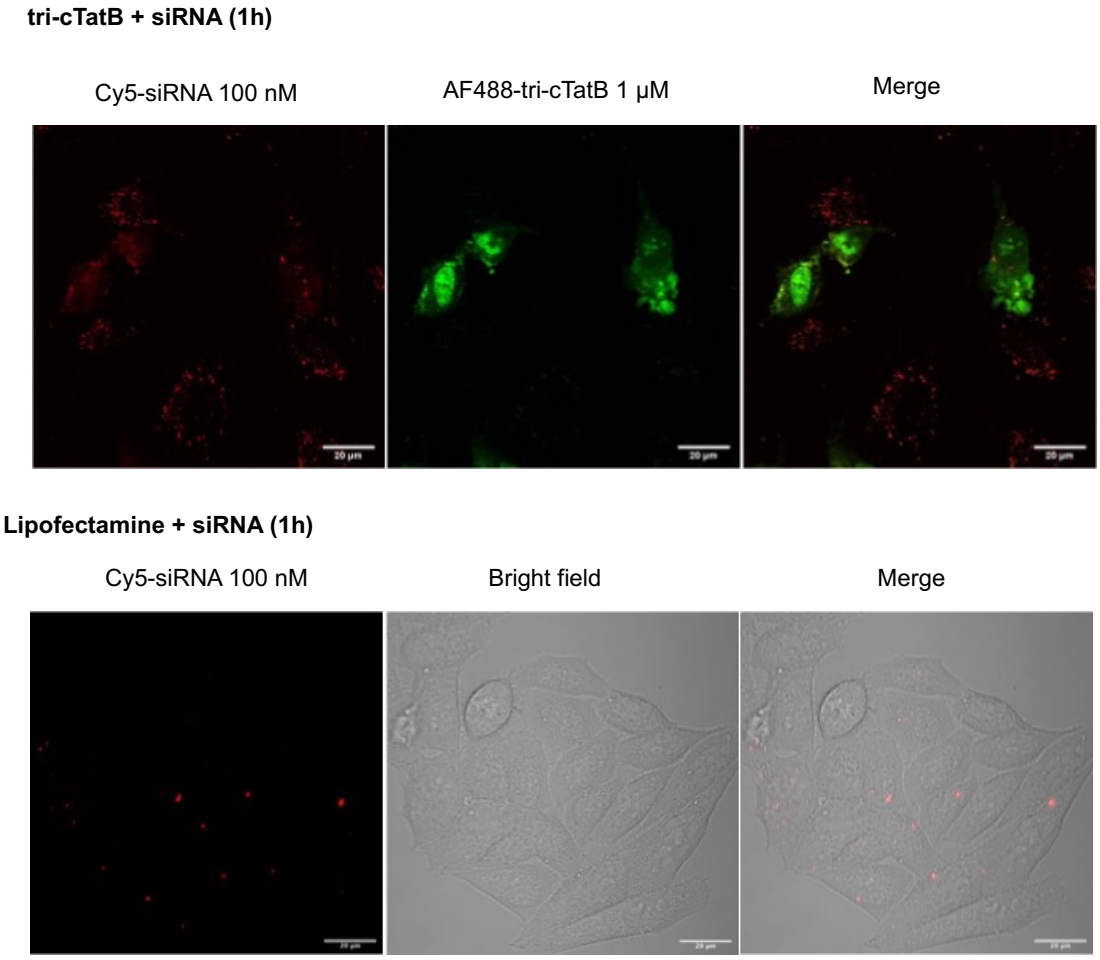

Figure 3.5. Live cell confocal imaging of tri-cTatB co-incubation with siRNA. 1 µM of AF488-tri-cTatB (green) was used to deliver 100 nM of Cy5-siRNA (red). Lipofectamine transfection of 100 nM siRNA was included. Cells were imaged after 1 hour of incubation. Scale bars: 20 µm.

3.3.3 Tri-cTatB mediated delivery of siRNA: self-assembled complex

Another commonly used non-covalent CPP-mediated siRNA delivery strategy is self-assembly of complexes of the 2 components via electrostatic interaction. To form complexes, positively charged tri-cTatB was mixed with negatively charged siRNA at different N/P ratios in PBS buffer for 30 minutes (Figure 3.6A). siRNA to tri-cTatB ratios of 1:1, 1:2, 1:5, 1:10 and 1:20

were tested. To assess complex formation, the mixture was assessed via running gel retardation assays. siRNA was also mixed with cTat monomers at different N/P molar ratios (1:1, 1:5, 1:10 1:20 and 1:40) and assayed (Figure 3.6B). Migration of the siRNA band was impeded at a siRNA:tri-cTatB molar ratio of 1:2 and prevented completely at a ratio of 1:10. This complete retardation was likely due to charge neutralisation of the RNA by the peptide and/or formation of large complexes between peptides and RNA. Since the siRNA band started to disappear at the N/P ratio of 1:10, a molar ratio of siRNA:tri-cTatB of 1:10 was used for subsequent experiments. In contrast to tri-cTatB, siRNAs mixed with monomeric cTat were not retarded on the gel, indicating that siRNA did not form condensed complexes with tri-cTatB at N/P ratios of less than 1:40.

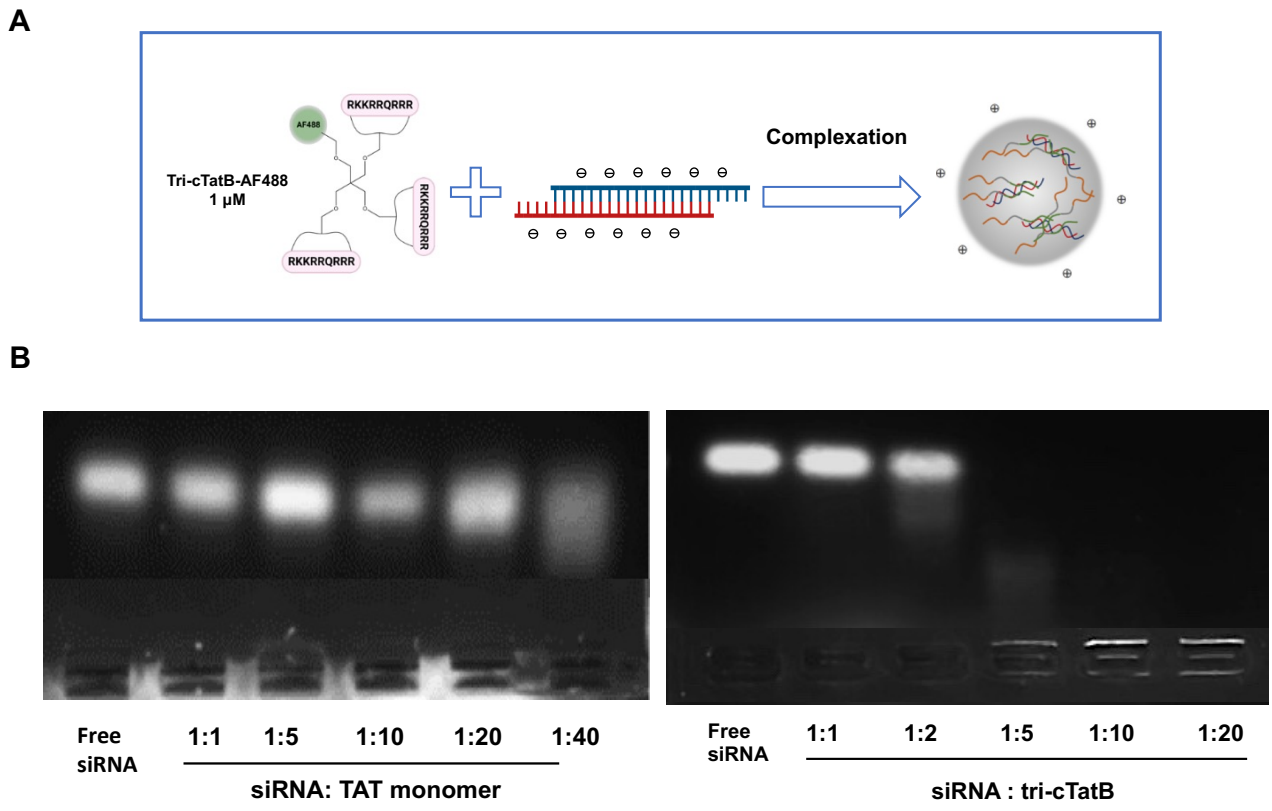

Figure 3.6. siRNA and tri-cTatB complex formation. (A) Schematic illustration of the complexation. Positively charged tri-cTatB incubated with natively charged siRNA in PBS buffer to form the complex via electrostatic interaction. **(B)** Complex formation was checked by gel retardation on agarose gel electrophoresis. siRNA was mixed with tri-cTatB at molar ratios of 1:1, 1:2, 1:5, 1:10 and 1:20. After incubation for 30 mins in PBS, samples were mixed with 6x loading dye and loaded onto 2% agarose gel stained with SYBR Gold.

To characterise the siRNA/tri-cTatB complexes, particle size, charge and morphology were measured. The hydrodynamic size distribution of siRNA/tri-cTatB complexes was measured by DLS (Figure 3.7A). The overall charge of free siRNA, tri-cTatB and siRNA/tri-cTatB complexes was measured by the zeta potential. The morphology of the complex at 1:10 N/P ratio was visualised by Cryo-EM (Figure 3.7D). The average diameter (Z-average) of the complex was 459 nm ± 42.2 (mean ± SD) with an average polydispersity index (PdI) of 0.26 (Figure 3.7A). Cryo-EM images revealed the spherical morphology of siRNA/tri-cTatB complexes with a diameter of approximately 450 nm (Figure 3.7C), confirming their self-assembly and that the measured size is consistent with the DLS result. In addition, the naked siRNA was negatively charged at -53 mV and tri-cTatB was positively charged at +21 mV. After complexation with tri-cTatB, this negative charge of siRNA is masked (Figure 3.7B). siRNA/tri-cTatB complexes were positively charged: the potential was +14.7 mV at a N/P ratio of 1:5 and +30 mV at a ratio of 1:10, indicating that the overall complex surface charge is positive and in the range where repulsive charge between neighbouring particles will prevent aggregation.

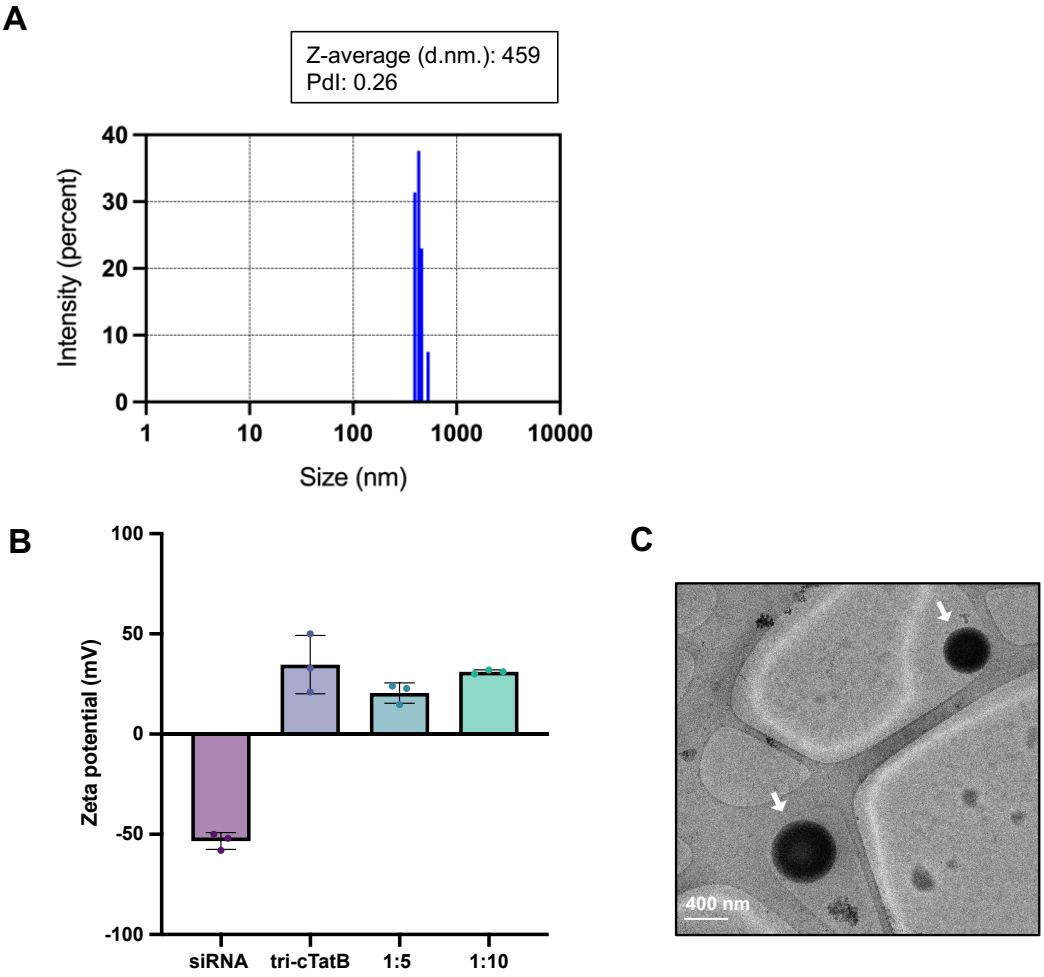

Figure 3.7. Characterisation of siRNA/tri-cTatB complex. (A) size distribution by intensity of freshly made siRNA/tri-cTatB complexes measured by dynamic light scattering (DLS). **(B)** Zeta potential of free siRNA, tri-cTatB peptide and siRNA/tri-cTatB complexes, all samples were tested in triplicate. Bars represented the average ± standard deviation. **(C)** Cryo-EM of siRNA/tri-cTatB complex at 1:10 N/P ratio. The siRNA/tri-cTatB complex presented as spherical shape (indicated by arrows).

To test the serum stability of siRNA/tri-cTatB complexes and whether tri-cTatB provides protection of siRNA without chemical modification, siRNA/tri-cTatB complexes or naked siRNA were incubated in 10% and 50% of FBS for up to 48 hours. Samples were analysed using gel electrophoresis to test complex integrity. As presented in Figure 3.8, the siRNA band begins to smear after 24 hours of incubation in 50% FBS, suggesting that the integrity of siRNA in siRNA/tri-cTatB complexes was preserved for up to 24 hours in 50% serum. In contrast,

free siRNA degraded after incubation for 2 hours. Following incubation in a low concentration of FBS (10%), free siRNA remained intact for up to 24 hours.

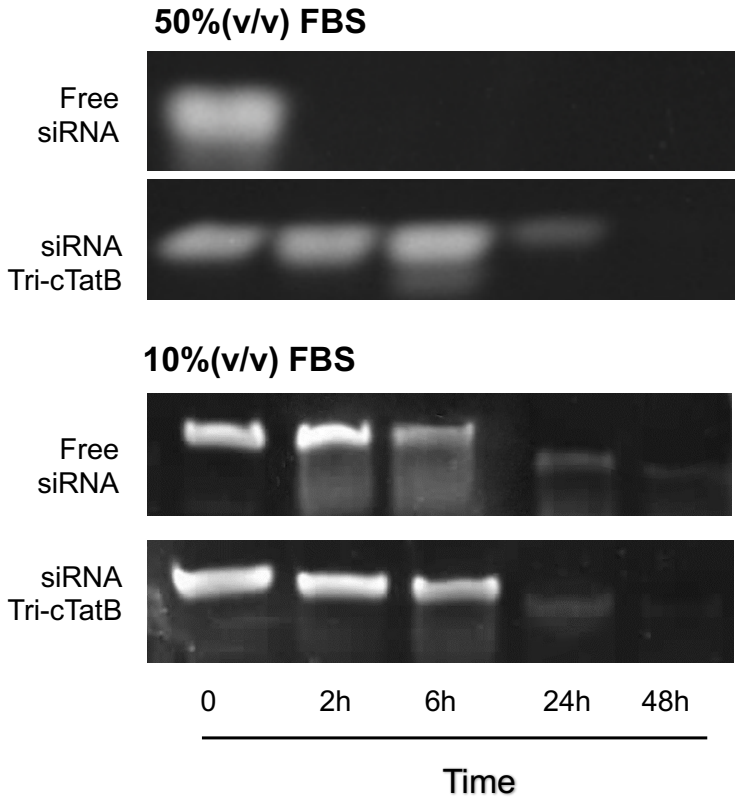

Figure 3.8. Serum stability test of siRNA/tri-cTatB complex. 20% PAGE is used to determine the stability of siRNA in the complex (1:10 N/P) and free siRNA following incubation in 50% and 10% FBS serum from 0 to 48 hours.

3.3.4 siRNA/tri-cTatB self-assembled complexes: cellular uptake

The intracellular delivery efficiency of the siRNA/tri-cTatB was investigated by live cell confocal imaging (Figure 3.9A). In this experiment, the cellular uptake of siRNA/tri-cTatB complexes with a N/P ratio of 1:5 or 1:10 was tested. Lipofectamine-mediated delivery was included for comparison. Here tri-cTatB was not labelled and siRNA was labelled with FAM. The internalisation efficiency is reflected by the amount of intracellular FAM-siRNA. siRNA/tri-cTatB at 1:10 N/P molar ratio showed more marked cellular uptake compared to lipofectamine, siRNA/tri-cTatB at 1:5 N/P ratio, and siRNA alone at 1 hour delivery. As a negative control, free siRNA was not internalised as shown by the absence of green

fluorescence. To quantify the internalisation of siRNA, regions of interest (ROIs) corresponding to the cytoplasm were delineated manually by Fiji. Mean fluorescence intensities for each ROI were calculated and plotted (Figure 3.9A). siRNA/tri-cTatB complexes with an N/P ratio of 1:10 showed greater internalisation compared to complexes with N/P ratio of 1:5 (p=0.0001) or lipofectamine transfected siRNA (p<0.0001).

To further quantify the percentage of cellular uptake of siRNA mediated by tri-cTatB and cyclic TAT monomer, flow cytometry was run after 1 hour of delivery. As indicated by Figure 3.9 C, in 1 hour delivery, 1 μM Tat monomer mediated 4% (of total 10,000 cell events) cell uptake of siRNA and 60% of cells were transduced with 1 μM tri-cTatB complexed with siRNA at 1:10 N/P ratio.

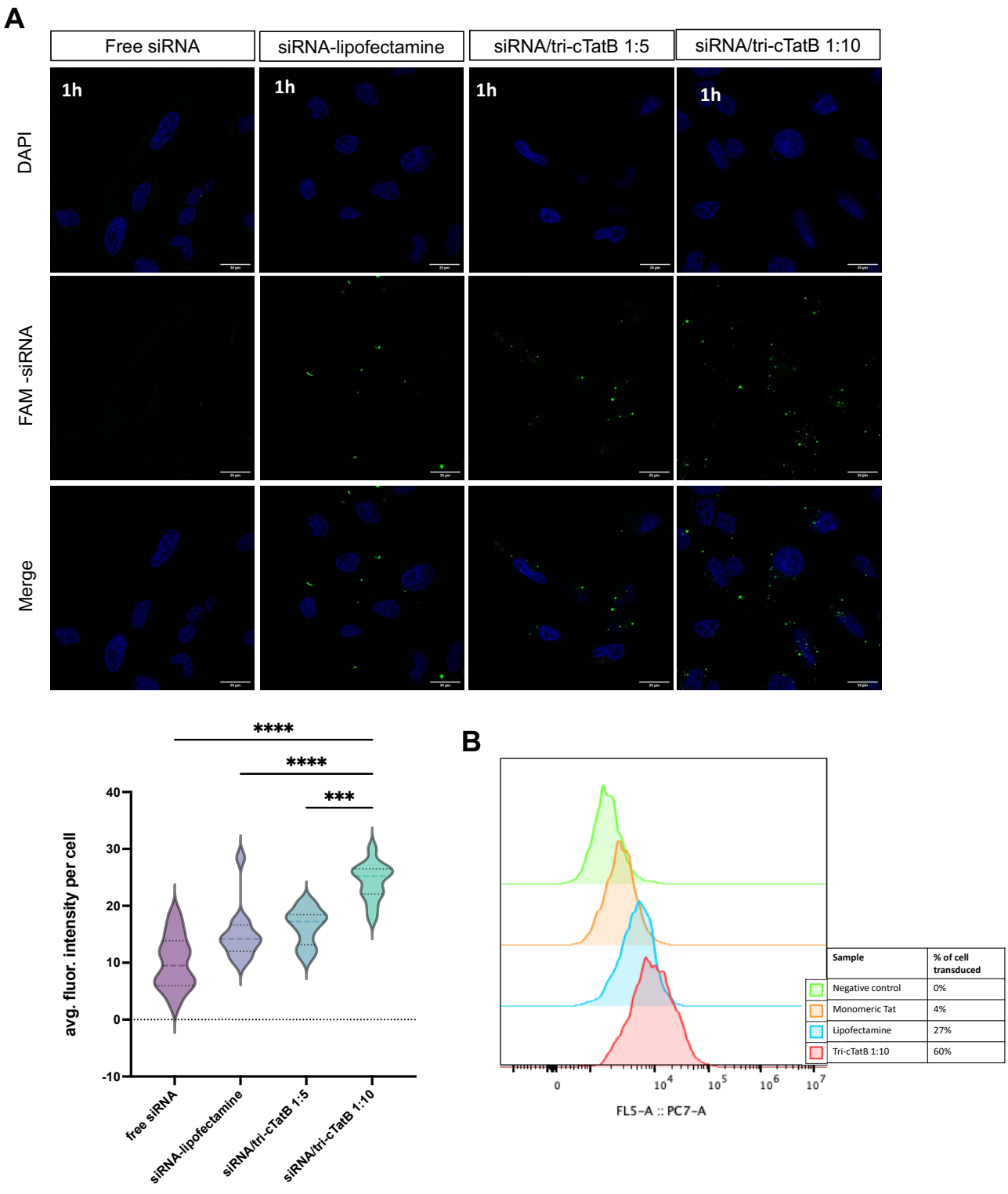

Figure 3.9. The uptake of the siRNA/tri-cTatB complex in HeLa cells. (A) The cellular uptake efficiency of siRNA/tri-cTatB was evaluated by live cell imaging. Here tri-cTatB was not labelled and siRNA was labelled with FAM. Nuclei were stained with Hoechst (blue), Scale bars: 20 µm. The intracellular fluorescence intensity per cell of FAM-siRNA was quantified in the below image (n=20, error bars represent the standard deviation, ****P<0.0001). **(B)** Flow cytometry analysis to quantify the siRNA internalisation mediated by the tri-cTatB complex at 1:5 and 1:10 ratio, Tat monomer and lipofectamine in 1 hour of delivery.

It was observed that intracellular localisation of siRNA/tri-cTatB complexes was remarkably different from non-complexed tri-cTatB. As the live cell imaging shows in Figure 3.10, non-complexed FAM-tri-cTatB (green) signals were homogenously distributed in the cytoplasm and was present in the nucleoli which is in accordance with the free Tat peptide. In comparison, when formulated as siRNA/tri-cTatB complexes, the distribution of Cy5-siRNA (red) and FAM-tri-cTatB (green) was noted to be mainly cytosolic, appearing as bright fluorescent foci, indicating that complexes were likely located in endo/lysosomes. The red and green fluorescence are also highly co-localised, which suggests that the siRNA and tri-cTatB are still in physical association in the cytoplasm after 1 hour of incubation. This observation led to the next step set of the experiments to identify the nature of the vesicle-like foci and the mechanism of the complex internalisation.

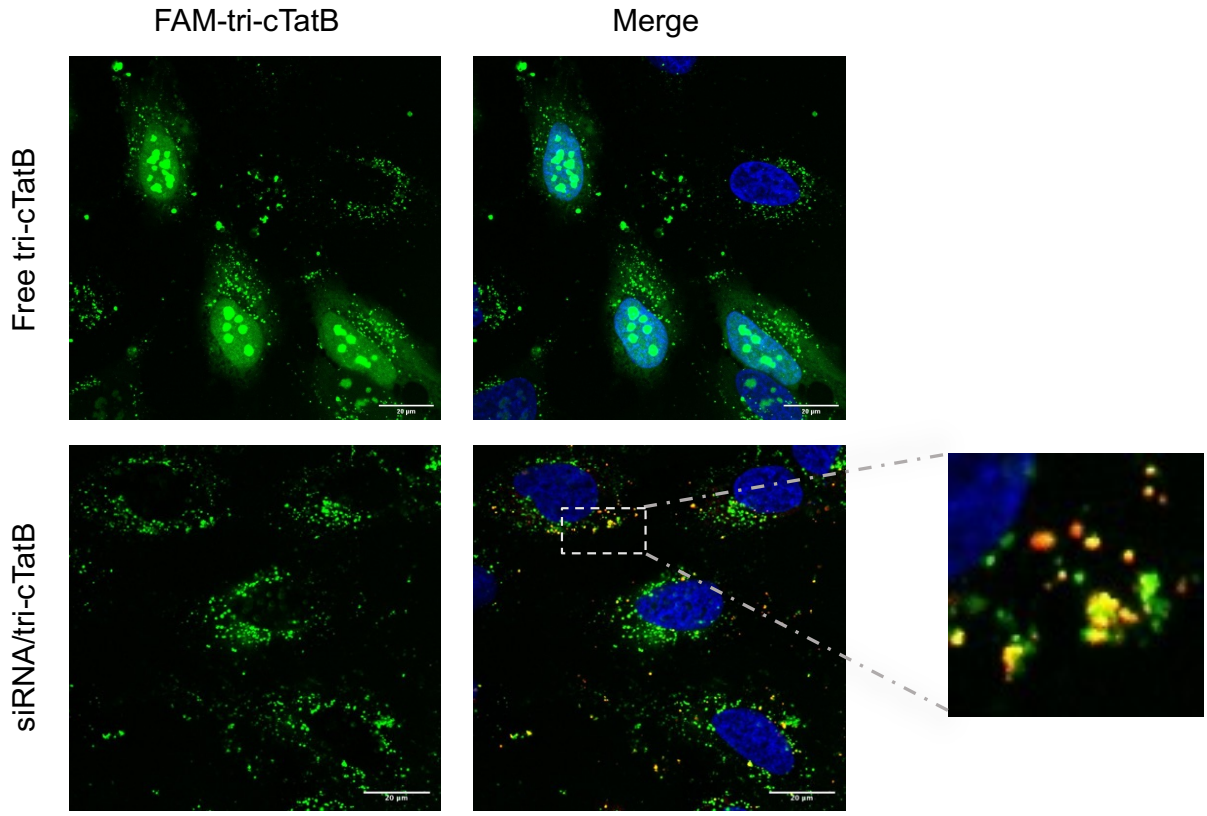

Figure 3.10. Subcellular localisation of free FAM-tri-cTatB compared to tri-cTatB/siRNA complexes. FAM-labelled tri-cTatB (1 μM) and tri-cTatB/siRNA complexes (siRNA labelled with Cy5, 100 nM) were treated to cells. Nuclei were stained with Hoechst (blue). Scale bars: 20 μm.

3.4 Discussion and conclusion

Intracellular delivery of macromolecules is a critical procedure for biological research and therapeutic applications. Macromolecules, normally larger than 1 kDa, including proteins and nucleic acid drugs hold great promise in cancer therapy. However, they cannot spontaneously cross the cell membrane due to their weight and charge. Since the discovery of the HIV transcription factor Tat in the late 1980s, the use of CPPs as non-viral vectors has been seen as a viable way to deliver macromolecules into cells without affecting their integrity and function. This chapter introduced a peptide recently developed by our lab, which is an arranged cyclic Tat peptide into multimeric clusters on a defined chemical scaffold. This peptide has shown significantly improved delivery efficiency compared to previously reported CPPs in antibody delivery. Its potential in delivering nucleic acids has not been studied. This chapter explored the synthesis of this novel peptide, tri-cTatB and its potential in delivering siRNA into HeLa cells via different strategies.

3.4.1 tri-cTatB mediated siRNA delivery by co-incubation

The first and simplest strategy of using tri-cTatB to deliver siRNA was co-incubation, which was the same protocol as tri-cTatB co-delivery of antibodies[90]. This strategy is based on the hypothesis that a CPP might induce a cell to "drink-up" macromolecules present in its surrounding media[106]. The sample preparation of co-incubation is relatively easy, siRNA was added to cells following the addition of 1 μM tri-cTatB. The results showed that 1 μM tri-cTatB mediated more siRNA internalisation than commercial transfection agent lipofectamine in HeLa cells in 1 hour delivery time. Cy5-siRNA is mostly located around the membrane while AF488 labelled tri-cTatB was located in the cytosol and also accumulates in the nucleus, which is consistent with Tietz's observation. It was found that Tat and other arginine CPPs induce the accumulation of their conjugated cargoes at the nucleoli of cells[106]. Therefore, it was not surprising that siRNA in this co-incubation was not localised with the peptide in the nucleus

which is an undesirable place for siRNA. This indicates that the siRNA had no association with the peptide during the intracellular delivery. Although this co-incubation delivery has shown success in antibodies, it is might not ideal for siRNA delivery because siRNA was not properly protected in this process and very likely to be degraded in cells. The bioactivity of delivered siRNA needs to be further accessed and other strategies that can provide protection to fragile nucleic acids are required to be developed.

3.4.2 tri-cTatB form complexes with siRNA via electrostatic interaction

Another non-covalent CPP delivery of nucleic acids is via the complexation of polycationic CPP and negatively charged nucleic acids by electrostatic interaction. This strategy avoids the need for chemical modifications of oligonucleotides and allows large amounts of nucleic acids to be efficiently incorporated into nano-sized complexes[103]. It was observed that tri-cTatB can influence the siRNA movement on gel electrophoresis which confirmed the interaction between peptides and siRNAs (Figure 3.6B). The siRNA band was completely retarded at the siRNA/tri-cTatB molar ratio of 1:10 due to the high positive charges of tri-cTatB. In contrast, monomeric Tat peptide, with weaker positive charges, could not build a condensed complex based on almost no retardation of siRNA bands. This result aligns with the hypothesis that a highly dense, positively charged region of peptide is crucial for the formation of nanocomplexes with nucleic acids[108].

Characterisation of the complexes could help in understanding intracellular uptake. According to the DLS and Zeta potential of the complex (Figure 3.7), the positive charges of tri-cTatB have been masked by charge interaction and the complex at 1:10 N/P ratio exhibits overall positive surface charge which is essential for efficient complex internalisation ability. The positive charges of the complex meant that the CPPs were exposed to the surface of the complex which might explain the enhanced stability of siRNA/tri-cTatB complex compared to siRNA only (Figure 3.8). The hydrodynamic size of siRNA/tri-cTatB at a 1:10 ratio was

measured by DLS, result showed the size at around 469 nm in diameter. Cryo-EM investigation revealed the siRNA/tri-cTatB complexed in a spheroid manner with an approximate diameter of 400 nm, which is in agreement with DLS results.

One advantage of CPPs and siRNA complexation delivery strategy is that siRNA can be protected without chemical modifications, and this is confirmed by our stability test. The stability of siRNA in the complex could be affected by charge neutralization and cohesive strength caused by electrostatic attraction between the peptide and the siRNA[59].

3.4.3 siRNA/tri-cTatB complex cellular uptake

Clear evidence has been presented that supports the cellular internalisation and co-localisation of the nanocomplex. Live cell images showed higher HeLa cell uptake of siRNA/tri-cTatB at 1:10 complexes than 1/5 complexes in 1 hour delivery time. This can be due to the more condensed structure and higher positive charges of the 1:10 complexes. The complexes also demonstrated a quicker delivery route than the well-known transfection agent lipofectamine. Since lipofectamine is known to be limited in *in vivo* experiments due to low efficiency and cytotoxicity, this tri-cTatB demonstrated the potential to be developed as a promising nucleic acids transfection reagent. Flow cytometry was used to quantify the internalisation, at the same concentration (1 μM) and delivery incubation time (1 hour), the tri-cTatB has shown much higher transfection of siRNA compared to the cTat monomer. This significantly improved delivery efficiency proved the hypothesis that the cyclisation of Tat, along with its subsequent trimeric formation, enhances the efficacy of internalisation. Given that most Tat-derived CPPs require higher working concentrations exceeding 10 μM, which are normally toxic to cells, their clinical applicability is compromised[109]. Therefore, our results provide evidence for the use of tri-cTatB as a potential clinically applicable delivery strategy.

Co-localisation of the complex was identified via a yellow fluorescence pixel merged between the red fluorescence of the siRNAs and the green fluorescence of the tri-cTatB (Figure 3.10).

Presumably, due to charge masking, tri-cTatB was not able to translocate into the nucleus as it usually does after forming a complex with siRNA. The co-localised siRNA and tri-cTatB were distributed peripherally around the nucleus in particle-like forms within the cytoplasm, indicating that siRNA and tri-TatB are not disassociated after entering the cell so tri-cTatB could not be translocated into the nucleus. These particle-like foci might represent endosomes or lysosomes that contain complexes according to previous reports[110,111]. Therefore, it is crucial to investigate if the complexes were trapped in endosomes and if the siRNA transfected using complexation with tri-cTatB has maintained its biological activities.

Chapter 4

The cellular uptake mechanism of siRNA/tri-cTatB complexes and biological effects of internalised siRNA

4.1 Introduction

In the previous chapter, the use of tri-TatB to deliver siRNA via co-incubation and complex formation was explored. Although both of these strategies resulted in successful HeLa cell uptake of siRNA, it is important to demonstrate that internalised siRNA retains its biological function.

As discussed before, it was hypothesised that the strategy of siRNA/tri-cTatB complex delivery could provide greater protection to nucleic acids compared to the co-incubation delivery method. Therefore, the research presented in this chapter focuses on self-assembled complex delivery. In the last chapter, it was reported that internalised siRNA and tri-cTatB tended to co-localise, presenting as puncta-like foci, likely due to their uptake into endosomes or lysosomes. Since endosomal compartment entrapment is one of the main reasons for the poor efficiency of nucleic acid delivery, it is crucial to understand the delivery mechanism of siRNA/tri-cTatB complexes.

4.1.1 Mechanism of CPP-mediated intracellular uptake

The exact nature of the mechanism through which CPPs internalise remains elusive. The complexity of interactions that occur at the cell surface in addition to the physicochemical diversity of different CPPs has resulted in a variety of internalisation mechanisms being reported[112]. The preferred internalisation mechanism of different types of CPP is dependent on myriad factors, such as temperature, extracellular concentration and associated cargo[113,114]. The mechanisms exploited by different CPPs can be broadly divided into two categories, energy-independent direct translocation pathways and the energy-dependent endocytic pathways (Figure 4.1). The internalisation mechanism of nucleic acids delivered by CPPs also follows the two main categories[115]. The precise pathway utilised by CPPs is dependent on various parameters and elucidation through a series of experiments is needed.

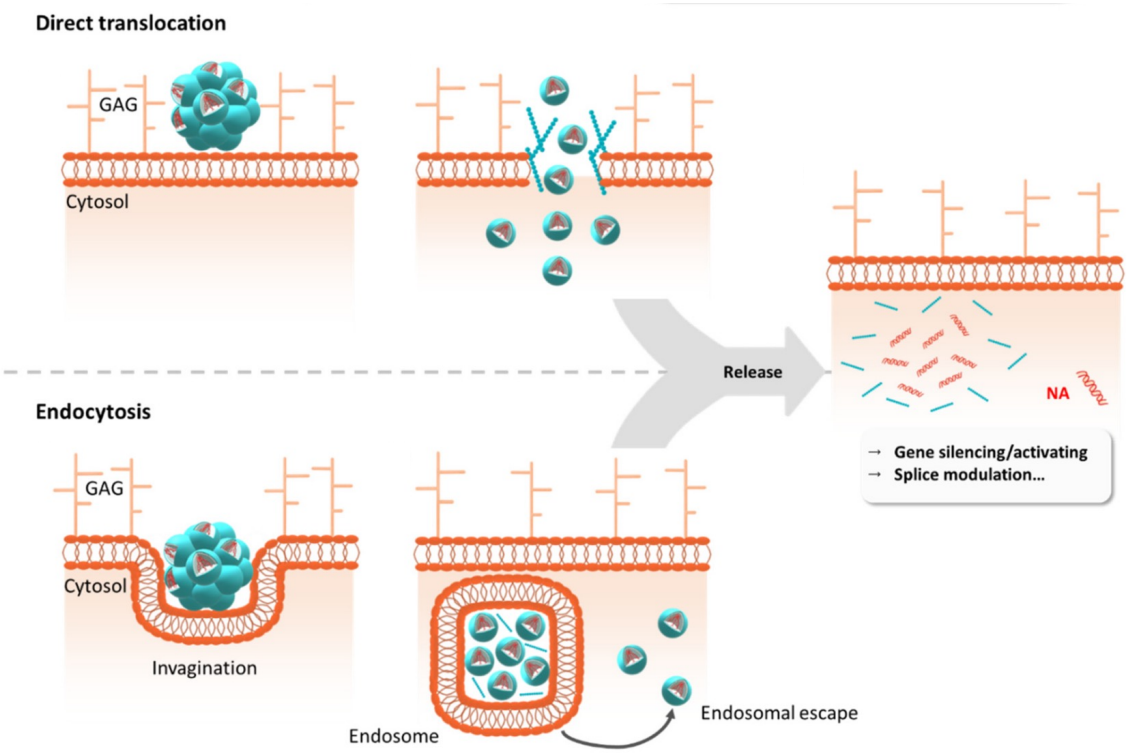

Figure 4.1. Two main categories of CPP-mediated delivery of nucleic acid cargoes: Direct translocation via the cell membrane or endocytosis-dependent pathway. Then nucleic acid cargoes can be directly released or escape from endosomes to the cell cytoplasm to perform their activity. GAGs (glycosaminoglycans). Figure adapted from Boisguérin *et al*. 2021[115].

4.1.2 Direct translocation mechanism

The initial evidence of peptide penetration via direct translocation was found from experiments showing internalisation to occur at low temperatures (approximately 4ºC), suggesting the mechanism happens without an active process facilitated by the cell[116]. In general, direct translocation requires the interaction of positively charged CPPs with negatively charged components of the cell membrane such as GAGs and the phospholipid bilayer (see Figure 4.1), which then leads to CPP penetration[116]. Moreover, direct translocation requires permanent or temporary destabilisation of the cell membrane for internalisation to happen. It has often been reported that the mechanism of direct translocation of CPPs is favoured when they are at high extracellular concentrations and is most likely to occur with amphipathic CPPs such as transportan analogues and MPG[93].

As an energy-independent process, direct translocation is regarded as a single-step process, including mechanisms involving the formation of inverted micelles, carpet and pore models. The translocation mechanism to be discovered first was inverted micelle formation, which was reported to be exploited by the CPP, penetratin[117]. The process starts with the formation of electrostatic interaction between the CPP and the lipid bilayer that causes modification of the curvature of the membrane, with the subsequent formation of an inverted micelle containing the CPP-cargo.

The pore formation models are in general associated with primary amphipathic peptides, including Pep-family and MPG peptides[118]. Pore formation involves two mechanisms, the formation of CPP bundles that form a structure in the lipid bilayer with a hydrophilic core or the interaction between positively charged side chains of amphipathic CPPs and phosphate head groups of the cell membrane, exposing a hydrophilic pocket. In addition, the carpet destabilisation model involves positively charged amino acids of the CPP interacting with acidic phospholipid head groups of the cell membrane, causing multiple CPPs to accumulate in an orientation parallel to the cell surface, forming a 'carpet'[119].

Regarding the delivery of nucleic acids, there is sparse evidence to show that direct translocation of CPP and cargoes occurs. Boisguerin and colleagues found that WRAP-siRNA nanoparticle internalisation uses a balance between direct translocation and endocytosis, favouring direct translocation through the plasma membrane[120].

4.1.3 Endocytosis pathways

It is generally accepted that CPPs, especially when associated with cargo molecules, are predominantly internalised via energy-dependent mechanisms involving different types of endocytosis prior to endosome escape (Figure 4.2 for illustration of uptake pathways and trafficking events associated with CPPs). In this context, all major endocytic pathways, including macropinocytosis, caveolae-mediated endocytosis (CvME) and clathrin-mediated

endocytosis (CME), have been found to be involved in the uptake of CPPs[94,121]. Distinct from direct translocation, endocytosis driven mechanisms predominate in cases of low extracellular CPP concentration (< 10 μM) and when delivering macromolecular cargoes[122].

Macropinocytosis is a rapid, lipid raft-dependent and receptor-independent mechanism of endocytosis[123]. It is a process that involves the rearrangement of the actin cytoskeleton to form protrusions from the cell membrane, creating an endocytic vesicle within the cell cytoplasm called a macropinosome and the internalised vesicles or macropinosomes can have sizes up to 5 μm. The role of macropinocytosis in the uptake of cationic CPPs was established by finding that the uptake of CPPs was reduced under conditions where macropinocytosis was inhibited, such as low cell culture temperature (4℃), or in the presence of macropinocytosis specific inhibitors, including amiloride and actin polymerisation cytochalasin inhibitor[123,124].

Caveolae-mediated endocytosis (CvME) is a receptor and dynamin dependent mechanism. Caveolae are characterised by bulb-shaped invaginations comprised of oligomerised proteins of the caveolin family in association with cavin proteins. Electron microscopy data suggest that caveolae are tightly connected to the actin filaments and the The interior of caveolae, around 50 nm in diameter, can only accommodate relatively small cargo[124]. Several reports have suggested that CvME is a preferred mechanism for CPP internalisation. One study demonstrated that the knockdown of caveolin-1 led to a reduction in the internalisation of the amphipathic CPP Transportan when bound to biotin in a complex with avidin[124]. This study suggested that the CvME endocytosis mechanism involves CPPs that are conjugated to relatively large molecular cargoes.

Clathrin-mediated endocytosis (CME) is the best-characterised endocytosis mechanism so far. Like CvME, it is a receptor-dependent, clathrin-mediated process, that occurs in all mammalian cells. CME is characterised by the formation of a polyhedral lattice comprised of clathrin proteins assembled into a triskelion formation that promotes invagination of the cell membrane

and then forms an endocytic vesicle via dynamin mediated vesicle fission[124]. This process can be divided into five stages: (i) initiation of endocytic events, (ii) cargo loading, (iii) membrane bending, (iv) vesicle scission and (v) disassembly of the coat. Each of the stages mentioned is highly orchestrated by a series of molecular interactions. CME has so far been reported as a pathway used by CPPs, including TAT peptide, oligo-arginines and anionic CPPs. It was first reported by Richard *et al.* (2005) that the uptake of TAT peptides in HeLa cells was via CME, which could be inhibited when using chlorpromazine and K^+ depletion[125]. Around the same time, it was reported that MPGα/siRNA complexes were also taken up by CME, although MPG had earlier been shown to enter cells in an energy-independent manner[126].

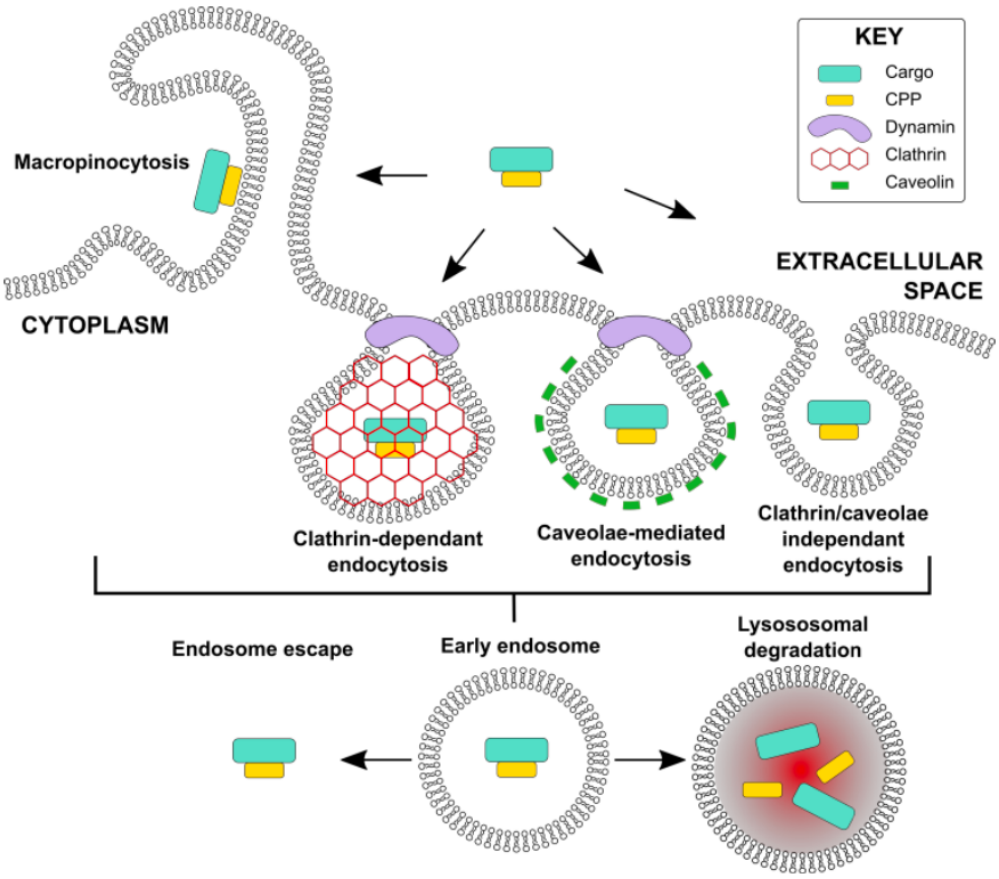

Figure 4.2. Endocytic mechanisms of CPP internalisation. Reports from several studies have shown that CPPs can exploit a range of endocytic pathways to achieve cell entry. Unlike direct translocation, these mechanisms are energy dependent and are favoured at lower extracellular concentrations of CPP (<10 μM). Once a CPP-NA complex has been endocytosed,

it must undergo endocytic escape to avoid lysosomal degradation and gain access to the cell cytoplasm. Figure adapted from Trabulo *et al*. 2010[127].

4.1.4 Trafficking and endosomal release

Once CPPs and nucleic acid cargoes have been internalised into the cell by endocytosis, they are largely trafficked to endo-lysosomal compartments, which is a process called endosomal entrapment. The cargo must be released from the endosome in order to reach the cytoplasm where it can perform its biological action[80]. In normal circumstances, vesicles formed by endocytosis are first trafficked to an early endosome, which has a slightly acidic environment (pH ~6.5). Then the early endosome undergoes maturation to a late endosome, becoming more acidic (pH ~5.5), and finally is processed to a lysosome (pH ~4.7)[80]. The contents in lysosomes are very likely to be degraded by hydrolytic enzymes. Therefore, endosomal escape or release of nucleic acid cargos before degradation in lysosomes is a critical step for effective CPP and its cargo delivery. Extensive studies have focused on understanding the endosomal escape mechanism and how to increase the delivery efficiency of CPP and cargo to the cytoplasm.

Several mechanisms of endosomal escape have been postulated and different types of CPP likely utilise different mechanisms under certain physiological conditions. One possible mechanism is based on the ability of the CPP to disrupt the membrane. Positively charged CPPs are thought to interact with negatively charged phospholipids of the endosomal membrane, resulting in the formation of a membrane pore and leakage[128]. The Tat peptide has been reported to induce leakage of endosomes through this mechanism. Another possible mechanism is called the 'proton-sponge' hypothesis which, it has been suggested, facilitates the endosomal escape of large, polycationic CPPs[129]. This mechanism relies on the ability of polycationic CPPs to buffer endosomes to a pH of 5-7, forcing the endosome to increase the influx of H^+ ions to counteract the CPP buffering capacity. The increased charge of endosomes containing CPPs leads to the influx of Cl^- ions causing an increase in osmotic pressure and lysis of the endosome, releasing the contents into the cytosol.

4.1.5 Challenge of nucleic acids delivery: endosome entrapment

As introduced in Chapter 1.5, endosomal entrapment is a critical bottleneck for CPP-mediated delivery and one of the main challenges for the delivery of nucleic acid therapeutics. Chapter 1.5 introduced some strategies that can trigger endosome escape of nucleic acids, including endolytic small molecules endolytic peptides and photo-induced endosomal escape. In this study, the use of some of the strategies to enhance the endosomal release of the siRNA/tri-cTatB complexes was investigated.

4.1.5.1 Small molecule

Endolytic small molecule agents, typified by chloroquine, an antimalarial agent, embody some of the earliest direct attempts to enhance endosomal escape of RNA therapeutics[130]. Chloroquine and related compounds are membrane permeable and freely diffuse into cells; however, once they diffuse into the low pH environment of endosomes they become protonated (positively charged) and trapped inside (Figure 1.7A). Due to this sink effect, the endosomal concentration increases logarithmically resulting in endosomal rupture due to the insertion of chloroquine's bicyclic aromatic rings into the endosomal lipid bilayer[78]. Various of studies have demonstrated the ability of chloroquine to enhance siRNA and ASO. A recent study by Rietz *et al*. (2020) has shown that membrane damage caused by small molecules results in the efficient release of cholesterol-conjugated siRNA, which results in an increase in knockdown efficiency by 47-fold[131].

4.1.5.2 Endolytic Peptides

The ability of endolytic peptides, such as melittin and endoporter, to enhance the endosome escape of RNA therapeutics has been extensively studied[78]. Due to its cationic charge, melittin (GIGAVLKVLTTGLPALISWIKRKRQQ) aggregates anionic RNA therapeutics and plays an effective role in forming pores via electrostatic interaction of melittin with negatively charged

lipid headgroups of endosome membrane. However, because of its potent membrane disruption ability, melittin is thought to be too antigenic, toxic, and uncontrollable for clinical use[132].

Endosomal escape domain (EED) is a recently developed short endolytic peptide. They constitute a group of short peptides, with various hydrophobic features, which have previously been described to play important roles in the endosomal escape of viruses and are also known to modulate PTD/CPP uptake[133,134]. A recent study by Lonn *et al*. (2016) found that the addition of EEDs with specific hydrophobic patches, containing either two aromatic indole rings or one indole ring and two aromatic phenyl groups, at a fixed distance of six polyethylene glycol (PEG) units from TAT, significantly enhanced cytoplasmic delivery without causing cytotoxicity (Figure 4.3)[133]. The amino acid residues Trp (W) and Phe (F) are both known to destabilise cellular membranes by burying their hydrophobic R groups into the lipid bilayer[135]. Therefore, the EED consisting of an aromatic ring containing amino acids, Phe (F) and Trp (W), including an optimal six PEG unit (PEG_6) spacer was selected for this study.

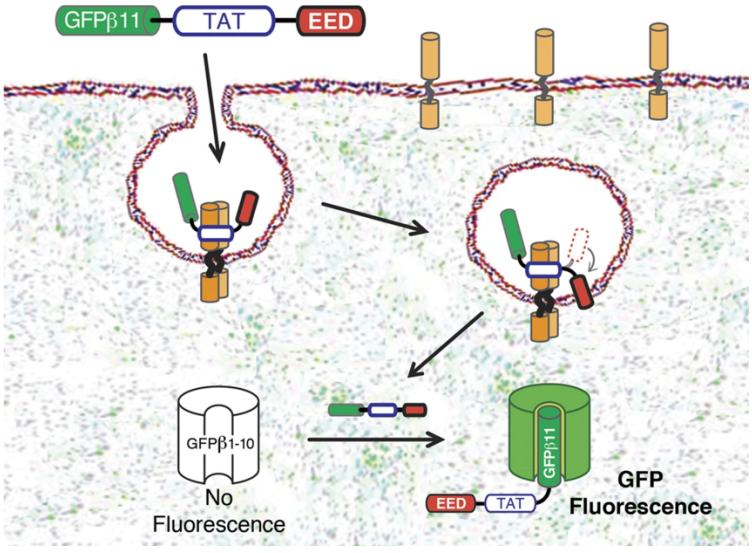

Figure 4.3. Conjugation of EED to TAT-cargo via covalent bonds. In the study by Lonn *et al*., it was shown that when TAT was concentrated in the endosomes, the hydrophobic EED motif buried itself into the lipid bilayer of the endosomal membrane, leading to localised membrane destabilisation and the enhancement of endosomal escape into the cytoplasm. Figure adapted from Lonn *et al*. 2016[133]. Copyright by Springer Nature.

4.1.5.3 Photo-induced endosomal escape: photosensitizer

Photochemical internalisation (PCI) is an intervention that involves the release of endocytosed macromolecules into the cytoplasmic matrix. PCI is based on the use of photosensitizers (PS) localised in endocytic vesicles which, following light activation, leads to the rupture of the endosomal vesicles and the release of the macromolecules into the cytoplasm[136]. Many investigators have speculated that PCI works for CPP-mediated internalisation because cationic CPPs tend to accumulate near the anionic endosome membrane, the site where PSs are most active. As shown in Figure 4.4A, CPP-PS conjugates and cargo are taken up by cells via endocytosis and trapped in the endo-lysosomes, gathering at the membrane due to the cationic nature of the CPP. After light irradiation, the photoexcited PS generates reactive oxygen species (ROS), specifically, singlet oxygen ($^1O_2$), which can cause oxidation of the endosomal membrane. Oxidation leads to membrane destabilisation, causing endosome leakage to release trapped contents. Therefore, photo-induced endosomal release of CPP-cargoes provides an efficient and controllable strategy to improve delivery efficiency[137].

Many photosensitizers have been developed for PCI and photodynamic therapy (PDT). The earliest photosensitizers to be developed, such as chlorin p6 derivatives and tetra(4-sulfonatophenyl)porphine (TPPS4), are able to localise to the endo-lysosomal compartment[138]. However, some reports suggested that amphiphilic photosensitizers achieve greater PCI effect because they enter cells through endocytosis and localise to the lipid–aqueous interface of the membrane[139]. Widely used PSs includes disulfonated aluminum phthalocyanine (AlPcS2a), meso-tetraphenyl porphyrindisulphonate ($TPPS_{2a}$), and disulfonatedtetraphenyl chlorin ($TPCS_{2a}$). Among them, TPCS2a, also called fimaporfin, has shown improved permeability and was suitable for *in vitro* and *in vivo* applications.

Fimaporfin ($TPCS_{2a}$), approved by FDA, was developed by di-imide reduction of disulfonated tetraphenyl porphine ($TPPS_{2a}$). Fimaporfin is solubilised in Tween80, mannitol and Tris-buffer at pH 8.5, with an excitation wavelength of ~652nm[140]. As demonstrated in Figure 4.4B,

fimaporfin accumulates in endosomes and lysosomes where it produces ROS upon light excitation. ROS then damage membranes by reacting with membrane components and causing membrane permeabilisation. Many studies have suggested that fimaporfin constitutes a flexible and efficient system for nucleic acid delivery. Jørgensen *et al*. (2013) have developed a peptide-based carrier for siRNA delivery, 90% mitogen-activated protein kinase kinase-1 (MEK1) silencing was achieved with the application of fimaporfin and light[141]. The endosome/lysosome targeting property of fimaporfin has been tested clinically in combination with bleomycin and vaccine peptide/protein-based antigens[142]. Thus, we hypothesised that the combination of fimaporfin-based PCI with siRNA/tri-cTatB self-assembled complexes could build an efficient and light-controlled delivery platform for siRNA.

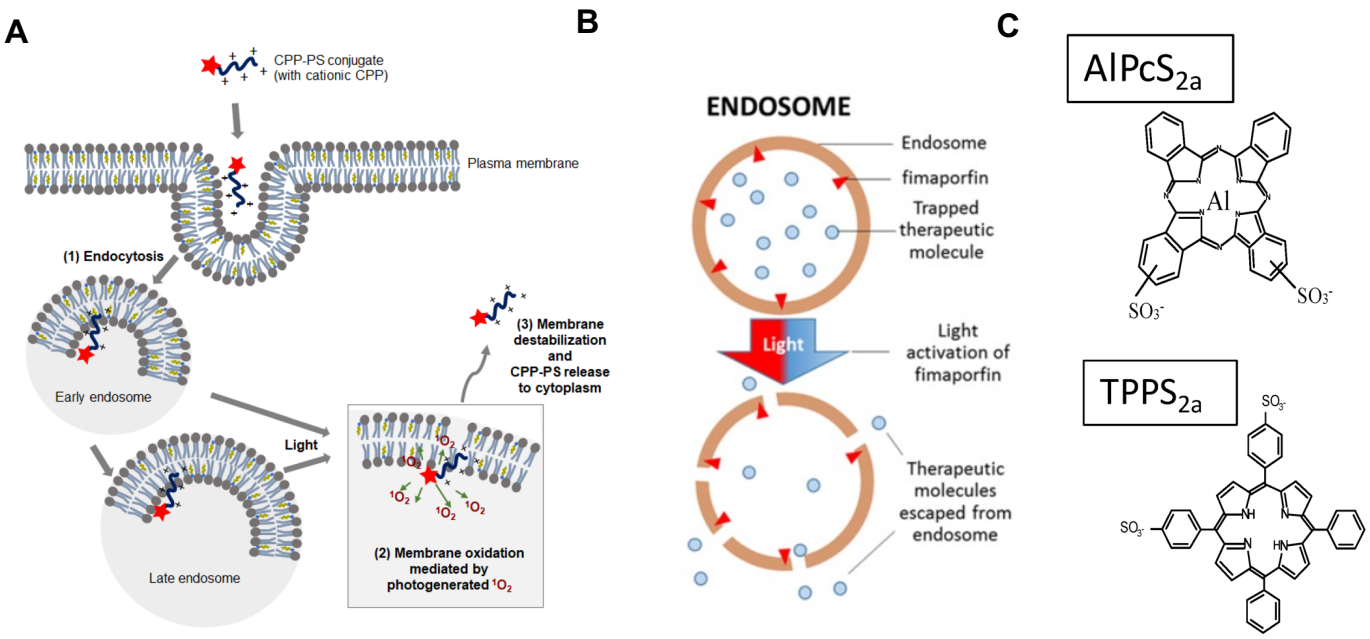

Figure 4.4. Illustration of photo-induced endosomal escape. (A) Mechanism of CPP-photosensitizer mediated PCI. Image adapted from Soe *et al* (2020)[143]**. (B)** Illustration of how fimaporfin works as a small molecular photosensitizer for PCI. Fimaporfin can be assimilated into endocytic vesicle membranes, upon 405 or 652 nm light irradiation, PS-generated oxidation disrupts the endosome, and endocytosed contents are released. **(C)** Chemical structures main photosensitizers used in PCI.

4.2 Aims

The aims of the research presented in this Chapter were to:

1) Investigate the intracellular localisation of nucleic acid cargoes delivered by siRNA/tri-cTatB complexes through subcellular trafficking studies.
2) Study the mechanism of tri-cTatB/siRNA internalisation, to identify the endocytosis pathway used.
3) Investigate the bioactivity of delivered siRNA by using siRNA targeting GAPDH, and to evaluate siRNA downregulation by means of the GAPDH activity assay.
4) Develop strategies to trigger the endosome escape of endocytosed siRNA: endolytic peptides or photo-activation.

4.3 Results

4.3.1 Gene silencing effect of the siRNA internalised by tri-cTatB

In Chapter 3 it was shown that tri-cTatB can mediate siRNA internalisation via both co-incubation and self-assembling complexes. Next, it was crucial to evaluate the intracellular bioactivity of the internalised siRNA. The colorimetric enzymatic GAPDH activity assay was used as a quick method to evaluate GAPDH downregulation under various conditions. The GAPDH protein level is indicated by measuring NADH production at 450 nm using a fluorescence spectrophotometer (Figure 4.5A). HeLa and HEK293T cells were treated with 1 μM tri-cTatB co-delivered siGAPDH or siGAPDH/tri-cTatB complexes for 1 hour respectively, and lipofectamine transfected siGAPDH was included as a positive control. Considering GAPDH is a housekeeper gene that is hard to knock down, we collected cells after 48 and 72 hours of treatment. As shown in Figure 4.5B, no significant knockdown of GAPDH was observed in HeLa cells for the 2 methods of tri-cTatB and siGAPDH transfection compared to the negative control, while the lipofectamine mediated transfection was successful, with a reduction in GAPDH activity of 62 and 65% after 48 and 72 hours, respectively. Similar results

were observed in HEK293T cells: at 48 hours post-treatment siGAPDH/tri-cTatB and lipofectamine plus siGAPDH showed 26% and 74% reduction in GAPDH activity compared to the negative control. No significant downregulation was observed at 48 or 72 hours when tri-cTatB and siGAPDH were co-delivered.

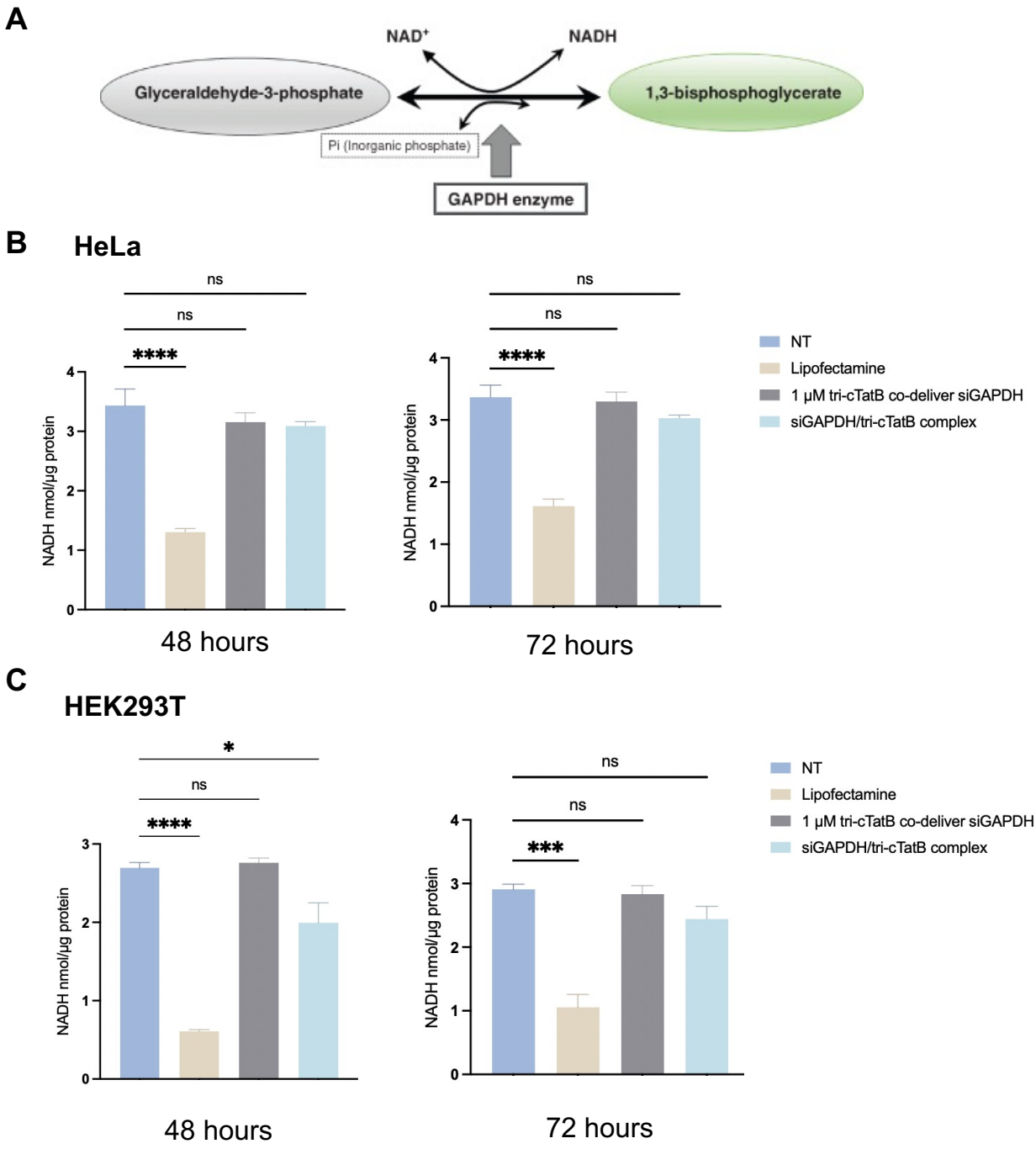

Figure 4.5. Gene silencing effect of the internalised siRNA evaluated by using the GAPDH activity assay. (A) The activity assay is based on GAPDH-mediated glycolysis. GAPDH catalyses the conversion of glyceraldehyde-3-phosphate into bisphosphoglycerate and an

intermediate, which reacts with a developer to form a red product that absorbs maximally at 450 nm. **(B, C)** GAPDH enzymatic activity. HeLa and HEK293T cells were treated with tri-cTatB (1 μM) co-delivered siGAPDH (100 nM) and siGAPDH/tri-cTatB complexes (tri-cTatB 1 μM, siGAPDH 100 nM). Lipofectamine delivery of siGAPDH was included as a positive control (NT: no treatment, n = 3, error bars represent the standard deviation, **P*<0.05, *****P*<0.0001).

4.3.2 tri-cTatB/siRNA internalisation mechanism study: subcellular trafficking and endocytosis pathway

As discussed in Chapter 3.4.3, a plausible explanation for the intense fluorescent foci seen in confocal microscopy images is that they represent endosomes or lysosomes containing fluorophore-labelled siRNA/tri-cTatB complexes. This suggested that the inefficient GAPDH knockdown observed after the delivery of siRNA/tri-cTatB complexes was due to endosome entrapment. Therefore, the next step was to study the subcellular trafficking of siRNA delivered by siRNA/tri-cTatB complexes.

To determine the mechanism of cell internalisation of siRNA/tri-cTatB, cells were incubated with endocytosis inhibitors individually, including the clathrin-mediated endocytosis inhibitor chlorpromazine, the energy-dependent endocytosis inhibitor sodium azide (NaN_3), the pinocytosis inhibitor amiloride and lipid raft-mediated endocytosis inhibitor methyl-β-cyclodextrin (MβCD). Based on confocal microscopy images (Figure 4.6), the extent of uptake and intracellular distribution of the green signal (FAM labeled siRNA) were not significantly affected by NaN_3, amiloride or methyl-β-cyclodextrin. However, uptake was markedly reduced in cells pre-treated with the clathrin-mediated endocytosis inhibitor chlorpromazine indicating that siRNA/tri-cTatB complexes are internalised through clathrin-mediated endocytosis. As introduced in Chapter 4.1.3, clathrin-mediated endocytosis is a common endocytic pathway for cellular uptake which suggests siRNA/tri-cTatB complexes will likely be entrapped in endosomal compartments after cellular uptake.

Inhibitors	Mechanism of action
Chlorpromazine	Sequesters clathrin and AP2 to intracellular vesicles
Amiloride	Inhibits Rac1 and cdc-42, pinocytosis inhibitors
M ßCD	Forms soluble inclusion complexes with membrane cholesterol
NaN_3	Energy-dependent endocytosis inhibitors

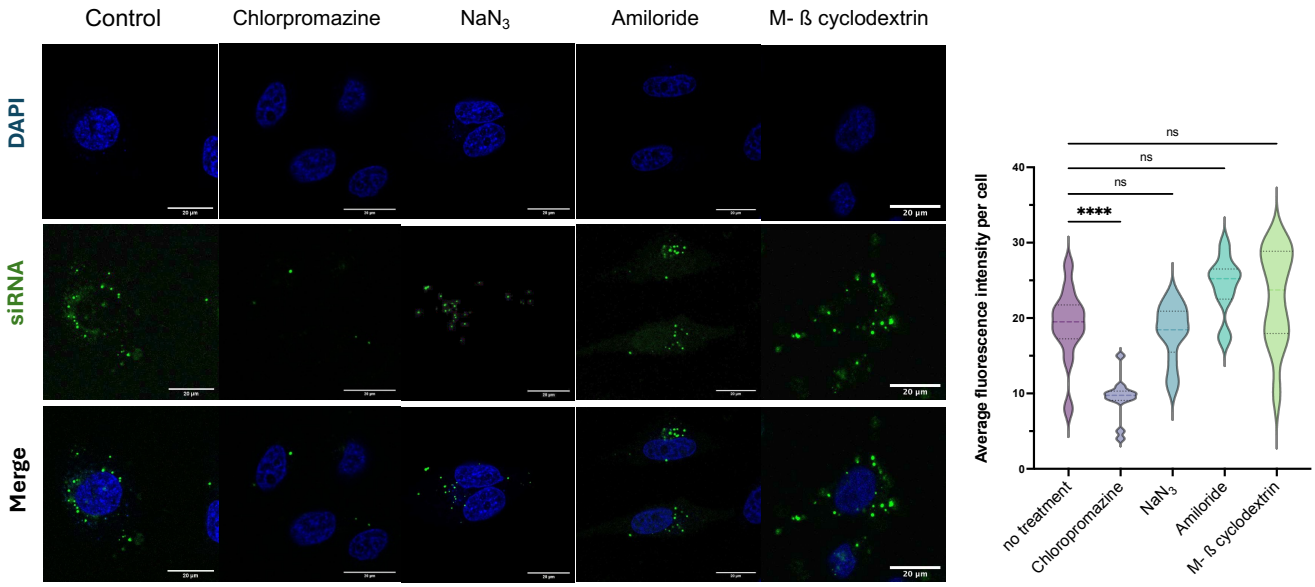

Figure 4.6. Internalisation mechanism study of the siRNA/tri-cTatB complexes. Cells were pre-treated with 4 types of endocytosis inhibitors, which could inhibit certain or multiple endocytosis pathways by blocking the cell surface receptors. Cells were then treated with FAM-labelled siRNA/tri-cTatB complexes for 1 hour before live-cell imaging. Results were evaluated by confocal microscopy imaging of FAM-labelled siRNA (green) internalisation of HeLa cells and fluorescence intensity was quantified by Fiji. Nuclei were stained with Hoechst (blue), scale bar=20 µm. Groups were statistically compared using One-Way ANOVA, error bars represent the standard deviation ****P<0.0001.

To determine whether the siRNA/tri-cTatB complexes are trapped in endosomal compartments, endosomes and lysosomes were identified using Rab5a and Lamp1 protein tracking. Following incubation of cells with siRNA/tri-cTatB for 1 hour, confocal microscopy images showed that the FAM-siRNA in complexes (green) co-localise in endosomes (red) (Figure 4.7). In contrast, Cy5-siRNA in complexes (red) did not co-localise with lysosomes (green).

However, 5 hours after the addition of siRNA/tri-cTatB (Figure 4.8), it was observed that the fluorescence of siRNA (red) co-localised predominantly with lysosomes (green) while its co-localisation with endosomes was reduced compared to the 1-hour image. These results confirmed that the delivery of siRNA/tri-cTatB is mediated by endocytosis, and complexes are initially entrapped in endosomes and then gradually processed to lysosomes.

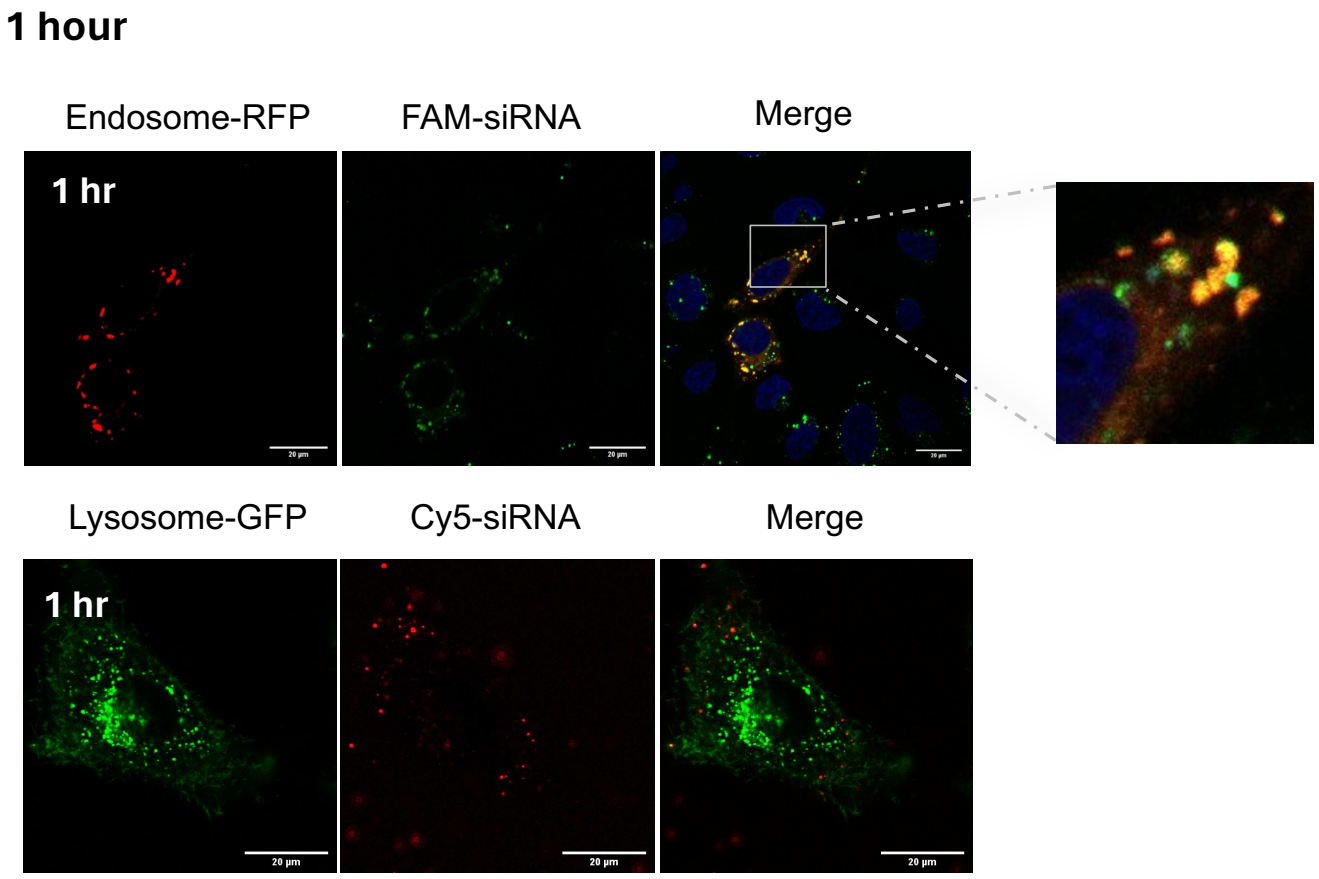

Figure 4.7. Subcellular trafficking of siRNA delivered by siRNA/tri-cTatB complexes after 1 hour of delivery. Confocal microscopy images of FAM-siRNA co-localisation with the endosome marker, Rab5a-RFP, and Cy5-siRNA co-localisation with the lysosome marker, Lamp1-GFP. Scale bars: 20 µm.

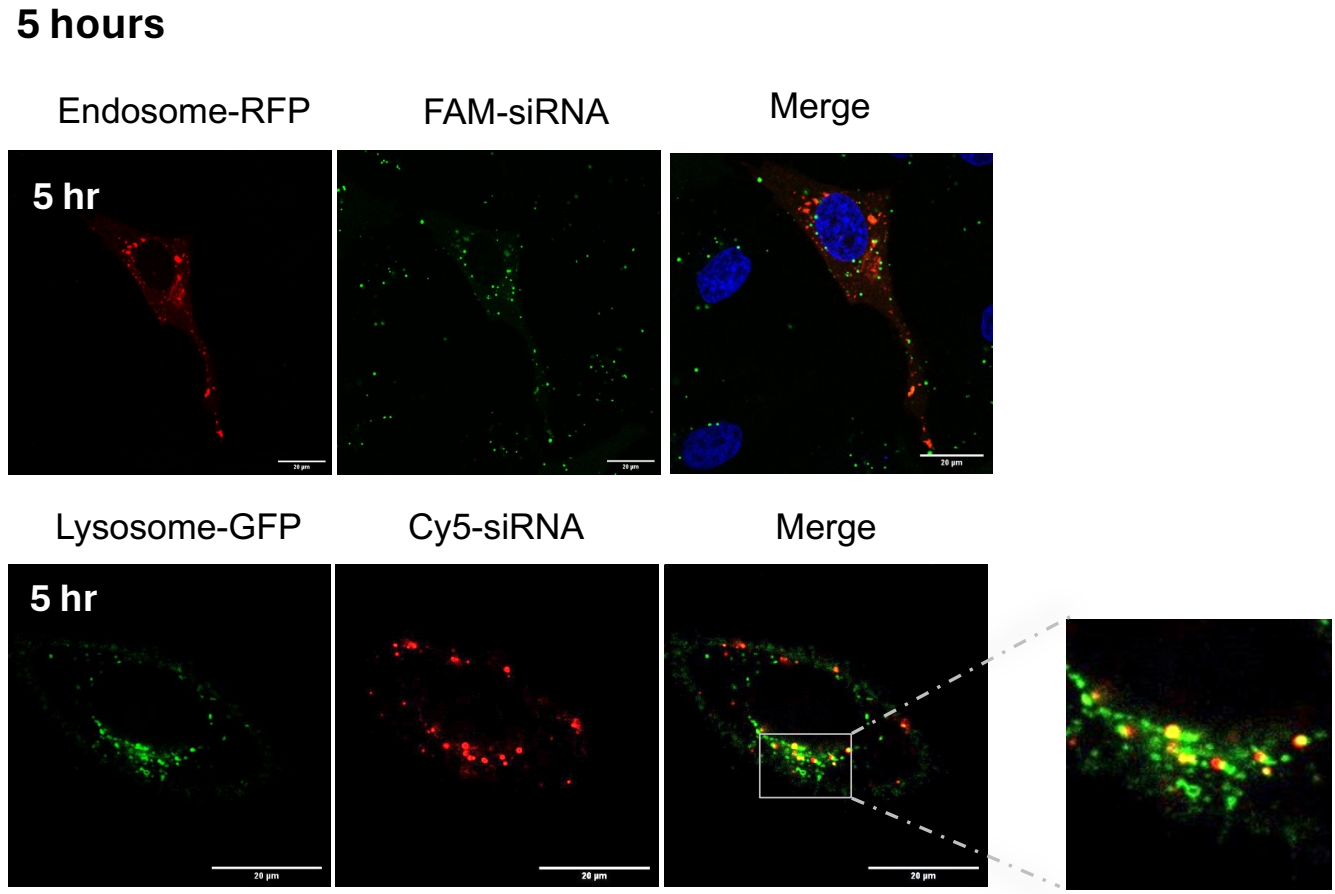

Figure 4.8. Subcellular trafficking of siRNA delivered by siRNA/tri-cTatB complexes after 1 hour. Confocal microscopy images of FAM-siRNA co-localisation with the endosome marker, Rab5a-RFP, and Cy5-siRNA co-localisation with the lysosome marker, Lamp1-GFP. Scale bars: 20 μm.

4.3.3 Strategy to trigger endosome escape: endosome escape domain

Having confirmed that siRNA/tri-cTatB complexes internalise via clathrin-mediated endocytosis and that endosome entrapment of siRNA reduces siRNA bioactivity, the next step was to develop strategies to trigger endosomal escape. As discussed in Chapter 4.1.5, endolytic peptides and photo-induced endosome escape are two proven methods to initiate the escape of the entrapped nucleic acids from endosomes. First, a type of endolytic peptide - the EED was conjugated to the sense strand of siRNA. Here the EED sequence was linked with a PGE six spacer according to Lonn *et al*'s study to enhance the cytosolic deliveryAs illustrated in Figure 4.9A, the sense strand of siRNA-GAPDH which was synthesised with a DBCO at the 3' end reacted with azide-PEG6 modified EED (GFWFG) via a copper-free click reaction SPAAC.

The reaction was allowed to proceed at room temperature for 3 hours at a 1:25 DBCO to azido ratio. The desired product is sense strand siRNA with EED at the 3' end (siRNA-EED). Mass spectrometry confirmed the presence of this product, with the correct molecular mass of 8206.0 $g \cdot mol^{-1}$.

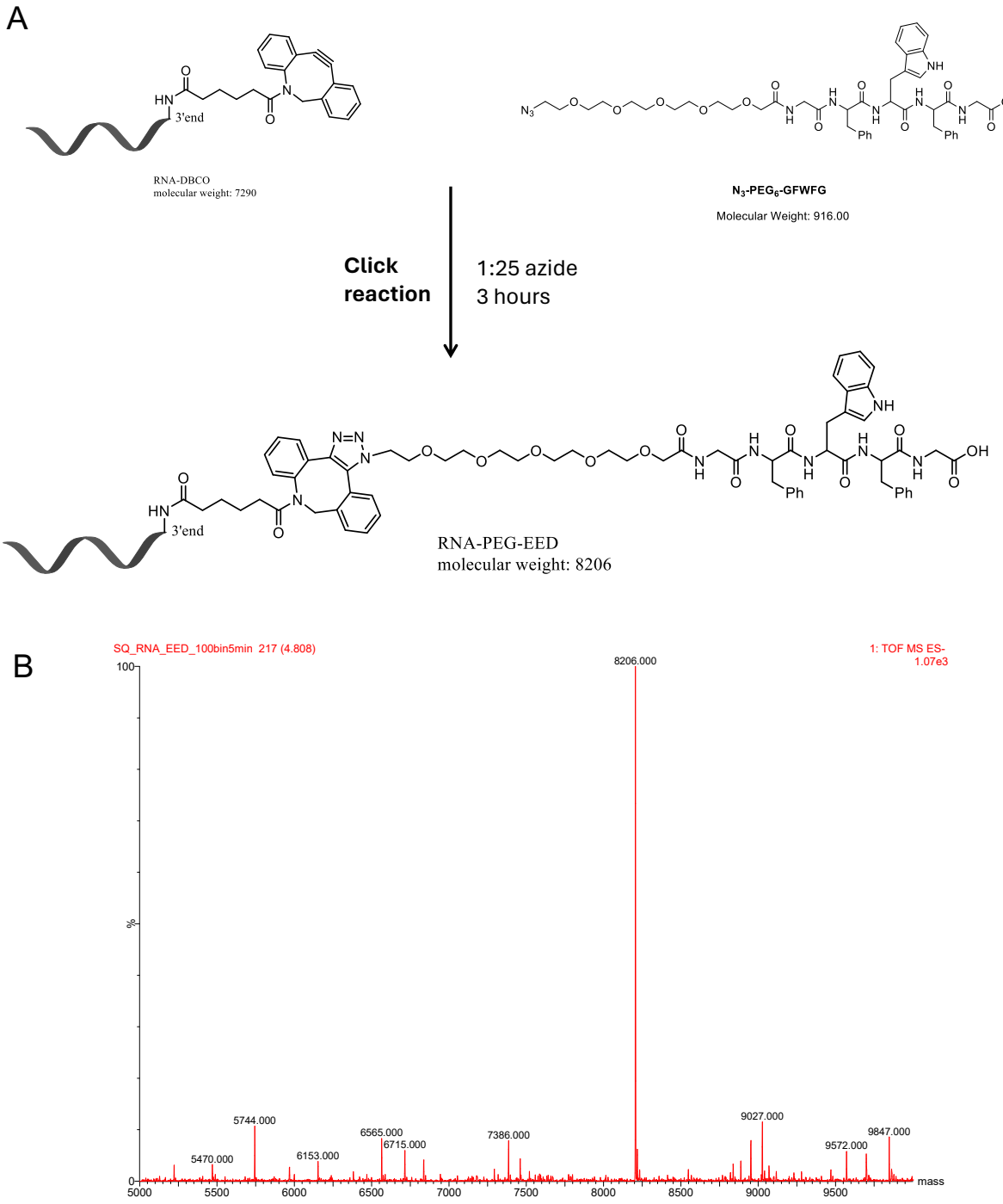

Figure 4.9. Synthesis of the EED-modified siRNA-GAPDH. (A) The EED (GFWFG) was modified with a 6 PEG linker and an azide end (N3-PEG6-GFWFG), reacting with the DBCO-modified siRNA-GAPDH sense strand at the 3' end via copper-free click reaction. **(B)**

Maximum entropy deconvoluted MS QTOF mass spectra of RNA-PEG-EED (theoretical molecular weight at 8206 g·mol^{-1}) confirmed the right product at mass 8206.0 g·mol^{-1}.
The ability of internalised EED-siGAPDH to function was evaluated using the GAPDH activity assay (Figure 4.10). HeLa cells were exposed to siGAPDH/tri-cTatB and EED-siGAPDH/tri-cTatB for 1 hour and assayed after 48 hours. The positive control lipofectamine transfected EED-siGAPDH has shown significant GAPDH downregulation compared to no treatment (NT), indicating that the EED peptide modification on siRNA did not affect its bioactivity. Compared to the NT, the EED modified siRNA/tri-cTatB complexes showed 22% of GAPDH knockdown while the non-modified siGAPDH did not significantly change the GAPDH level.

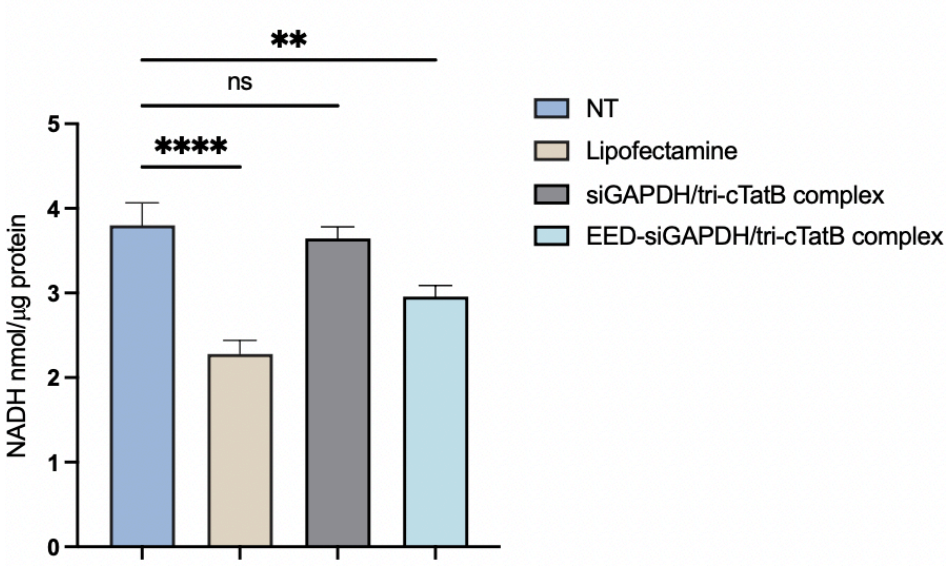

Figure 4.10 GAPDH downregulation by the EED modified siGAPDH. The endosome escape capability and bioactivity of the EED-modified siRNA was investigated by treating HeLa cells with EED-modified siGAPDH/tri-cTatB complexes (1 µM tri-cTatB), non-modified siGAPDH/tri-cTatB was included as a comparison. (Groups were statistically compared using One-Way ANOVA, n = 3, error bars represent the SD, **P<0.01, ****P<0.0001).

4.3.4 Strategy to trigger endosome escape: small molecular chloroquine

In this study, the small molecular triggered endosomal escape of the siRNA delivered by siRNA/tri-cTatB complexes was tried. Here HeLa cells were incubated with siGAPDH/tri-cTatB complexes in Opti-MEM for 1 hour followed by the addition of 60 µM chloroquine for

6 hours of incubation in complete medium. As shown in Figure 4.11, the positive control lipofectamine transfected siGAPDH has shown significant GAPDH downregulation compared to no treatment while there was no knockdown was observed for the siGAPDH/tri-cTatB complexes with chloroquine co-incubation. This result suggested that the small molecular chloroquine is not an ideal strategy for improving our delivery platform.

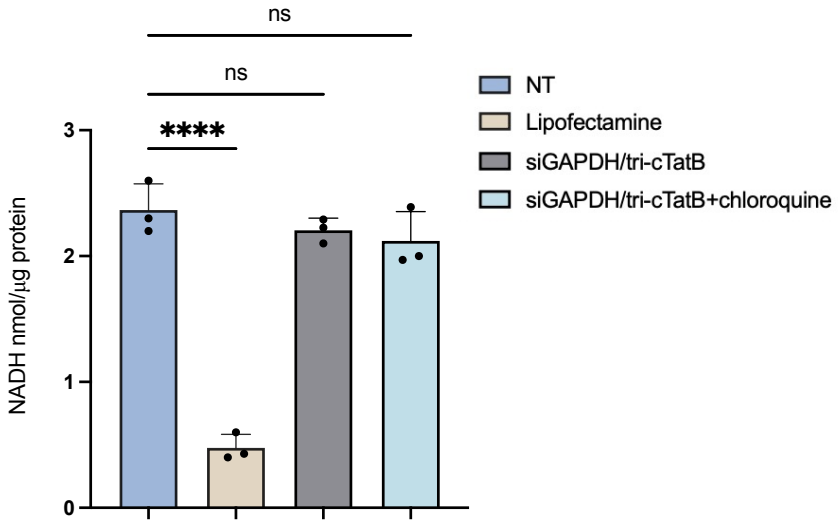

Figure 4.11 GAPDH downregulation by the siGAPDH/tri-cTatB with chloroquine addition. The endosome escape capability and bioactivity of the chloroquine-assisted siRNA endosome escape was investigated by treating HeLa cells with siGAPDH/tri-cTatB complexes (1 µM tri-cTatB) with or without the addition of chloroquine (60 µM) (Groups were statistically compared using One-Way ANOVA, n = 3, error bars represent the SD, ****P<0.0001).

4.3.5 Strategy to trigger endosome escape: Photochemical internalisation

Another strategy to initiate the siRNA escape from endosomes is photo-induced internalisation. To simplify the delivery process, we used a small molecular photosensitizer fimaporfin/TPCS2a (Figure 4.12A) which can passively diffuse into cells and localise in endocytic compartments. The measurement and normalisation of the absorption spectrum of fimaporfin revealed different peaks in the range of 350–700 nm when it was dissolved in Tween80, mannitol and tris-buffer at pH 8.5 (Figure 4.12B). The maximum absorption peak was detected at approx. 420 nm. A peak was also visible at 650 nm in the longer wavelength

range. Based on this result, LED light at 415 nm, being close to 420 nm was used in the light-irradiation experiment setup (Figure 4.12C).

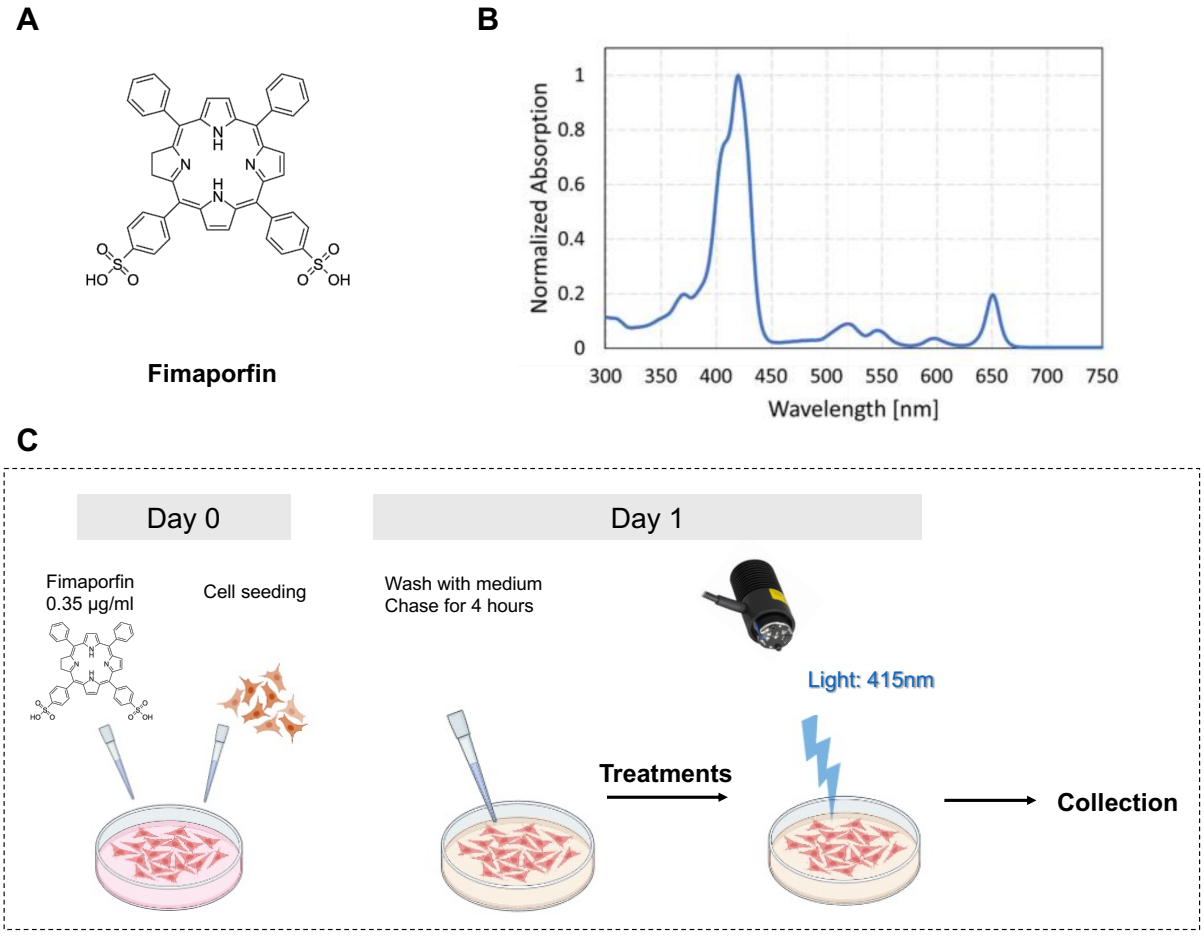

Figure 4.12. Illustration of the photo-induced endosome escape experiment. **(A)** The chemical structure of fimaporfin (TPCS2a). **(B)** The absorption spectrum of fimaporfin dissolved in Tween80, mannitol, and tris-buffer. **(C)** Illustration of the light-irradiation experiment setup. Cells were pre-treated with fimaporfin during cell seeding and on the next day cells were washed with fresh medium and incubated for another 4 hours to remove free fimaporfin. After treatments for 1 hour, cells were washed and irradiated using 415 nm light.

To find the optimal duration and energy of light exposure, HeLa cells were pre-stained with the lysosome marker Lamp1-GFP and exposed to light for different times between 0 and 60 s and the level of lysosome disruption was observed (Figure 4.13). Following light exposure for 60 seconds, there was a marked reduction in lysosomes in cells treated with fimaporfin, due to

lysosome rupture, while cells without added fimaporfin showed almost no change. Therefore, in subsequent photo-irradiation experiments light exposure at 20 mA for 60 seconds (corresponding to 11 J/ cm^2) was used. Phototoxicity was observed when cells were exposed for longer (more than 60s) under 415 nm light.

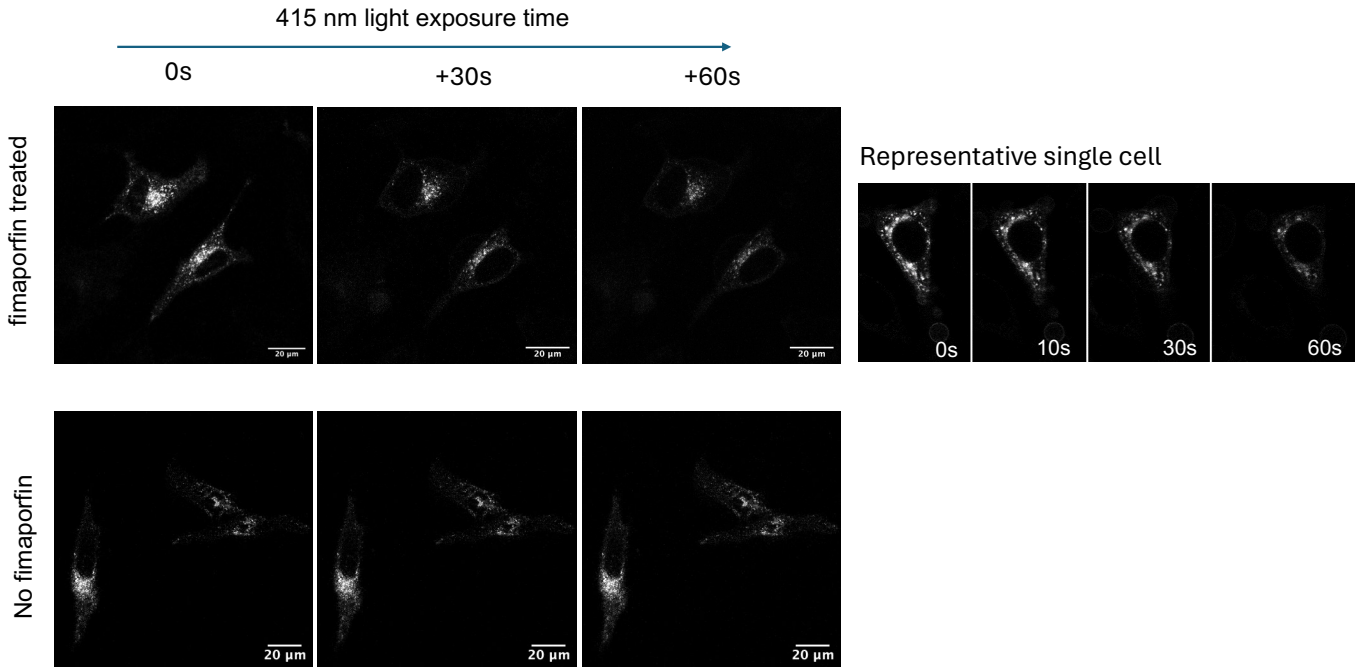

Figure 4.13. Lysosome disruption triggered by photo-irradiation. Confocal microscope images of HeLa cells stained with the lysosome marker Lamp1-GFP (white). Cells were treated with the photosensitizer fimaporfin the day before light exposure to cause lysosomal damage. Images were captured at the indicated time points (scale bar = 20 µm).

To investigate the effect of photo-activated endosomal escape of siRNA by complexes delivery, HeLa cells were pre-treated with fimaporfin and incubated with Cy5-siRNA/tri-cTatB for 1 hour. The intracellular distribution of Cy5 fluorescence was monitored before and after light irradiation (Figure 4.14). Prior to light stimulation, the Cy5-siRNA signal (red) was seen to have a punctate distribution. After light exposure for 60 seconds, Cy5 signals were seen to be homogeneously distributed throughout the cytosol, indicating endosomal disruption and release of Cy5- siRNA.

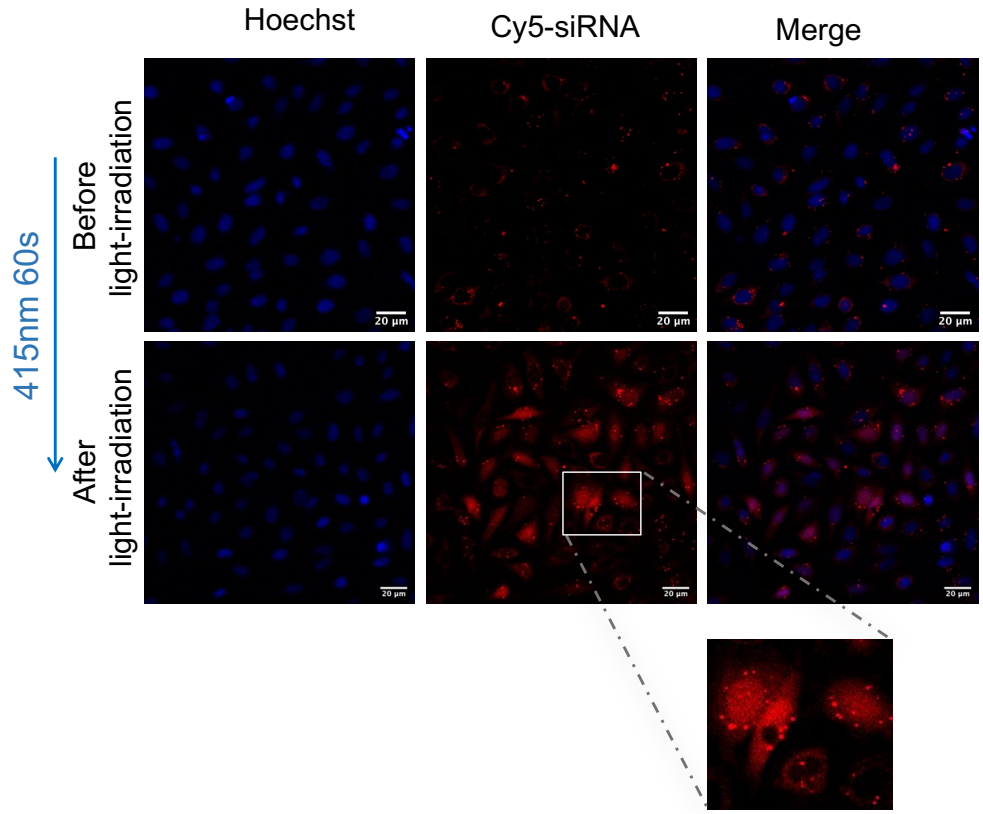

Figure 4.14. Photo-activated endosome release of siRNA. Confocal microscope images showing the photoinduced endosomal escape of Cy5 labelled siRNA/tri-cTatB at 1 hour. Blue light (415 nm) was applied to cells for 60 seconds. Scale bars = 20 μm.

4.4 Discussion and Conclusion

In recent years major efforts have been made to develop a platform for the efficient and nontoxic delivery of nucleic acids to tissues and cells, for the purpose of the diagnosis or treatment of disease. There are two main classes of barriers that must be overcome by carriers: extracellular and intracellular barriers, both of which may capture and/or destroy nucleic acid therapeutics before they reach their target site. As reported in Chapter 3.3, it was found that tri-cTatB provides a new non-covalent carrier for siRNA to help address the extracellular barrier. However, siRNA cannot efficiently perform its biological function if it is unable to cope with intracellular barriers, mainly endocytic vesicles[81]. It is well recognised that the critical bottleneck is the escape of siRNA from endosomes into the cytoplasm in a non-cytotoxic

fashion. Therefore, it was vital to track the tri-cTatB mediated siRNA internalisation route and then to trigger the release of siRNA from the endosomal compartment.

4.4.1 Inefficient siRNA downregulation due to endosomal entrapment

Successful delivery of macromolecules into the cytoplasm of cells requires three critical steps: 1) cell association, 2) stimulation of endocytosis, and 3) facilitation of endosomal escape[144]. From the last chapter, two methods were established for tri-cTatB mediated siRNA delivery via co-incubation or self-assembling complexation. Although successful internalisation of siRNA has been observed for both methods, it was also found that both siRNA and tri-cTatB signals presented within spot-like foci which are likely to be endosomes or lysosomes. Consequently, it was hypothesised that the siRNA is delivered by siRNA/tri-cTatB via endocytosis.

The efficiency of siRNA-GAPDH internalisation by both methods was first assessed by measuring the GAPDH downregulation level (Figure 4.10). There was almost no knockdown for the 2 methods in HeLa or HEK293T cells apart from the siGAPDH/tri-TatB transfection of HEK293T cells. This result was consistent with the hypothesis that very limited siRNA spontaneously escapes from endo/lysosomes and therefore the knockdown efficiency was minimal compared to a commercial transfection reagent. Considering the lack of protection and insignificant biological activity of the siRNA delivered using the strategy of tri-cTatB plus siRNA co-delivery, we focused on developing the siRNA/tri-cTatB self-assembling complexes platform for subsequent experiments.

To further understand the siRNA/tri-cTatB internalisation mechanism, cells were then treated with endocytosis inhibitors. None of these inhibitors affected the uptake of siRNA/tri-cTatB complexes but the cells pre-treated with chlorpromazine showed almost no uptake of siRNA/tri-cTatB complexes (Figure 4.6). The effect of chlorpromazine is to inhibit clathrin-coated pit formation by a reversible translocation of clathrin and its adapter proteins from the

plasma membrane[145], suggesting that the mechanism uptake of siRNA/tri-cTatB complexes is clathrin-mediated endocytosis. This result is consistent with the cellular uptake mechanism of Tat and most arginine-rich peptides, indicating that tri-cTatB can bind to cell surface receptors and form clathrin-assembled clusters [125,146].

The typical fate of molecules internalised via clathrin-mediated endocytosis is to be sorted to early endosomes, late endosomes, and ultimately lysosomes. Since lysosomes contain various degradative enzymes (such as nucleases and phosphatases), failure to escape rapidly from lysosomes usually results in entrapment and degradation of nucleic acids. Therefore, the release of nucleic acid cargo before getting processed in lysosomes is a critical step for effective CPP-mediated delivery of therapeutic cargo[147]. The intracellular trafficking of siRNA/tri-cTatB showed that there is marked co-localisation of the complex with early endosomes at 1 hour, and by 5 hours, siRNA signals are processed to co-localise with lysosomes (Figure 4.7, 4.8). Hence, to enhance the siRNA/tri-cTatB delivery efficacy, the entrapped siRNA must be released before lysosome degradation, that is at the endosome stage.

4.4.2 Endolytic peptide triggered endosome escape.

In this study, two strategies were introduced to assist in inducing the endosome escape of siRNA/tri-cTatB complexes as soon as they are transported to early endosomes. EEDs are fusogenic or lytic peptides derived from viruses, which can disrupt endosomal membranes without damaging the plasma membrane or membranes of other organelles[148]. The EED was selected for testing because it has been proven to be inactive at neutral pH but shifts to an active, membrane-disruptive state under the acidic pH environment of the endosome. The EED we attempted to use was developed by Dowdy and co-workers, they established EED-TAT conjugation with enhanced cellular delivery and endosomal release ability[133]. It was suggested that a 3' end modification of the sense strand minimises any chance of steric hindrance or interference with RNAi and a free 5’-OH group on the antisense strand is necessary for

functional siRNA[149]. The EED peptide was applied to siRNA/tri-cTatB delivery by ligating the peptide to the 3'end of the siRNA-GAPDH guide strand via copper-free click reaction (Figure 4.9).

The knockdown efficiency of EED-modified siGAPDH was evaluated by the GAPDH activity assay (Figure 4.10). The EED modified siGAPDH showed superior GAPDH knockdown efficiency compared to the non-modified siGAPDH when delivered by siGAPDH/tri-cTatB, indicating enhanced endosome release of the EED modified siRNA. Although the delivery efficacy was improved by the EED, it was still less efficient than the commercial transfection reagent, lipofectamine. A possible explanation for this is that the Trp/Phe-containing EEDs conjugated to siRNA undergoes hydrophobic collapse, whereby the aromatic residues aggregated and precipitated the conjugate molecule, resulting in enhanced endosome escape but also partial inactivation of siRNA molecules. In future studies, additional chemistry improvements to mask the hydrophobicity could be undertaken to address the hydrophobic collapse problem. Another concern on EED addition is that many EEDs lead to endosomal bursting releasing a wide array of its luminal content into the cytosol, resulting in activation of the innate immune system and toxic pathways, which narrows the oligonucleotide therapeutic index[130,150].

4.4.3 Light irradiation triggered endosome escape.

Another strategy to trigger siRNA endosome escape in this study was photo-activated internalisation. This system relies on endosome membrane destabilisation caused by ROS, which is produced by a photo-activatable photosensitizer upon light excitation[128]. As discussed in Chapter 4.4.1, the aim was to control the release of siRNAs before they are processed to lysosomes, which might be achieved by applying the light at the optimal delivery time point. Consequently, a driving question was whether the combination of PCI with the delivery siRNA/tri-cTatB complexes could assist with endo-lysosomal escape.

It has been suggested that for $^1O_2$ to damage a membrane, its production should be in the vicinity of the target membrane. Therefore, the small molecule fimaporfin was selected to act as the photosensitizer because it passively diffuses into cells as a separate entity, and localises near the membrane of endocytic compartments[136]. In several studies, the preferred strategy has been to covalently conjugate the photosensitizer to the carrier or cargo to have all components on one entity. However, this study decided to use a separate photosensitizer to make the synthesis and formulation process easier. Also, when all the components are covalently linked it may be difficult to achieve optimal concentrations of all of them at the same time. Based on the light-induced lysosome disruption experiment in HeLa cells (Figure 4.13), the adverse effect of photosensitizer plus light irradiation on lysosome integrity was confirmed. This experiment also allowed the optimal irradiation energy for the siRNA/tri-cTatB complexes in HeLa cells to be defined. According to live-cell microscopy, light irradiation successfully triggered the escape of Cy5 labelled siRNA from endosomes, since a change of the Cy5-siRNA signal from punctate foci to homogeneous staining of cytoplasm was observed. This result revealed that the application of light-irradiation to the delivery of siRNA/tri-cTatB complexes holds promise for achieving the controlled and enhanced release of siRNA cargoes from endosomes to the cytoplasm.

4.4.4 Conclusion

The aims of this chapter were to illuminate the mechanism of tri-cTatB-mediated delivery of siRNA, to determine whether endo-lysosomal entrapment was a problem and, if so, to develop strategies to overcome the endosomal barrier. An important initial observation was that there was inefficient siRNA-associated protein downregulation when the siRNA was co-delivered with tri-cTatB. Further investigation revealed that siRNA/tri-cTatB complexes internalise into cancer cells via the clathrin-mediated endocytosis pathway and that once internalised, the siRNA traffics to early endosomes by 1 hour and is then gradually routed to lysosomes. To

maximise the bioactivity of internalised siRNA, strategies to trigger the endosomal release of siRNA before the lysosome stage were developed.

In this chapter, strategies including small molecules, endolytic peptides and PCI induced endosome escape were tried. Among them, the small molecule, chloroquine didn't induce significant endosomal escape for this siRNA/tri-cTatB delivery platform. This method was not further optimised due to its potential toxicity. It was reported that at the effective concentration, chloroquine invariably lyse not only the endosome containing the siRNA cargo, but many other endosomes inside the cell resulting in substantial and unacceptable toxicity[151].

Although the method of addition of EED to siRNA has shown improved knockdown efficiency, it was not comparable to the commercial transfection reagent. One possible reason is that the EED-siRNA conjugation couldn't allow EED to perform its function at its optimal concentration. And its potential risks of causing activation of the innate immune system and other toxic pathways narrow the oligonucleotide therapeutic index. Since the aim was to establish a modular delivery platform that can be used to transfect many types of nucleic acid without the need for different synthetic protocols, this study did not further explore the application of EED assisted siRNA/tri-cTatB complex delivery.

The method of photo-induced endosomal escape has shown great potential in improving siRNA/tri-cTatB delivery efficacy. It provided a clue to establish an efficient and controllable platform for siRNA delivery. Another major advantage of PCI as a delivery tool is its intracellular site-specific action. The fact that the photochemical-induced delivery of the specific macromolecule is confined only to the illuminated area is an advantage for *in vivo* studies. siRNA delivery would be limited to the targeted cells, thereby further reducing non-specific effects[152]. However, it is crucial to acknowledge the importance of finding the balance between enhancing endosomal escape for better efficacy, maintenance of cargo biological activity, and cytotoxicity. These endpoints are considered in the next Chapter.

Chapter 5

Photo-activated delivery and function of siRNA/tri-cTatB and mRNA/tri-cTatB complexes

5.1 Introduction

In Chapter 4, the promise of introducing light irradiation into siRNA/tri-cTatB complex delivery was demonstrated. To further investigate the safe and effective application of a light-controlled delivery platform, it is necessary to assess cytotoxicity and siRNA downregulation efficiency. As a noninvasive treatment modality, photochemical internalisation (PCI) therapy has emerged as a promising treatment for cancer[153]. Therefore, this study aim to expand the light-controlled siRNA transfection platform to oncology applications. Furthermore, no covalent bonding or specific modification of the nucleic acid cargo is required, and therefore it was hypothesised that the platform has the potential to be used for other types of nucleic acid therapeutics such as mRNA.

5.1.1 Nucleic acid therapeutics: powerful tools for cancer therapy

As introduced in Chapter 1, cancer is an enormous public health challenge, and it is urgent to implement precise and individualised treatment and to increase investment in advancing cancer research. Traditional therapeutic approaches such as chemotherapy and radiation therapy are highly effective but often carry arduous physical and psychological challenges for patients. Encouragingly, over the last 20 years, the landscape of cancer treatment has undergone a comprehensive and remarkable transformation. Since cancer is associated with single or multiple gene defects, much research has focused on incorporating genetic materials as one of the means to treat various types of malignancy.

5.1.1.1 siRNA in cancer therapy

Increasing numbers of cancer-related gene targets are being elucidated, providing a mechanistic basis for a range of cancers. The potential use of siRNA as a therapeutic modality to attack cancer at these gene targets has several attractive features: (1) siRNA therapeutics can selectively and preferentially target any gene of the cancer cell, including targets that are

otherwise hard to drug[154,155]; (2) they are easy to be synthesised and modified, in addition to having good efficacy and safety profiles with minimal off-target effect and immunostimulatory effects[156,157]; (3) the RNAi mechanism of action is catalytic, resulting in extended siRNA inhibition of mRNA target expression even after a single dose. That is, siRNA-loaded RISC allows further cycles of mRNA binding and cleavage after initial mRNA binding[158].

The early and now well-established use of siRNA in clinical studies involved the local administration of naked siRNA molecules to organs that contain few nucleases, such as the eye[159]. Although local administration continues to be explored, systemic administration of siRNA is more used for cancer clinical trials. To date, nine siRNA-based therapies have been investigated clinically (Table 1.1). For example, preclinical studies have shown ideal antineoplastic activity in xenograft tumour models, and the inhibition of PLK1 expression was maintained for 7–10 days after administration of a single dose. TKM-080301 (TKM-PLK1) is a lipid nanoparticle-based formulation developed by Tekmira Pharmaceuticals and contains anti-PLK1 (polo-like kinase 1) siRNA for treating solid cancer[160]. Both phase I/II studies have reported tumour reduction in advanced hepatocellular carcinoma and adrenocortical cancer[160].

5.1.1.2 mRNA in cancer therapy

From 2005 to 2024, there were at least 150 oncologic clinical studies of mRNA. Among them, research targeting neoantigens has progressed rapidly since the onset of COVID-19, highlighting the feverish pace of mRNA research. Compared to the risk of integration into the host genome that is associated with DNA vaccines, mRNA is produced through *in vitro* transcription and can be directly translated into protein once it enters the cytoplasm. A single mRNA vaccine can encode multiple antigens, strengthening the immune response against resilient pathogens[161,162]. So far, mRNA has shown promising efficacy in encoding neoantigens for cancer vaccines, tumour suppressor factors for inhibiting tumour progression, tumour-associated antigens (TAAs) for activating dendritic cells, CAR for engineered T-cell therapies,

and genome-editing proteins for gene therapy[163]. Among them, mRNA-based cancer vaccines that express TAA have gained tremendous attention as an alternative cancer immunotherapy because they can specifically attack and destroy cancer cells through immune stimulation[164]. For example, the mRNA-based vaccine mRNA-4359 that targets the immunomodulatory enzyme indoleamine 2,3-dioxygenase 1 (IDO1) and immune checkpoint molecule programmed cell death-1 ligand 1 (PD-L1) has recently been given to patients with advanced solid cancer in the UK[165].

Naked mRNA molecules are not stable *in vitro* and are susceptible to degradation by exonucleases and endonucleases, necessitating high-quality storage and transportation systems. Although lipid nanoparticles are the most used delivery system for mRNA, challenges remain concerning the stability of the mRNA-LNPs, which must be stored at ultra-low temperatures[166]. Additionally, non-specific uptake of LNP by non-target cells can reduce therapeutic efficacy and increase the risk of off-target effects. CPPs are thought to offer great promise in meeting the requirement of simple production, high transfection efficiency, and improved biocompatibility for mRNA delivery systems[115]. Peptide-based vectors also take advantage of the versatility of peptide sequences, which can be equipped with desired properties. Although CPPs have been widely studied for delivering macromolecules such as antibodies and siRNA, little is known about their delivery capability of mRNA. One of the aims of this chapter was to study the transfection efficiency of mRNA delivered the novel CPP, tri-cTatB.

5.1.2 Polo-like kinase 1 (PLK1): a potential target for cancer therapy

Polo-like kinases (PLKs) are a family of serine/threonine protein kinases that are widespread in eukaryotic cells. The human PLK family includes five members: PLK1, PLK2, PLK3, PLK4, and PLK5. PLK1 is the most extensively investigated protein among the PLK family[167]. PLK1 plays essential roles in the cell cycle, including controlling mitotic entry and the G2/M checkpoint, coordinating the centrosome and cell cycles, regulating spindle assembly and

chromosome segregation, and facilitating DNA replication[168]. The PLK1 protein has a highly conserved N-terminal kinase catalytic domain, C-terminal polo-box domain (PDB) and the connecting region in the middle. The C-terminal PDB mediates PLK1 subcellular localisation and protein interactions and regulates the N-terminal serine/threonine kinase domain (Figure 5.1). Mechanistically, PLK1 directly binds to the phosphopeptide of certain proteins through the PBD and phosphorylates different substrates by the kinase domain in a spatiotemporal-dependent manner, thereby regulating different cellular activities[169].

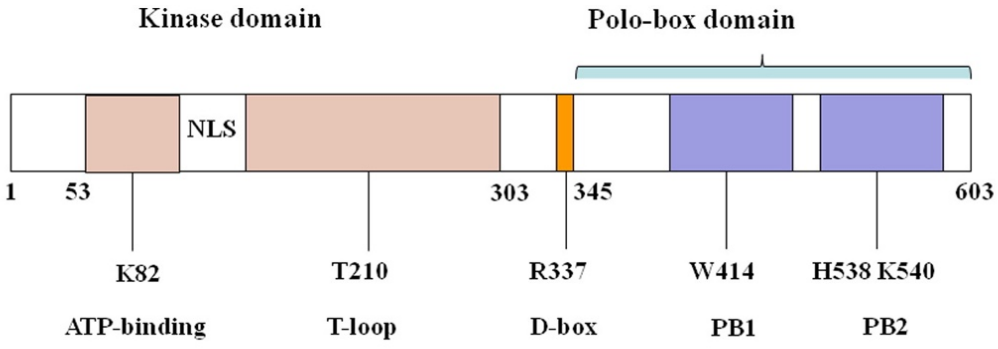

Figure 5.1. The domain structure of PLK1. PLK1 protein involves a highly conserved N-terminal kinase catalytic domain (harbouring 252 amino acids), C-terminal polo-box domain (harbouring 60-70 amino acids), and the connecting region in the middle. PB1: polo-box 1; PB2: polo-box 2. Figure adapted from Liu *et al*. (2017)[170].

Previous studies have revealed that PLK1 is overexpressed in various types of cancer compared to normal controls tissue and its overexpression is associated with a poor prognosis in cancer patients[171]. According to the PLK1 signaling pathway (Figure 5.2), the inhibition of PLK1 in cancer cells leads to inhibition of Cdc25 activation, resulting in the elimination of cancer cells via inactivation of cdc2/cyclin B1-mediated mitotic arrest followed by apoptosis[172]. Additionally, several studies have revealed that targeting PLK1 may be a novel approach for overcoming drug resistance in cancer chemotherapy and that PLK1 inhibition results in radiosensitisation[170]. For example, Jimeno *et al*. confirmed that PLK1 mediated the resistance

of pancreatic cancer cells to gemcitabine[173], and Rodel *et al*. showed that PLK1 silencing could enhance the sensitivity of rectal cancer to radiotherapy[174].

Therefore, PLK1 could be a promising therapeutic target for cancer since PLK1 downregulation could induce apoptosis, decrease cancer cell survival and increase the sensitivity to chemotherapy drugs and radiotherapy, whereas it has little effect on normal cells. For these reasons, PLK1 was selected as the first target to investigate the oncogenic application of the light-controlled siRNA/tri-cTatB delivery platform.

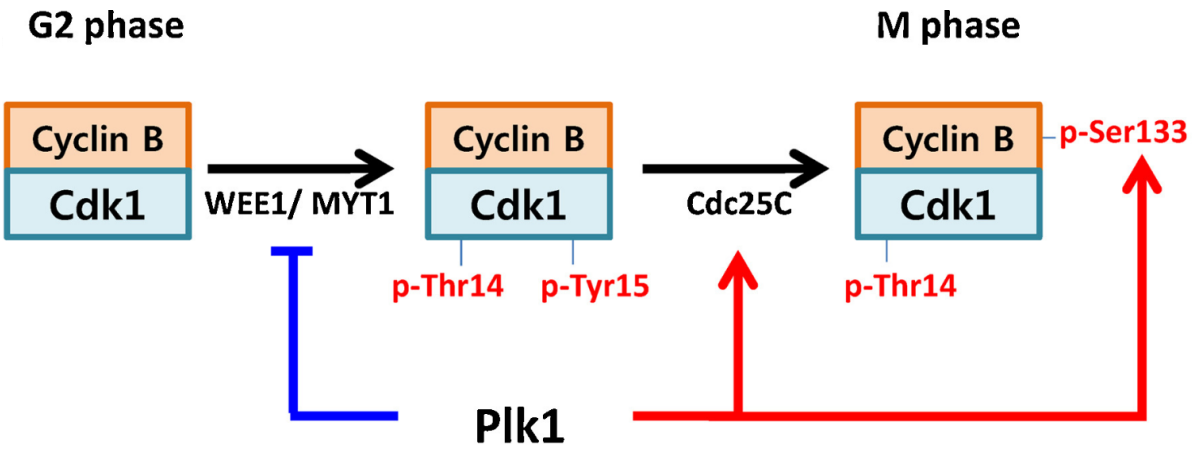

Figure 5.2. Signalling pathway of PLK1 in G2/M transition. During interphase, Cdk1 is phosphorylated and inactivated by Wee1 and MYT1. At the boundary between G2 and mitosis, Plk1 phosphorylates and activates Cdc25C, which results in dephosphorylation of Cdk1[175]. In addition, PLK1 phosphorylates Ser133 of cyclin B1, a cofactor of Cdk1, to stimulate mitotic entry. Figure adapted from Yim and Erikson (2014)[172].

5.2 Aims

The aims of the research presented in this Chapter were to:

1) Investigate the safety and bioactivity of the new light-controlled siRNA/tri-cTatB delivery system.
2) Evaluate a therapeutic application of the delivery platform: downregulation of the oncogene, PLK1.

3) Test the versatility of the delivery platform by extending the application to another nucleic acid format, mRNA.

5.3 Results

5.3.1 The light-controlled siRNA/tri-cTatB delivery platform

The successful cytosolic release of siRNA from endosomes after light irradiation of HeLa cells treated with the photosensitizer fimaporfin was reported in Chapter 4.3.4. In this chapter the cytotoxicity of the light-irradiation delivery system and whether the bioactivity of siRNA is preserved after endosome escape were investigated. The *in vitro* cell viability of HeLa and MDA-MB-231 cells was evaluated after incubation with various treatments by Cell Counting Kit – 8 (CCK8) (Figure 5.3). Here, the commonly used transfection reagent lipofectamine was included for comparison. Fimaporfin alone and siRNA/tri-cTatB alone had no effect on cell viability. Following the siRNA/tri-cTatB treatment and light exposure, the cell viability of MDA-MB-231 cells was 84.7% and the HeLa cell was reduced by 18.3% (p=0.042) compared to controls. Of note, lipofectamine delivery of siRNA resulted in a significant loss of cell viability compared to negative control (49%, p<0.0001) in HeLa cells and 86.3% viability in MDA-MB-231 cells.

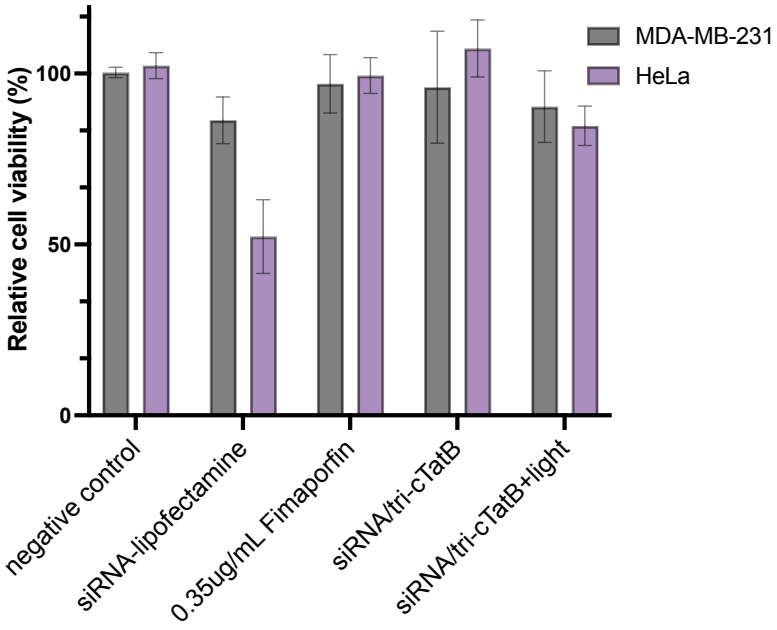

Figure 5.3. Cell viability of the delivery platform. Cell viability of HeLa and MDA-MB-231 cells after pre-treatment with fimaporfin (0.35 μg/mL) and then treated with siRNA and tri-cTatB (1 μM) complexes with or without light irradiation. CCK8 assay was performed 24 hours post-treatments. The commercial transfection reagent lipofectamine was included for comparison (Error bars represent mean ± SD, n=3).

After successful delivery and release into the cytoplasm, it is critical that the interfering activity of siRNA is demonstrated since siRNA is easily degraded in the intracellular environment. Likewise, it is important to ensure that the light irradiation does not disrupt siRNA activity. GAPDH knockdown assays were used to investigate whether siRNAs delivered through tri-cTatB complexes plus photo-activated endosomal release retain gene silencing capability. HeLa, HEK293, and MDA-MB-231 cells were exposed to siGAPDH/tri-cTatB complexes for 1 hour followed by light irradiation. Lipofectamine transfected siGAPDH was included as a positive control. Here, scrambled siRNA was utilised to distinguish sequence-specific silencing from off-target or non-specific effects and was incorporated into scrRNA/tri-cTatB complexes using the same protocol as siGAPDH/tri-cTatB. According to Figure 5.4, after 48 hours, a greater than 50% reduction of GADPH enzymatic activity was noted in all 3 cell lines treated by light-controlled siGAPDH/tri-cTatB (87, 66 and 44% for HeLa, MDA-MB-231 and HEK293T cells, respectively). In the absence of light irradiation, there was no statistically significant change in GAPDH enzymatic activity following siGAPDH/tri-cTatB transfection in any of the cell lines.

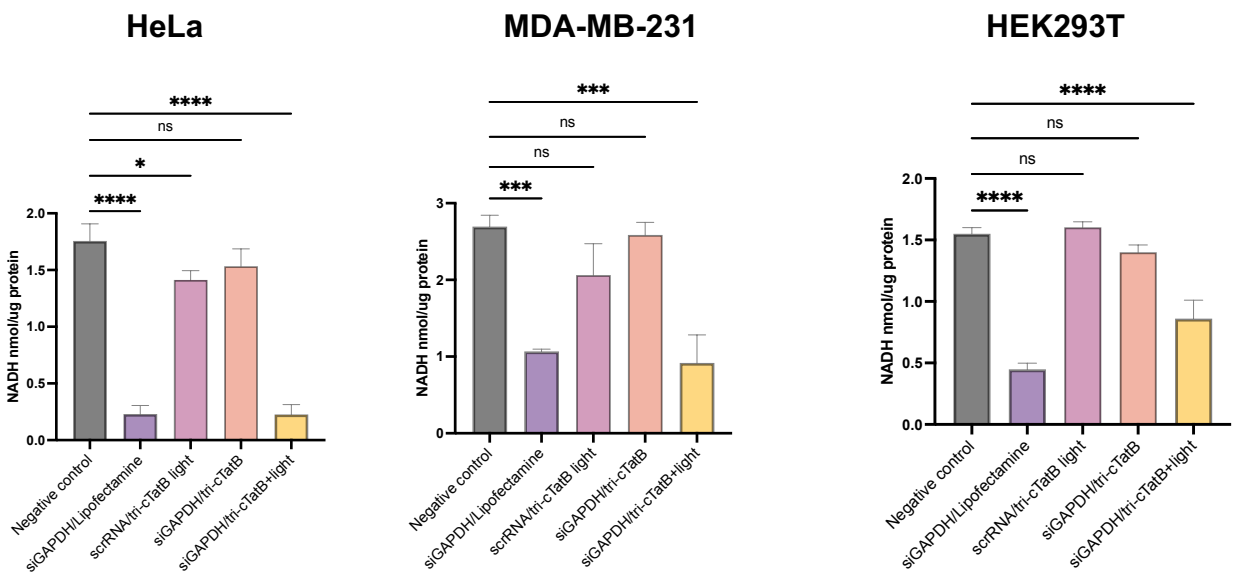

Figure 5.4. Light-activated tri-cTatB mediated siRNA delivery and downregulation. GAPDH enzymatic activity of HeLa, HEK293T and MDA-MB-231 cells was assayed by GAPDH activity assay to investigate the delivery efficiency of siGAPDH/tri-cTatB complexes (tri-cTatB 1 μM, siGAPDH 100 nM) plus light activation (light 11 J/cm^2). The GAPDH assay was performed 48 hours post-treatment (n = 3 biological replicates, error bars represent the SD, the significance of the differences was evaluated by one-way ANOVA, ***P<0.001, ****P<0.0001).

5.3.2 Oncogenic application of the delivery platform

Following the demonstration that the light-activated siRNA/tri-cTatB delivery system shows transfection efficiency with retained cell viability and siRNA silencing capability, the next step was to explore the functionality and versatility of the system, especially its potential in cancer therapy. In this study, the system was used to downregulate the oncogene PLK1, which is overexpressed in breast cancer. Therefore, the delivery platform was assessed in breast cancer cell lines MDA-MB-231 and MCF-7. Both cell lines were pre-treated with fimaporfin and then exposed to siPLK/tri-cTatB complexes and scrRNA/tri-cTatB complexes for 1 hour followed by 11 J/cm^2 light irradiation, or lipofectamine siPLK transfection. The western blot results (Figure 5.5) showed a marked reduction of PLK1 protein following incubation of cells with

siPLK/tri-cTatB complexes followed by light activation. The bar graphs were generated following three repeats of the western blots, with bands quantified and normalised to a loading control, showing 55.2% and 53.8% reduction of PLK1 compared to the untreated control sample in MDA-MB-231 and MCF-7 cells, respectively. In contrast, neither scrRNA/tri-cTatB plus light nor siPLK/tri-cTatB alone (without light irradiation) caused a significant reduction of PLK1.

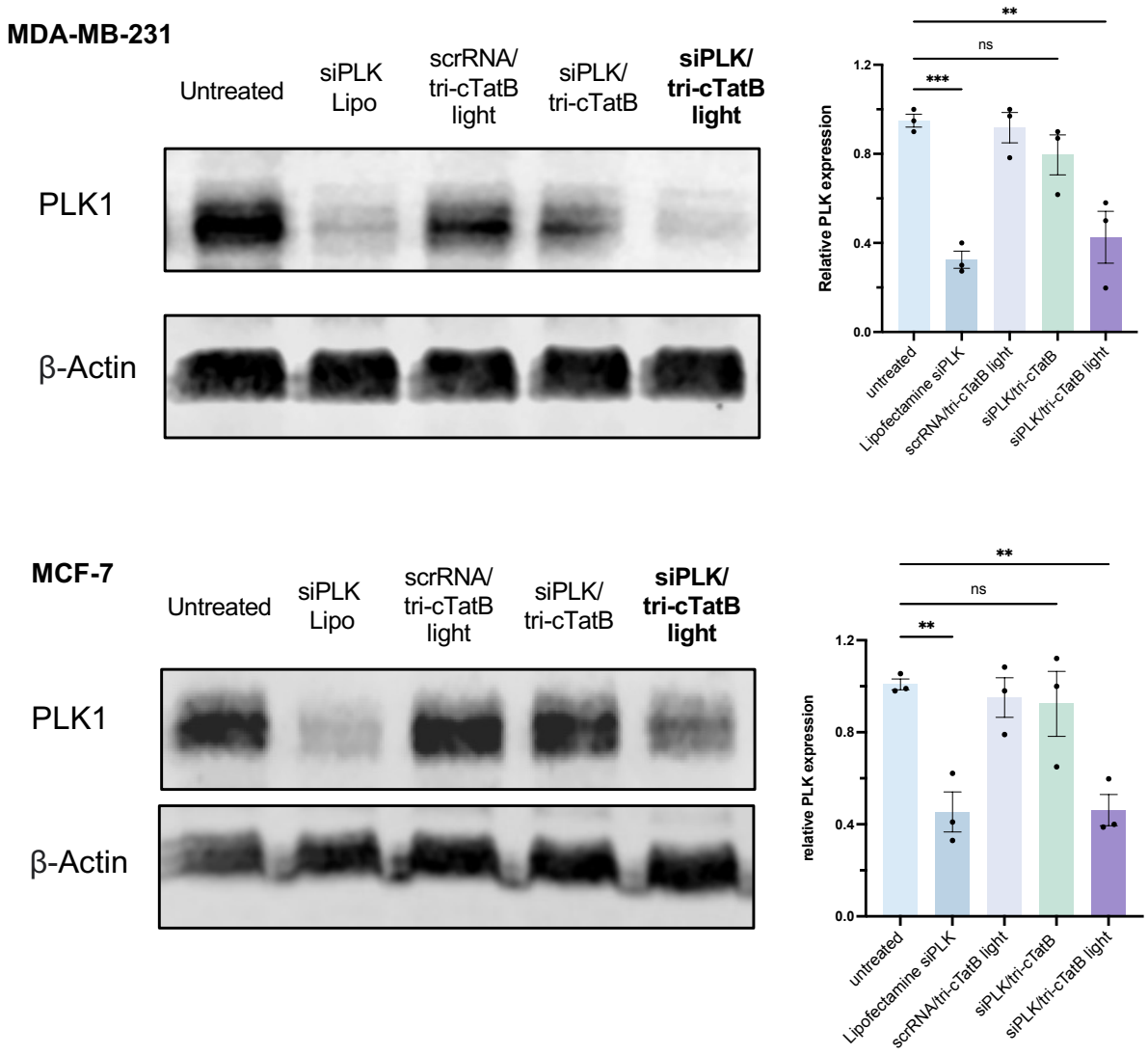

Figure 5.5. Downregulation of PLK1 by the siPLK/tri-cTatB + light platform. Western blot analysis indicates the PLK1 expression level in MDA-MB-231 and MCF-7 cells following various treatments (siRNA concentration of 100 nM). Beta-actin was used as a loading control, lipofectamine siPLK transfection was included as a positive control. Bar figures were generated

by band quantification (calculated by ImageJ) to demonstrate the relative PLK1 expression level (n = 3 biological replicates, error bars represent the SD, $^{**}P<0.01$).

As previously introduced, the downregulation of PLK1 results in cell apoptosis, thus the early apoptosis of MDA-MB-231 and MCF-7 cells due to the reduction of PLK1 was tested. Both cell lines were treated with siPLK/tri-cTatB complexes or scrRNA/tri-cTatB complexes followed by 11 J/cm^2 light irradiation, and with lipofectamine plus siPLK. 24 hours post-treatment, Annexin-V APC/PI flow cytometric analysis was performed to quantify apoptotic cells (Figure 5.6). Cells undergoing early apoptosis sort to quadrant 2 (Annexin V positive, PI negative). There was a higher percentage of MDA-MB-231 cells in early apoptosis following treatment with siPLK/tri-cTatB plus light exposure compared to cells where light was omitted: 29% vs 13%, respectively. MCF-7 cells also showed a higher rate of early apoptotic cells following treatment with light-activated siPLK/tri-cTatB compared to cells where light was omitted: 22% vs 8%, respectively. The proportion of cells undergoing apoptosis following exposure to scramble siRNA/tri-cTatB complexes plus light was 5.2% and 11.3% for MDA-MB-231 and MCF-7 cells, which was similar to untreated control cells.

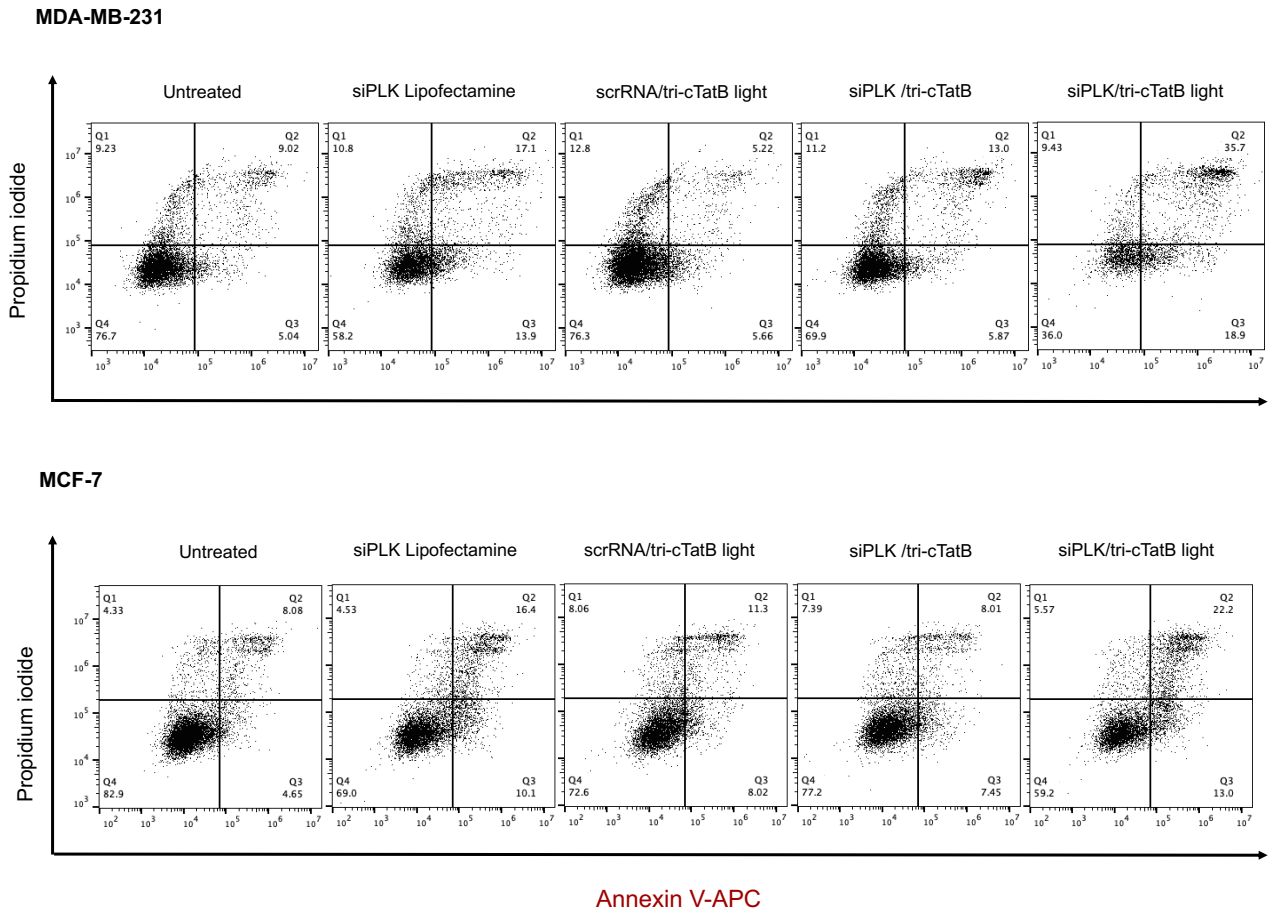

Figure 5.6. Early apoptosis caused by PLK downregulation was detected by the Annexin-V assay. The annexin-V APC conjugation assay was used to detect early apoptosis and analysed by flow cytometry. MDA-MB-231 and MCF-7 cells were incubated with siPLK/tri-cTatB complexes (+/- light irradiation), scrRNA/tri-cTatB + light irradiation, siPLK lipofectamine (siPLK 100 nM). The assay was performed 24 hours post-treatments.

Following early cell apoptosis, late apoptosis/death of MDA-MB-231 cells caused by PLK1 downregulation was tested 48 hours after treatments. Figure 5.7 demonstrates the viability of MDA-MB-231 cells harvested 48 hours post all treatments. According to the morphology of MDA-MB-231 cells under phase-contrast microscopy (Figure 5.7A), more rounded cells were detected in the group of siPLK/tri-cTatB plus light treatment and lipofectamine plus siPLK compared to other groups. The CCK8 viability assay (Figure 5.7B) suggested that before light-irradiation, siPLK transfection mediated by tri-cTatB complexes exhibited no significant cell death while under light-irradiation MDA-MB-231 cell viability was inhibited by around 50%.

This was attributed to reduced PLK1 expression mediated by light-activated siPLK/tri-cTatB therapy.

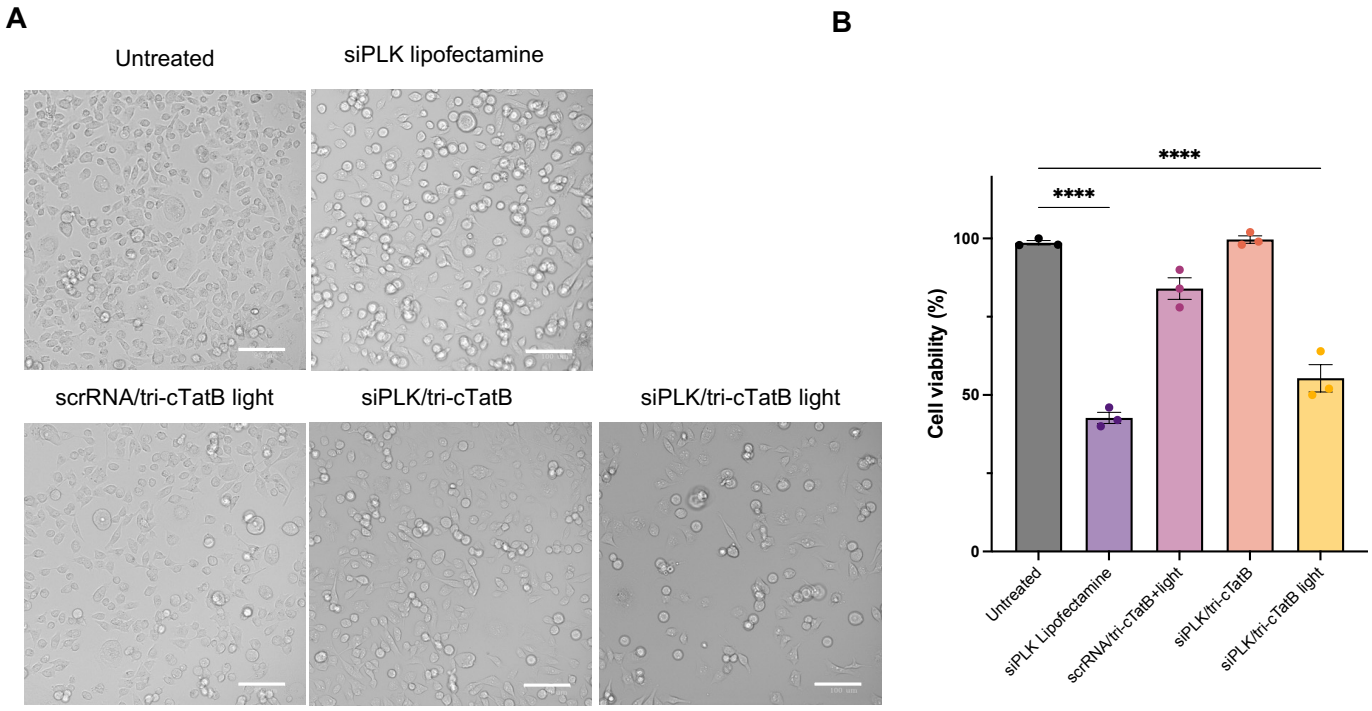

Figure 5.7. The cell late apoptosis and death caused by PLK downregulation were tested by viability assay. MDA-MB-231 cells were collected 48 hours post-treatment (siPLK 100 nM), and the viability was investigated by (A) Phase-contrast microscopy (scale bar = 100 μm) and (B) the CCK8 viability assay. (n = 3 biological replicates, error bars represent the SD, ****P<0.0001).

5.3.3 Extended application of the delivery platform: mRNA delivery

Up to this point it has been established that a light-controlled self-assembled siRNA/tri-cTatB complex delivery system results in successful siRNA cytosolic release and effective downregulation of the target protein. To further explore the universality and versatility of the system for nucleic acid therapeutics, the potential of the system for mRNA delivery was investigated. Following the same protocol as for siRNA and tri-cTatB self-assembly, in this study 2 μM of tri-cTatB peptide and 2.5 μg/mL mRNA were mixed to form self-assembled

complexes via electrostatic interaction. The mRNA/tri-cTatB complexes were applied to cells followed by 11 J/cm^2 light irradiation to trigger the endosomal escape of Cy5-mRNA.

Live-cell confocal images showed efficient internalisation of Cy5-mRNA following incubation of mRNA/tri-cTatB with HeLa cells for 1 hour (Figure 5.8). Similar to the siRNA internalisation route, the mRNA signals were detected intensively within cells but presented as particle-like foci. After light irradiation, the Cy5 signals changed to homogeneous staining of the cytoplasm, indicating the release of mRNA into the cytosol.

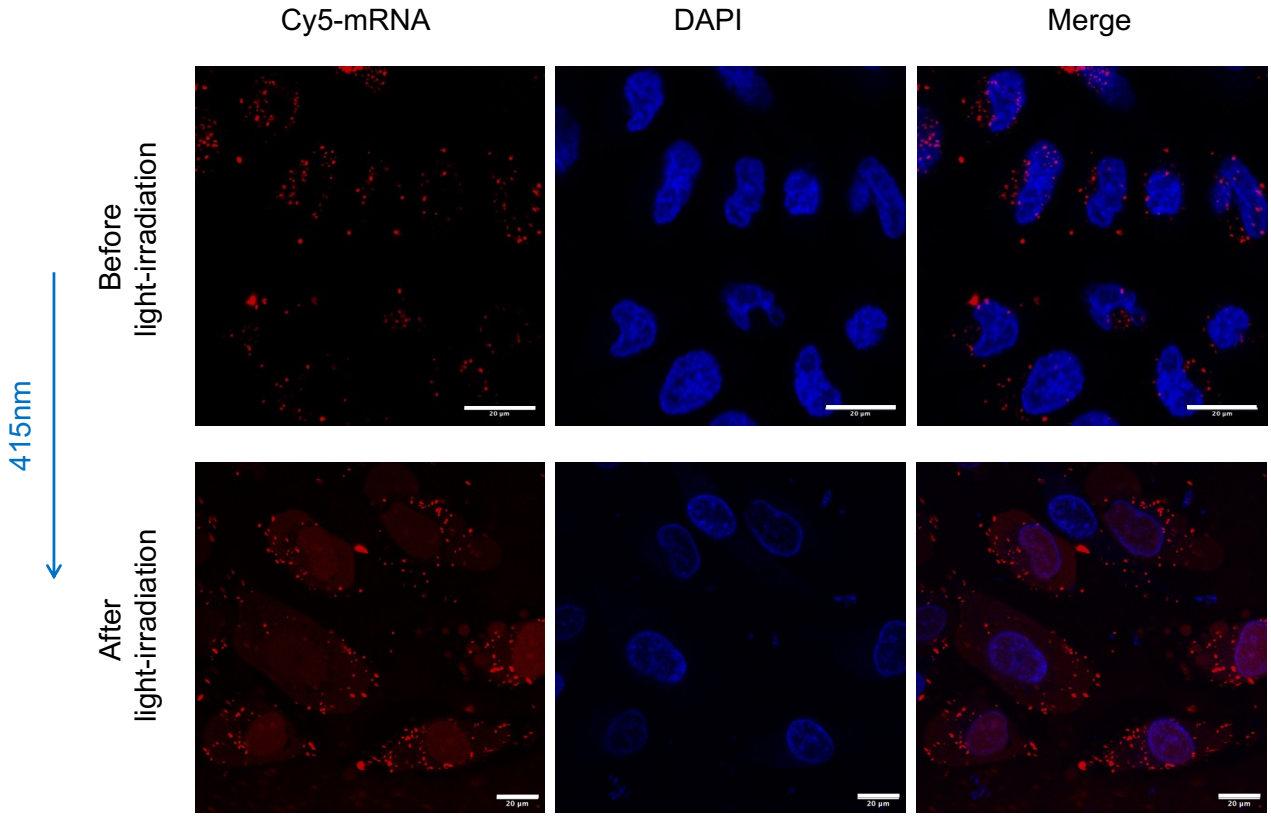

Figure 5.8. Live-cell imaging of Cy5 labeled mRNA/tri-cTatB delivery. HeLa cells uptake of Cy5 labeled mRNA mediated by mRNA (2.5 µg/ml) and tri-cTatB (2 µM) complexes for 1 hour, fimaporfin was pre-treated. Images were taken before and after light irradiation (scale bar=20 µm).

mRNA encoding the eGFP reporter protein was used to investigate transfection efficiency and mRNA intracellular activity. 24 hours post-delivery of eGFP-mRNA, microscopy images of

eGFP were captured. Based on the fluorescence micrographs shown in Figure 5.9, before light activation, only a small proportion of cells expressed weak eGFP protein while after light activation, a markedly increased proportion of HeLa cells exhibited green fluorescence. It was also noted that the intensity of the green signal was stronger than that of cells in which mRNA was transfected by lipofectamine. This indicates the amount of mRNA transfected per cell by tri-cTatB at 1 hour is higher than that transfected by lipofectamine at 4 hours.

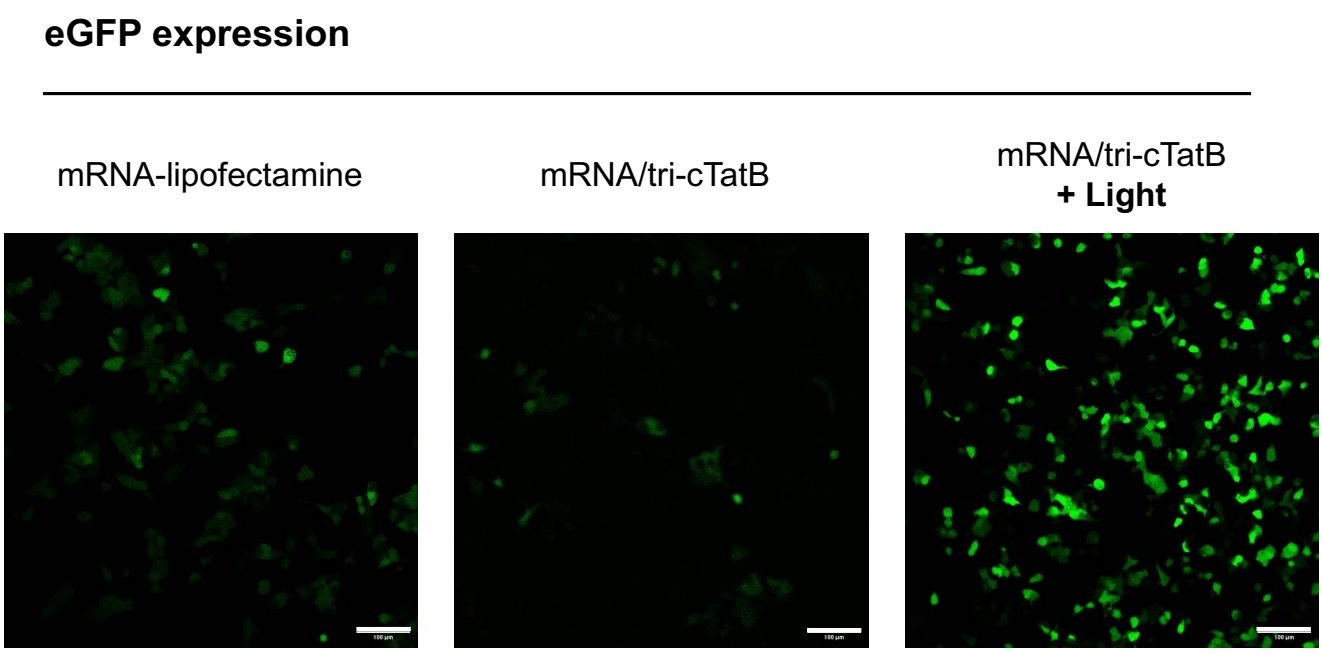

Figure 5.9. Expression of eGFP by light-controlled mRNA/tri-cTatB transfection. Fluorescence micrograph showing the expression of eGFP in HeLa cells under different delivery conditions. The delivery period of mRNA/tri-cTatB is 1 hour followed by light irradiation (mRNA 2.5 μg/ml, light 11 J/cm^2). mRNA was transfected by lipofectamine for 4 hours. Images were taken 24 hours post-delivery (Scale bar=100 μm).

The transfection efficiency of mRNA encoding eGFP in HeLa and HEK293T cells was quantified by flow cytometry (Figure 5.10). Lipofectamine transfection of mRNA-eGFP was included as the positive control. Flow cytometry was carried out after exposure of cells to the mRNA/tri-cTatB complexes for 1 hour, followed by incubation for a further 24 hours. The combination of the delivery of mRNA-loaded tri-cTatB complexes and PCI resulted in

successful transfection and then the expression of eGFP in both HeLa and HEK293T cells. 95.2% of HEK293T cells expressed eGFP following light activation and mRNA/tri-cTatB delivery, while only 7% of cells expressed eGFP in the absence of light activation. 54.1% of HeLa cells transfected by light-activated mRNA/tri-cTatB expressed eGFP while only 2.2% of cells expressed eGFP without light activation. The efficiency and rapidity of mRNA transfection suggested that the novel self-assembled mRNA/tri-cTatB platform functions and with PCI significantly activated its performance, making it a promising platform for mRNA gene therapy.

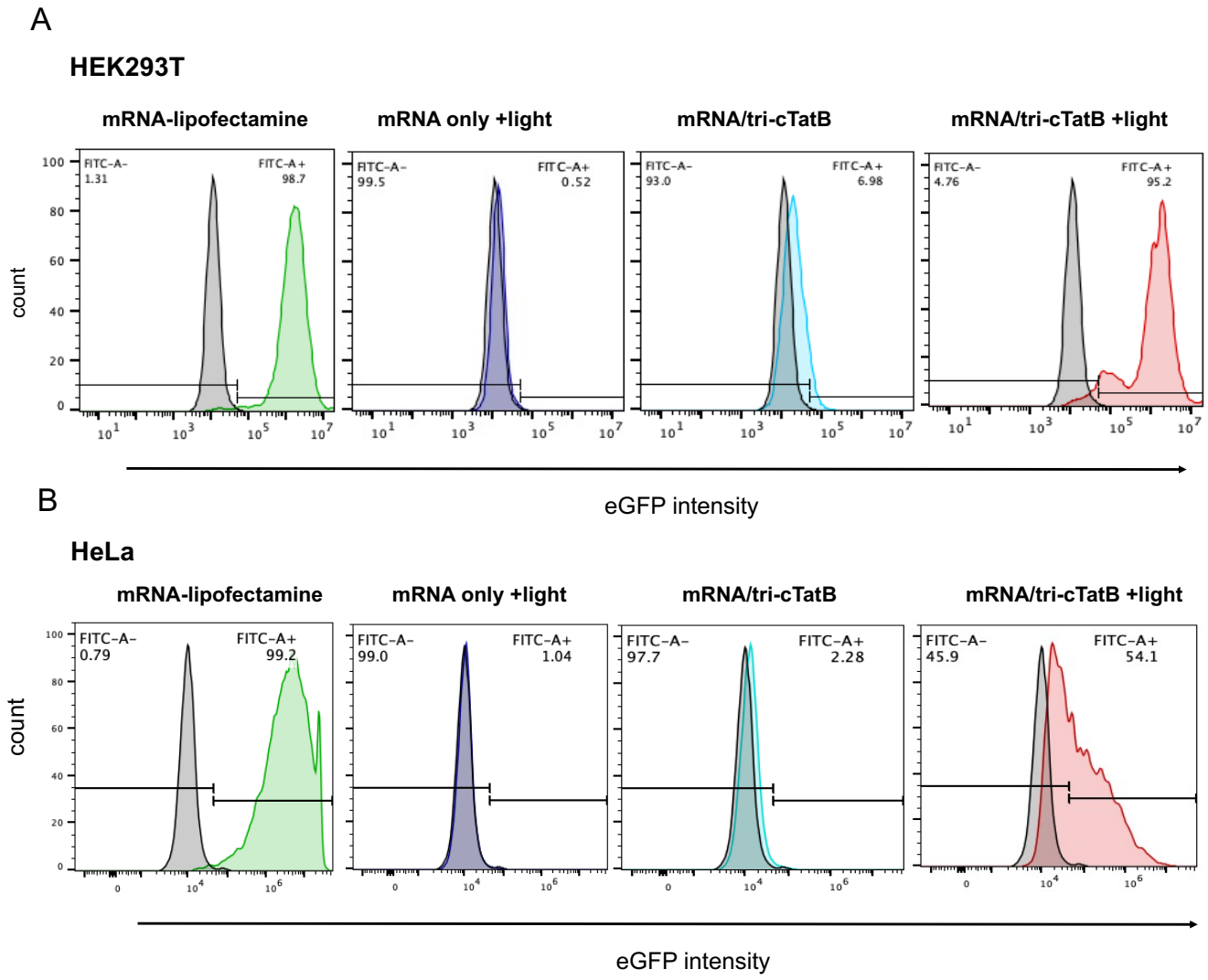

Figure 5.10. The expression of eGFP mediated by mRNA/tri-cTatB transfection. Flow cytometry quantification of HEK293T and HeLa cells eGFP expression level. Fimaporfin was

pre-treated to cells. The delivery period of all conditions is 1 hour apart from the positive control lipofectamine-mRNA. Cells were collected and assessed after 24 hours of incubation

5.4 Discussion and Conclusion

5.4.1 Gene silencing by light-activated siRNA/tri-cTatB delivery

In this chapter, a CPP-mediated light-activated system was used to internalise siRNA into cancer cells. siRNA that was conveyed into cells through the action of self-assembled siRNA/tri-cTatB peptide complexes retained the ability to knockdown target protein and predicted biological outcomes. The rationale for introducing light irradiation relies on photochemical internalisation (PCI), a novel minimally invasive treatment which has shown promising preclinical results in enhancing the effect of anticancer drugs through initiating localised drug release[176]. To understand the safety profile of PCI, the viability of cells when treated with fimaporfin, light, siRNA/tri-cTatB and combinations of these were investigated. The results showed that HeLa and MDA-MB-231 cells remained almost fully viable when they were treated with the photosensitiser fimaporfin alone (0.35 μg/ml), siRNA/tri-cTatB alone, or light alone (Figure 5.3). This was consistent with earlier reports that treatment with fimapofin and the appropriate dosage of visible light illumination alone does not substantially affect the viability of most cell types, although some studies have shown that fimaporfin was slightly cytotoxic in some cell lines without irradiation[177]. The combination of fimaporfin and light induces PCI in the membrane of endocytic vesicles, causing membrane structure damage and, inevitably, associated cytotoxicity[178]. This explains the slightly decreased cell viability (10% of MDA-MB-231 and 17.2% of HeLa cells) when fimaporfin was combined with light irradiation. The cytotoxicity of PCI (PS and light combined) is a desired feature in cancer treatment applications, with the advantage that the toxicity is limited to the area exposed to light irradiation. PCI-mediated therapy can be considered to be a more selective procedure than systemic chemotherapy, with reduced systemic effects and activity restricted to irradiated tissues[179]. Notably, a marked reduction in cell viability was observed when cells were

transfected with the commercial transfection reagent Lipofectamine, consistent with its recognised limitation for *in vivo* applications due to systemic toxicity[180].

A major advantage of the light-controlled delivery system is its intracellular site-specific action. The fact that the photochemical-induced delivery of the specific macromolecular drug is confined to the illuminated area only is an advantage for *in vivo* studies. siRNA delivery would be limited to the desired cells, thereby further reducing non-specific effects[152]. In Chapter 4, it was shown that in combination with PCI, the intracellular localisation of siRNA shifts from vesicles to the cytosol. To examine whether the redistributed siRNA can induce RNAi-mediated gene silencing, the protein downregulation efficacy of the system was evaluated. 1 hour of siGAPHD/tri-cTatB internalisation followed by light irradiation was found to induce significant downregulation of the abundant protein GAPDH compared to the treatment without light (Figure 5.4). This result indicated that tri-cTatB complexes can transfect a sufficient amount of siRNA in a short time and that light triggered the function of siRNA with spatiotemporal precision, revealing the great potential of light-controlled tri-cTatB complexes for delivery of nucleic acids in broader applications.

5.4.2 Light-controlled transfection of siRNA by tri-cTatB for cancer therapy

A system that can deliver siRNA rapidly and at low carrier concentration and which triggers the gene silencing effect at a specific time and site has now been established. The next step was to apply this system to cancer therapy. In 2009, the first-in-man dose-escalation trial of PCI for bleomycin delivery in patients with different types of solid malignancies started (phase 1, NCT00993512, ClinicalTrials.gov)[181]. The trial ended with the results demonstrating the safety of the photosensitizer used for PCI, which is TPCS2a, illuminated by 652-nm laser light with an energy of 60 J/cm^2. Oliveira S. and co-workers first applied PCI to siRNA delivery in 2007 and proved the efficient anti-EGFR effect of the siRNA/lipofectamine complexes when using

TPPS2a as the photosensitizer[152]. Those studies provided evidence to support combining PCI with the siRNA/tri-cTatB complex delivery system in oncogenic applications.

In this study, significant oncogene PLK1 protein downregulation was observed under the treatment of siPLK1/tri-cTaB plus light in breast cancer cell lines, MDA-MB-231 and MCF-7 (Figure 5.5). In contrast, siPLK1/tri-cTaB transfection in the absence of light did not exhibit significant gene silencing compared to the negative (untreated) control, indicating that the gene silencing effect was light-activated. Since downregulation of PLK1 leads to cell cycle arrest followed by apoptosis[172], cancer cell apoptosis was examined as an experimental endpoint. Early cell apoptosis and late apoptosis/death (Figure 5.6, 6.7) were both observed after 24 hours and 72 hours of treatments, respectively, demonstrating the cancer therapeutic potential of this novel delivery platform. Notably, in the viability assay, PCI induced 14% phototoxicity in MDA-MB-231 cells, highlighting that PCI not only regulated siRNA function but also contributed to cancer cell apoptosis on its own.

A major challenge, however, for this system in future applications, is the difficulty of efficiently exciting photosensitisers located deeper than 1 cm from the tumour surface. Nevertheless, this has been attenuated by the development of lasers that can be coupled into fibre optics, which in turn can be inserted into endoscopes (e.g., nasendoscopy and laryngoscopy). Nowadays, it is possible to illuminate regions in the human body that were previously inaccessible, e.g., lungs, gastrointestinal tract and bladder[182,183]. As this system does not require conjugation or specific modification, future studies could explore delivering siRNAs targeting various oncogenic proteins using tri-cTatB in combination with light, aiming to develop multiple cancer therapeutics simultaneously.

5.4.3 Light-controlled delivery of mRNA

mRNA-based gene therapy shows promising potential in novel vaccine development against infectious diseases and new therapeutics for a wide range of indications including cancer.

Peptide-based mRNA delivery systems are gaining momentum due to the versatility of peptide sequences. The potential of using CPP for mRNA delivery has been explored before but not widely studied[115]. For example, PepFect14 has been developed as a platform for ovarian cancer therapy by forming complexes with reporter mRNA[62]. Given the successful delivery and function of light-controlled tri-cTatB delivery of siRNA, we wished to expand the delivery system to mRNA. Similar to the method of siRNA/tri-cTatB complexes, the mRNA was allowed to form complexes with tri-cTatB non-covalently, which occurs between the anionic phosphate group of mRNA and the cationic amino acid of the CPP. This method is facile, consistent, and preserves the function of mRNA[184].

In this study, it was hypothesised that mRNA could form complexes with tri-cTatB and internalise into cells via the endocytosis pathway, and that the application of PCI could trigger the endosomal escape of mRNA. According to Figure 5.8, this hypothesis was proved: tri-cTatB successfully facilitated the internalisation of mRNA via complex co-delivery, and light irradiation triggered the Cy5-mRNA signals from particle foci to a homogeneous distribution in the cytosol, indicating the endosome release of mRNA. The expression of eGFP from mRNA transfected by tri-cTatB complexes (Figure 5.9, 5.10) suggested that mRNA function was maintained during delivery. The bioactivity of internalised mRNA may have been preserved due to protection provided by the condensed complex of mRNA and tri-cTatB, a hypothesis that requires further investigation in future studies. Compared to the complexes delivery alone, light has significantly improved the mRNA endosome release and expression in HeLa and HEK293T cells. Since this proof-of-concept study demonstrated efficient mRNA internalisation through mRNA/tri-cTatB complexes and light-activated expression in cancer cells, further investigation into delivering antigen-encoding mRNA using this platform for cancer therapy is warranted. We are particularly interested in delivering antibody-encoding mRNAs (such as anti-HER2 and anti-PD1) as antibody therapeutics in tumour models.

5.4.4 Conclusion

In this Chapter, the light-activated tri-cTatB and siRNA self-assembled complexes delivery platform was studied and its great potential in cancer application was demonstrated. The platform also demonstrated versatility due to its success in delivering mRNA. The successful application of this novel delivery platform to siRNA and mRNA transfection suggests that light-induced CPP-based delivery may represent an efficient and universal platform for gene therapy and vaccines. To illustrate this, it is envisioned that other nucleic acids such as plasmid DNA, and microRNA could, in principle, be delivered using this platform. In addition to the protein (antibody) delivery ability of tri-cTatB that was presented in previous work, tri-cTatB and nucleic acid complexes may also be employed as a tool for the delivery of protein/nucleic complexes, which is a critical step in CRISPR/Cas9 genome editing[185]. Moreover, future work must be conducted to find the optimal photosensitiser, photosensitiser concentration, peptide and nucleic acid concentration, nitrogen to phosphate (N/P) ratio for complexation, and irradiation energy dose for different cell lines when planning *in vivo* work.

Chapter 6

Discussion and future work

The primary aim of this doctoral research was to develop strategies to enhance the delivery of nucleic acids. The therapeutic possibilities of nucleic acids have not yet been utilised to their full potential, mostly because of the underperformance of the carriers. Since the proven highly efficient delivery capability of the trimeric cyclic derivative of TAT peptide, tri-cTatB, in the co-delivery of antibodies in previous studies, this study now utilises this peptide to improve the delivery of nucleic acids. It was found that siRNA can form condensed complexes with tri-cTatB via electrostatic interactions and that the complex internalises into cells via the clathrin-mediated endocytosis pathway. Triggering endosomal release is a key strategy for enhancing nucleic acid efficacy. To this end, this study incorporated the concept of photochemical internalisation to further optimise the delivery system, achieving efficient endosomal escape following light irradiation while preserving the functionality of the nucleic acid cargo (Figure 6.1).

The emphasis of this chapter is the broader position of this work in the context of the related published literature, its limitations and potential avenues for future research.

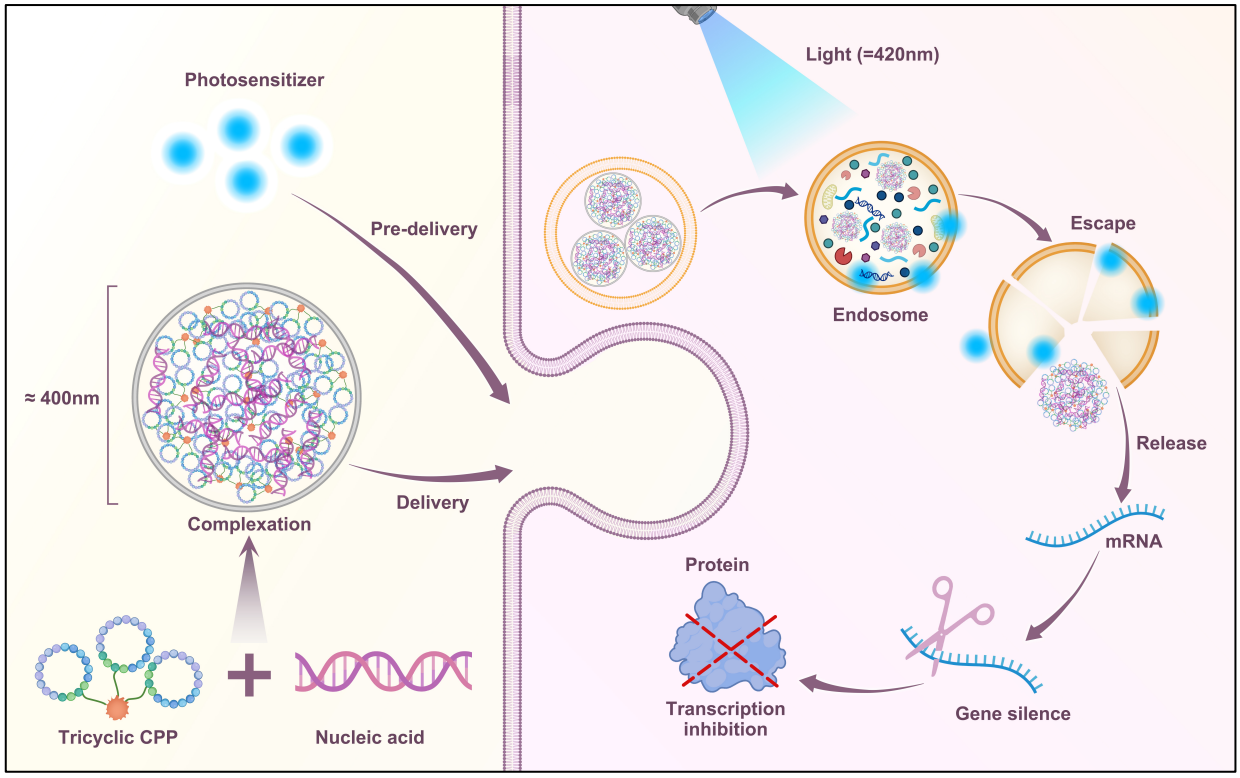

Figure 6.1 Graphical scheme of the light-activated siRNA/tri-cTatB delivery platform.

6.1 Nucleic acid delivery via self-assembled complexes

To insert tri-cTatB into the delivery of siRNA, the method of co-incubation, covalent linkage and complex formation was considered. We ultimately concentrated our research on the delivery of nucleic acids (NAs) and peptide self-assembled complexes. This approach leverages the electrostatic interaction between cationic CPPs and anionic nucleic acids, enabling the formation of versatile complexes through a simple "mix and incubate" technique at room temperature[186]. This strategy is not only easy to execute but also highly cost-effective, as it eliminates the need for additional reactions or purification steps. Notably, incorporating the payload by electrostatic interaction can lead to instability and premature release of nucleic acid[187]. It is crucial to find an optimal balance between peptide and siRNA, avoiding charge neutralisation, and preserving a positive overall charge of the particle. In Chapter 3, the N/P ratio of the siRNA and tri-cTatB was optimised and an overall positively charged complex was characterised.

Although the stability of siRNA/tri-cTatB in the presence of serum has been demonstrated *in vitro*, the maintenance of stability in the presence of physiological conditions (serum and blood) *in vivo* is more crucial. Indeed, the stability of complex particles is directly impacted by their size and homogeneity. The size of nano-complexes directly determines their surface area interacting with biological environments, thus influencing their blood circulation time and their biodistribution[115]. In general, the kidneys filter particles smaller than 6 nm, whereas complexes larger than 50 nm and smaller than 200 nm are captured by the liver and spleen[188]. While particles flow through the liver sinusoidal capillaries, it has been suggested that scavenger receptors on Kupffer cells recognize the opsonins adsorbed on the particle surface and engulf them. Particles with size lower than the human fenestrae diameter (103-113nm) are likely to be captured[189]. Since DLS and TEM suggested siRNA/tri-cTatB particle size at 450 nm in diameter, in future *in vivo* studies, it is important to control the size and homogeneity of the complex and to monitor the *in vivo* tissue biodistribution.

Peptide-based nanoscale complexes are well-suited for NA delivery due to their versatility. Compared to other carriers, CPPs are relatively non-cytotoxic and can be easily degraded into amino acids, making them suitable for preclinical and clinical studies. However, CPP-mediated strategies are still not used in clinical applications despite their efficiency in delivering therapeutic cargo into cells. To push forward with clinical translation, several features should be taken into account. First, the stability, size, and monodispersity of the peptide-assembled complexes should be controlled. It is possible that siRNA/tri-cTatB complexes might sequestrate in the liver *in vivo* due to the large particle size. To address this, in future studies, the size could be optimised by grafting PEG motifs or fatty acids onto the CPPs, as reported by various publications[190,191]. Indeed, the PEGylation of nanoparticles reduces their size without influencing cellular internalisation or their siRNA knockdown efficacy[171]. PEGylation can also reduce the opsonisation of nanoparticles, minimising their clearance by the reticuloendothelial system (RES) and leading to longer blood circulation times and improved pharmacokinetic properties[192]. Secondly, the development of stimulus-responsive "smart" CPP-based systems that are pH- or enzyme-triggered has been predicted by some investigators[193]. The engineered "smart" peptide-based complex is expected to penetrate many physiological barriers without inducing undesirable host immune responses or losing its colloidal stability after intravenous injection. Finally, the cell or tissue specificity of internalisation of peptide-based complexes should be addressed, and will be discussed in the next section.

6.2 Site-specific delivery of nucleic acids

Although nucleic acid/tri-cTatB complexes have achieved efficient and controlled internalisation via light activation, strategies for targeted delivery and the specificity of the site of action require further research.

6.2.1 Delivery specificity achieved by CPP modification

To further optimise delivery efficiency in future studies, it is planned to improve the specificity of tri-cTatB based complexes for tumour targets by the addition of homing sequences that recognise specific cell surface proteins that are overexpressed by cancer cells[194]. Unlike passive targeting, which relies on the accumulation of nanoparticles in the liver, lungs, or tumours through enhanced permeability and retention effects, active targeting requires the appropriate ligand molecules to direct particles to specific organs or tumour sites. Therefore, identifying the optimal ligand to graft onto peptide complexes is a crucial factor for their successful tumour-targeted delivery[115]. There are several strategies to selectively target cancer cells with CPPs conjugated with targeting ligands such as tumour-targeting peptides. Screening of phage-display libraries has resulted in the discovery of several tumour-targeted peptides that selectively recognise molecular markers on tumour blood vessels[195]. For example, the five residue homing peptide CREKA, which was identified by *in vivo* screening of phage-displayed peptide libraries in tumour-bearing MMTV-PyMT transgenic breast cancer mice, has been combined with the pVEC peptide to yield a CPP with tumour-homing specificity[196]. To improve the tumour-targeting capability of nucleic acid and tri-cTatB complexes, it is possible to conjugate a tumour-targeted peptide onto tri-cTatB to make a chimeric peptide.

6.2.2 Site-specific delivery achieved by PCI

Given the nature of siRNA/tri-cTatB internalisation through endocytosis, combining the PCI strategy with the gene delivery platform could achieve site-specific delivery in oncologic applications. Due to the local and focused light-dependent activation, PCI is a method with a high site-specificity that limits the biological effect to illuminated areas only, a property that should lower potential systemic side effects of the delivered drug. In addition, photodynamic therapy has been established as an accepted cancer treatment modality showing low or no systemic side effects[136]. The current study has shown that PCI can re-localise siRNA from

endocytic vesicles into the cytosol. With the addition of light, siRNA and mRNA biological function was significantly enhanced.

Due to the advantage of site-specificity, gene delivery platforms involving PCI are especially promising for cancer therapy. Light illumination confined to the tumour area (including also a normal tissue margin) can guarantee that only the endo-lysosomes in the illuminated region will be ruptured and the trojan-horse carriers will only release their cargo within the cells resident in the irradiated region. For example, in recent work by Ekiner *et al*. a mesoporous organo-silica nanoparticle (PHT-PMO) based on a silylated Zn-phthalocyanine precursor was developed. PHT-PMO nanoparticles elicited no toxicity to MCF7 human breast adenocarcinoma cells in dark but were highly phototoxic when irradiated at 650 nm (71% death) and 810 nm (63% death) and even more so at 760 nm (80% death)[197].

6.3 Future perspectives and limitations of CPP PCI synergistic delivery

In this study, a particular point of interest in the application of the strategy of PCI in combination with the peptide tri-cTatB is that the cationic nature of tri-cTatB could play a role in bringing the singlet oxygen-generating photosensitizer in close proximity to endosomal membranes. Although many photosensitizers have been developed for photodynamic therapy, we chose to use an amphiphilic photosensitizer, TPCS2a/Fimaporfin, since it has good membrane permeability and has been used successfully in clinical applications. In previous studies, CPP-PS conjugation has been widely explored for photo-triggered cargo delivery. For example, Tat and chlorin e6 conjugation was used to enhance cytotoxin protein delivery[198], and Alexa546 was conjugated to TatU1A (TAT fuse with human U1A-derived RNA-binding protein) for cytosolic delivery of siRNA[137]. Our study first explored the co-delivery of photosensitizer in combination with CPP/RNA complexes, which proved to have a similar mechanism of action as CPP-PS conjugation but with a simplified synthesis process.

Sufficient light energy is a basic requirement for photosensitizers to easily generate ROS. Therefore, light dose is key in determining the efficacy of PCI. In most clinical uses of photosensitizers for PDT, the effective light dose is around 100–200 J/cm^2 [199]. Unlike PDT, PCI generally requires a lower-light dose. PCI of the Tat-porphyrin conjugate with saporin required 5 min irradiation with blue light at 2.1 J/cm^2 [200]. PCI with TatU1A-Alexa546 or TatU1A-Alexa633 required irradiation at 20 J/cm^2 [137]. Our study suggested that irradiation at 11 J/cm^2 can trigger sufficient siRNA and mRNA cargo release. Such a light dose causes very low cytotoxicity and allows for the repetitive delivery of cargo at different time points. In future studies, it would be worthwhile to optimise the light energy for various cancer cell lines and try low-intensity long-duration PCI (low energy for a long time) since it was reported to be more effective than standard acute PCI[92].

In cancer treatment, PCI combined with nanocarrier delivery has advantages and limitations. As discussed earlier, photosensitizers delivered with CPPs selectively accumulate in the tumour site and show cytotoxicity only in the area exposed to light irradiation. PCI-assisted therapy could be performed instead of surgery in inoperable patients. In addition, light irradiation of the surgical site in patients who underwent tumour removal surgery could decrease the risk of cancer recurrence[201]. However, *in vivo* and clinical studies of PCI are still limited to extensive superficial disease or tumours that can be reached by endoscopy because the local treatment using optical fibre makes it hard to kill the tumour cells present outside the focal area or alter the therapeutic outcomes in patients with advanced-stage cancer. The penetration efficiency of light into deep tissue is limited due to the absorption of light by endogenous biomolecules, making it challenging to effectively excite photosensitizers located more than 1 cm deep[202]. Although recent advancements in microendoscopic technology and laparoscopic light delivery systems have addressed some of these limitations, the application of PCI-activated therapy for treating large and deeply located tumours remains a significant challenge[183].

From the aspect of photosensitizer development, the first generation of photosensitizers approved for clinical use are derivatives of the porphyrin moiety[203], which have limitations including low singlet oxygen quantum yield, high doses needed for therapeutic efficacy, low selectivity to the tumour site, skin photosensitivity, and a long elimination half-life[204]. For cancer treatment, second-generation photosensitisers have been developed to show a higher molar extinction coefficient in the near-infrared region (NIR) than the first-generation photosensitizers and, therefore are capable of excitation in deeper tissue. For example, 5-aminolevulinic acid has shown higher molar extinction coefficient in the NIR and good clinical outcomes in bladder cancer treatment[205].

6.4 Remaining challenges of siRNA and mRNA

In this research, the challenges of inefficient intracellular delivery and endosomal entrapment of nucleic acids have been extensively studied, but other challenges must also be considered from a broader perspective. In addition to the challenges we already introduced in Chapter 1, the current clinical siRNA therapeutics have been limited to applications in hepatocytes since nanoparticles preferentially accumulate in the liver. The delivery of RNAi molecules to target non-hepatic diseases presents considerably greater challenges and will be a key point for the next step *in vivo* investigations of the siRNA/tri-cTatB delivery system. To broaden the applicability of siRNA beyond hepatic tissues, it is crucial to: (i) identify or determine unique receptors or small molecules as the targeted moieties[206]; (ii) propose specific screening or exploration strategies; and (iii) select genetically or clinically feasible target genes involved in specific diseases[207]. Of note, tri-cTatB has been shown *in vivo* in mice to pass across the blood-brain barrier (not published). Therefore, it will be particularly interesting to evaluate the potential of the siRNA/tri-cTatB platform brain and other extrahepatic tissues.

mRNA-based therapeutics show great potential for treating a diverse range of diseases, such as infectious diseases and cancer. Multiple studies have illustrated the advantages of internalised

mRNA over traditional protein because of its superior transfection efficiency, prolonged protein expression along with low risk of genomic integration. However, similar to siRNA, it is prone to degradation by native nucleases. The delivery platform described in this thesis showed not only high delivery efficiency but also effective protection of mRNA. One of the major hurdles to advancing mRNA is immunogenicity; injected or administered mRNAs can be recognized by the immune system as foreign entities, triggering an innate immune response that might reduce the therapeutic efficacy[208]. Attention needs to be paid to this aspect in future investigations of the mRNA/tri-cTatB platform: modifications of the structure or sequence of mRNA nucleotides, optimisation of the coding sequence, and immune system suppression should be considered.

The future of RNA-based drugs hinges on refining their biochemical properties to optimise potency while reducing off-target toxicity and immunogenicity. Specifically, siRNAs and mRNAs will require precise chemical modifications to mitigate nonspecific inflammatory responses, alongside the use of carriers to achieve efficient and targeted delivery to tissues of interest. These considerations have already played a pivotal role in yielding promising clinical outcomes for various drugs, including CALAA-01, TD101, ALN-VSP02, which are siRNA drugs with heavy chemical modifications.[209].

6.5 Conclusion and future work

For future studies, several aspects can be considered to expand the platform applications and facilitate *in vivo* research, including:

1) Add chemical modifications to the siRNA/mRNA/other nucleic acid candidates to enhance stability and circulation time.
2) Modify the tri-cTatB peptide with target ligands to enhance delivery specificity.

3) Optimise the light irradiation dosage for different cell lines or tissues for *in vivo* applications, to obtain a high cargo release rate with low phototoxicity.
4) Finalise research into mRNA transfection by the platform and expand its application in delivering antigen-encoding mRNA for cancer vaccine/therapy.
5) Explore the delivery of protein/nucleic complexes by the platform, which is a critical step in CRISPR/Cas9 genome editing.
6) Exploit the modular nature of the platform to deliver different siRNAs targeting various pathological genes, aiming to develop multiple cancer therapeutics.
7) Explore combination therapy: combining siRNA with other therapeutic agents, such as chemotherapy drugs and antibodies delivered by our platform to enhance efficacy.

From their discovery to date, nucleic acid therapeutics have helped to combat several disease conditions through gene regulations. Although the journey of nucleic acid formulations from *in vitro* to *in vivo* to market is still not in an advanced stage due to the reasons discussed in this thesis, it seems likely that advances in the development of novel, precise delivery systems will render nucleic acids tractable agents for the treatment of various hard-to-drug diseases in the near future. In this research, multiple strategies to enhance the efficacy of siRNA and mRNA were explored. Ultimately, a light-control delivery platform via nucleic acids self-assembling with tri-cTatB peptides was built and demonstrated high transfection efficiency at low carrier concentration in short incubation times in proof-of-concept experiments.

References

1. Organization, W. H. Global cancer burden growing, amidst mounting need for services. (2024).
2. Sung, H. *et al.* Global Cancer Statistics 2020: GLOBOCAN Estimates of Incidence and Mortality Worldwide for 36 Cancers in 185 Countries. *CA. Cancer J. Clin.* **71**, 209–249 (2021).
3. Hanahan, D. & Weinberg, R. A. Hallmarks of Cancer: The Next Generation. *Cell* **144**, 646–674 (2011).
4. Roy, A. & Li, S.-D. Modifying the tumor microenvironment using nanoparticle therapeutics. *Wiley Interdiscip. Rev. Nanomed. Nanobiotechnol.* **8**, 891–908 (2016).
5. Debela, D. T. *et al.* New approaches and procedures for cancer treatment: Current perspectives. *SAGE open Med.* **9**, 20503121211034370 (2021).
6. Pastor, F. *et al.* An RNA toolbox for cancer immunotherapy. *Nat. Rev. Drug Discov.* **17**, 751–767 (2018).
7. Kleinman, M. E. *et al.* Sequence- and target-independent angiogenesis suppression by siRNA via TLR3. *Nature* **452**, 591–597 (2008).
8. Kulkarni, J. A. *et al.* The current landscape of nucleic acid therapeutics. *Nat. Nanotechnol.* **16**, 630–643 (2021).
9. Sridharan, K. & Gogtay, N. J. Therapeutic nucleic acids: current clinical status. *Br. J. Clin. Pharmacol.* **82**, 659–672 (2016).
10. Hajj, K. A. & Whitehead, K. A. Tools for translation: non-viral materials for therapeutic mRNA delivery. *Nat. Rev. Mater.* **2**, 17056 (2017).
11. Gilboa, E., Berezhnoy, A. & Schrand, B. Reducing Toxicity of Immune Therapy Using Aptamer-Targeted Drug Delivery. *Cancer Immunol. Res.* **3**, 1195–1200 (2015).
12. Yin, H., Kauffman, K. J. & Anderson, D. G. Delivery technologies for genome editing. *Nat. Rev. Drug Discov.* **16**, 387–399 (2017).
13. Barber, G. N. STING: infection, inflammation and cancer. *Nat. Rev. Immunol.* **15**, 760–770 (2015).
14. Fire, A. *et al.* Potent and specific genetic interference by double-stranded RNA in Caenorhabditis elegans. *Nature* **391**, 806–811 (1998).
15. Elbashir, S. M. *et al.* Duplexes of 21-nucleotide RNAs mediate RNA interference in cultured mammalian cells. *Nature* **411**, 494–498 (2001).
16. Ahn, I., Kang, C. S. & Han, J. Where should siRNAs go: applicable organs for siRNA drugs. *Exp. Mol. Med.* **55**, 1283–1292 (2023).
17. Castanotto, D. & Rossi, J. J. The promises and pitfalls of RNA-interference-based

therapeutics. *Nature* **457**, 426–433 (2009).

18. Rand, T. A., Ginalski, K., Grishin, N. V. & Wang, X. Biochemical identification of Argonaute 2 as the sole protein required for RNA-induced silencing complex activity. *Proc. Natl. Acad. Sci.* **101**, 14385–14389 (2004).
19. Ameres, S. L., Martinez, J. & Schroeder, R. Molecular basis for target RNA recognition and cleavage by human RISC. *Cell* **130**, 101–112 (2007).
20. Elbashir, S. M., Lendeckel, W. & Tuschl, T. RNA interference is mediated by 21- and 22-nucleotide RNAs. *Genes Dev.* **15**, 188–200 (2001).
21. Rand, T. A., Petersen, S., Du, F. & Wang, X. Argonaute2 cleaves the anti-guide strand of siRNA during RISC activation. *Cell* **123**, 621–629 (2005).
22. Qin, S. *et al.* mRNA-based therapeutics: powerful and versatile tools to combat diseases. *Signal Transduct. Target. Ther.* **7**, 166 (2022).
23. Mascola, J. R. & Fauci, A. S. Novel vaccine technologies for the 21st century. *Nat. Rev. Immunol.* **20**, 87–88 (2020).
24. Deal, C. E., Carfi, A. & Plante, O. J. Advancements in mRNA Encoded Antibodies for Passive Immunotherapy. *Vaccines* vol. 9 (2021).
25. Conry, R. M. *et al.* Characterization of a messenger RNA polynucleotide vaccine vector. *Cancer Res.* **55**, 1397–1400 (1995).
26. Sahin, U., Karikó, K. & Türeci, Ö. mRNA-based therapeutics—developing a new class of drugs. *Nat. Rev. Drug Discov.* **13**, 759–780 (2014).
27. Eurofins. The Future of RNA Applications: Diagnostics, Therapeutics and Research. https://the-dna-universe.com/2021/04/29/the-future-of-rna-applications-diagnostics-therapeutics-and-research/.
28. Zhou, S., Chen, W., Cole, J. & Zhu, G. Delivery of nucleic acid therapeutics for cancer immunotherapy. *Med. Drug Discov.* **6**, 100023 (2020).
29. Pack, D. W., Hoffman, A. S., Pun, S. & Stayton, P. S. Design and development of polymers for gene delivery. *Nat. Rev. Drug Discov.* **4**, 581–593 (2005).
30. Neumann, E., Schaefer-Ridder, M., Wang, Y. & Hofschneider, P. H. Gene transfer into mouse lyoma cells by electroporation in high electric fields. *EMBO J.* **1**, 841–845 (1982).
31. Capecchi, M. R. High efficiency transformation by direct microinjection of DNA into cultured mammalian cells. *Cell* **22**, 479–488 (1980).
32. Plank, C. *et al.* The magnetofection method: using magnetic force to enhance gene delivery. *Biol. Chem.* **384**, 737–747 (2003).
33. Du, X. *et al.* Advanced physical techniques for gene delivery based on membrane

perforation. *Drug Deliv.* **25**, 1516–1525 (2018).

34. Bulcha, J. T., Wang, Y., Ma, H., Tai, P. W. L. & Gao, G. Viral vector platforms within the gene therapy landscape. *Signal Transduct. Target. Ther.* **6**, 53 (2021).
35. Wang, D., Tai, P. W. L. & Gao, G. Adeno-associated virus vector as a platform for gene therapy delivery. *Nat. Rev. Drug Discov.* **18**, 358–378 (2019).
36. Fukuhara, H., Ino, Y. & Todo, T. Oncolytic virus therapy: A new era of cancer treatment at dawn. *Cancer Sci.* **107**, 1373–1379 (2016).
37. Mendes, B. B. *et al.* Nanodelivery of nucleic acids. *Nat. Rev. Methods Prim.* **2**, 24 (2022).
38. Yan, Y. *et al.* Non-viral vectors for RNA delivery. *J. Control. Release* **342**, 241–279 (2022).
39. Shirley, J. L., de Jong, Y. P., Terhorst, C. & Herzog, R. W. Immune responses to viral gene therapy vectors. *Mol. Ther.* **28**, 709–722 (2020).
40. Felgner, P. L. *et al.* Lipofection: a highly efficient, lipid-mediated DNA-transfection procedure. *Proc. Natl. Acad. Sci.* **84**, 7413–7417 (1987).
41. Iyer, A. K., Duan, Z. & Amiji, M. M. Nanodelivery systems for nucleic acid therapeutics in drug resistant tumors. *Mol. Pharm.* **11**, 2511–2526 (2014).
42. Semple, S. C. *et al.* Rational design of cationic lipids for siRNA delivery. *Nat. Biotechnol.* **28**, 172–176 (2010).
43. Kulkarni, J. A. *et al.* On the formation and morphology of lipid nanoparticles containing ionizable cationic lipids and siRNA. *ACS Nano* **12**, 4787–4795 (2018).
44. Zhang, Y., Sun, C., Wang, C., Jankovic, K. E. & Dong, Y. Lipids and lipid derivatives for RNA delivery. *Chem. Rev.* **121**, 12181–12277 (2021).
45. Witzigmann, D. *et al.* Lipid nanoparticle technology for therapeutic gene regulation in the liver. *Adv. Drug Deliv. Rev.* **159**, 344–363 (2020).
46. Akinc, A. *et al.* The Onpattro story and the clinical translation of nanomedicines containing nucleic acid-based drugs. *Nat. Nanotechnol.* **14**, 1084–1087 (2019).
47. Guo, S. *et al.* Advances in peptide-based drug delivery systems. *Heliyon* **10**, e26009 (2024).
48. Paunovska, K., Loughrey, D. & Dahlman, J. E. Drug delivery systems for RNA therapeutics. *Nat. Rev. Genet.* **23**, 265–280 (2022).
49. Nair, J. K. *et al.* Multivalent N-acetylgalactosamine-conjugated siRNA localizes in hepatocytes and elicits robust RNAi-mediated gene silencing. *J. Am. Chem. Soc.* **136**, 16958–16961 (2014).
50. Springer, A. D. & Dowdy, S. F. GalNAc-siRNA conjugates: leading the way for

delivery of RNAi therapeutics. *Nucleic Acid Ther.* **28**, 109–118 (2018).

51. Debacker, A. J., Voutila, J., Catley, M., Blakey, D. & Habib, N. Delivery of oligonucleotides to the liver with GalNAc: from research to registered therapeutic drug. *Mol. Ther.* **28**, 1759–1771 (2020).
52. Hoyer, J. & Neundorf, I. Peptide Vectors for the Nonviral Delivery of Nucleic Acids. *Acc. Chem. Res.* **45**, 1048–1056 (2012).
53. Desale, K., Kuche, K. & Jain, S. Cell-penetrating peptides (CPPs): an overview of applications for improving the potential of nanotherapeutics. *Biomater. Sci.* **9**, 1153–1188 (2021).
54. González-Cruz, A. O., Hernández-Juárez, J., Ramírez-Cabrera, M. A., Balderas-Rentería, I. & Arredondo-Espinoza, E. Peptide-based drug-delivery systems: A new hope for improving cancer therapy. *J. Drug Deliv. Sci. Technol.* **72**, 103362 (2022).
55. Frankel, A. D. & Pabo, C. O. Cellular uptake of the tat protein from human immunodeficiency virus. *Cell* **55**, 1189–1193 (1988).
56. Joliot, A., Pernelle, C., Deagostini-Bazin, H. & Prochiantz, A. Antennapedia homeobox peptide regulates neural morphogenesis. *Proc. Natl. Acad. Sci. U. S. A.* **88**, 1864–1868 (1991).
57. Agrawal, P. *et al.* CPPsite 2.0: a repository of experimentally validated cell-penetrating peptides. *Nucleic Acids Res.* **44**, D1098-103 (2016).
58. Pooga, M. & Langel, Ü. Classes of Cell-Penetrating Peptides. *Methods Mol. Biol.* **1324**, 3–28 (2015).
59. Tai, W. & Gao, X. Functional peptides for siRNA delivery. *Adv. Drug Deliv. Rev.* **110**–**111**, 157–168 (2017).
60. Nakayama, F. *et al.* Fibroblast growth factor-12 (FGF12) translocation into intestinal epithelial cells is dependent on a novel cell-penetrating peptide domain: involvement of internalization in the in vivo role of exogenous FGF12. *J. Biol. Chem.* **286**, 25823–25834 (2011).
61. Cousins, M. J., Pickthorn, K., Huang, S., Critchley, L. & Bell, G. The safety and efficacy of KAI-1678- an inhibitor of epsilon protein kinase C (εPKC)-versus lidocaine and placebo for the treatment of postherpetic neuralgia: a crossover study design. *Pain Med.* **14**, 533–540 (2013).
62. van den Brand, D. *et al.* Peptide-mediated delivery of therapeutic mRNA in ovarian cancer. *Eur. J. Pharm. Biopharm.* **141**, 180–190 (2019).
63. Smith, K. M., Himiari, Z., Tsimbalyuk, S. & Forwood, J. K. Structural Basis for Importin-α Binding of the Human Immunodeficiency Virus Tat. *Sci. Rep.* **7**, 1650

(2017).

64. Truant, R. & Cullen, B. R. The arginine-rich domains present in human immunodeficiency virus type 1 Tat and Rev function as direct importin beta-dependent nuclear localization signals. *Mol. Cell. Biol.* **19**, 1210–1217 (1999).
65. McClorey, G. & Banerjee, S. Cell-Penetrating Peptides to Enhance Delivery of Oligonucleotide-Based Therapeutics. *Biomedicines* **6**, (2018).
66. Choi, S. W., Lee, S. H., Mok, H. & Park, T. G. Multifunctional siRNA delivery system: Polyelectrolyte complex micelles of six-arm PEG conjugate of siRNA and cell penetrating peptide with crosslinked fusogenic peptide. *Biotechnol. Prog.* **26**, 57–63 (2010).
67. Geng, J. *et al.* Emerging landscape of cell-penetrating peptide-mediated nucleic acid delivery and their utility in imaging, gene-editing, and RNA-sequencing. *J. Control. Release* **341**, 166–183 (2022).
68. Zeng, Z. *et al.* A Tat-conjugated peptide nucleic acid Tat-PNA-DR inhibits hepatitis B virus replication in vitro and in vivo by targeting LTR direct repeats of HBV RNA. *Mol. Ther. Acids* **5**, (2016).
69. Kanazawa, T., Akiyama, F., Kakizaki, S., Takashima, Y. & Seta, Y. Delivery of siRNA to the brain using a combination of nose-to-brain delivery and cell-penetrating peptide-modified nano-micelles. *Biomaterials* **34**, 9220–9226 (2013).
70. Simeoni, F., Morris, M. C., Heitz, F. & Divita, G. Insight into the mechanism of the peptide-based gene delivery system MPG: implications for delivery of siRNA into mammalian cells. *Nucleic Acids Res.* **31**, 2717–2724 (2003).
71. Crombez, L. *et al.* Targeting cyclin B1 through peptide-based delivery of siRNA prevents tumour growth. *Nucleic Acids Res.* **37**, 4559–4569 (2009).
72. Khaitov, M. *et al.* Treatment of COVID-19 patients with a SARS-CoV-2-specific siRNA-peptide dendrimer formulation. *Allergy* **78**, 1639–1653 (2023).
73. Wilhelm, S. *et al.* Analysis of nanoparticle delivery to tumours. *Nat. Rev. Mater.* **1**, 16014 (2016).
74. Han, X., Mitchell, M. J. & Nie, G. Nanomaterials for therapeutic RNA delivery. *Matter* **3**, 1948–1975 (2020).
75. Shi, J., Kantoff, P. W., Wooster, R. & Farokhzad, O. C. Cancer nanomedicine: progress, challenges and opportunities. *Nat. Rev. cancer* **17**, 20–37 (2017).
76. Faraji, A. H. & Wipf, P. Nanoparticles in cellular drug delivery. *Bioorg. Med. Chem.* **17**, 2950–2962 (2009).
77. Walkey, C. D. & Chan, W. C. W. Understanding and controlling the interaction of

nanomaterials with proteins in a physiological environment. *Chem. Soc. Rev.* **41**, 2780–2799 (2012).

78. Dowdy, S. F. Overcoming cellular barriers for RNA therapeutics. *Nat. Biotechnol.* **35**, 222–229 (2017).
79. Liberali, P., Rämö, P. & Pelkmans, L. Protein Kinases: Starting a Molecular Systems View of Endocytosis. *Annu. Rev. Cell Dev. Biol.* **24**, 501–523 (2008).
80. Hu, Y.-B., Dammer, E. B., Ren, R.-J. & Wang, G. The endosomal-lysosomal system: from acidification and cargo sorting to neurodegeneration. *Transl. Neurodegener.* **4**, 18 (2015).
81. Varkouhi, A. K., Scholte, M., Storm, G. & Haisma, H. J. Endosomal escape pathways for delivery of biologicals. *J. Control. release Off. J. Control. Release Soc.* **151**, 220–228 (2011).
82. Brown, C. R. *et al.* Investigating the pharmacodynamic durability of GalNAc-siRNA conjugates. *Nucleic Acids Res.* **48**, 11827–11844 (2020).
83. Juliano, R. L. Intracellular Trafficking and Endosomal Release of Oligonucleotides: What We Know and What We Don't. *Nucleic Acid Ther.* **28**, 166–177 (2018).
84. Czauderna, F. *et al.* Structural variations and stabilising modifications of synthetic siRNAs in mammalian cells. *Nucleic Acids Res.* **31**, 2705–2716 (2003).
85. Detzer, A. *et al.* Increased RNAi is related to intracellular release of siRNA via a covalently attached signal peptide. *Rna* **15**, 627–636 (2009).
86. Bramsen, J. B. & Kjems, J. Development of therapeutic-grade small interfering rnas by chemical engineering. *Front. Genet.* **3**, 154 (2012).
87. Juliano, R. L. *et al.* Structure–activity relationships and cellular mechanism of action of small molecules that enhance the delivery of oligonucleotides. *Nucleic Acids Res.* **46**, 1601–1613 (2018).
88. Bramsen, J. B. & Kjems, J. Development of Therapeutic-Grade Small Interfering RNAs by Chemical Engineering. *Front. Genet.* **3**, 154 (2012).
89. Miyoshi, Y. *et al.* Endosomal Escape of Peptide-Photosensitizer Conjugates Is Affected by Amino Acid Sequences near the Photosensitizer. *Bioconjug. Chem.* **31**, 916–922 (2020).
90. Tietz, O., Cortezon-Tamarit, F., Chalk, R., Able, S. & Vallis, K. A. Tricyclic cell-penetrating peptides for efficient delivery of functional antibodies into cancer cells. *Nat. Chem. 2021* 1–10 (2022) doi:10.1038/s41557-021-00866-0.
91. Schindelin, J. *et al.* Fiji: an open-source platform for biological-image analysis. *Nat. Methods* **9**, 676–682 (2012).

92. Shin, D. *et al.* The effects of low irradiance long duration photochemical internalization on glioma spheroids. *Photodiagnosis Photodyn. Ther.* **26**, 442–447 (2019).
93. Madani, F., Lindberg, S., Langel, Ü., Futaki, S. & Gräslund, A. Mechanisms of cellular uptake of cell-penetrating peptides. *J. Biophys.* **2011**, 414729 (2011).
94. Brock, R. The Uptake of Arginine-Rich Cell-Penetrating Peptides: Putting the Puzzle Together. *Bioconjug. Chem.* **25**, 863–868 (2014).
95. Lättig-Tünnemann, G. *et al.* Backbone rigidity and static presentation of guanidinium groups increases cellular uptake of arginine-rich cell-penetrating peptides. *Nat. Commun.* **2**, 453 (2011).
96. N, N. *et al.* Covalent attachment of cyclic TAT peptides to GFP results in protein delivery into live cells with immediate bioavailability. *Angew. Chem. Int. Ed. Engl.* **54**, 1950–1953 (2015).
97. Shirazi, A. N., Mozaffari, S., Sherpa, R. T., Tiwari, R. & Parang, K. Efficient Intracellular Delivery of Cell-Impermeable Cargo Molecules by Peptides Containing Tryptophan and Histidine. *Molecules* **23**, (2018).
98. Ovacik, M. & Lin, K. Tutorial on Monoclonal Antibody Pharmacokinetics and Its Considerations in Early Development. *Clin. Transl. Sci.* **11**, 540–552 (2018).
99. Freire, J. M., Almeida Dias, S., Flores, L., Veiga, A. S. & Castanho, M. A. R. B. Mining viral proteins for antimicrobial and cell-penetrating drug delivery peptides. *Bioinformatics* **31**, 2252–2256 (2015).
100. Fu, J., Yu, C., Li, L. & Yao, S. Q. Intracellular Delivery of Functional Proteins and Native Drugs by Cell-Penetrating Poly(disulfide)s. *J. Am. Chem. Soc.* **137**, 12153–12160 (2015).
101. Erazo-Oliveras, A. *et al.* The Late Endosome and Its Lipid BMP Act as Gateways for Efficient Cytosolic Access of the Delivery Agent dfTAT and Its Macromolecular Cargos. *Cell Chem. Biol.* **23**, 598–607 (2016).
102. Angeles-Boza, A. M., Erazo-Oliveras, A., Lee, Y. J. & Pellois, J. P. Generation of endosomolytic reagents by branching of cell-penetrating peptides: Tools for the delivery of bioactive compounds to live cells in cis or trans. *Bioconjug. Chem.* **21**, 2164–2167 (2010).
103. Lee, S. H., Castagner, B. & Leroux, J.-C. Is there a future for cell-penetrating peptides in oligonucleotide delivery? *Eur. J. Pharm. Biopharm.* **85**, 5–11 (2013).
104. Muratovska, A. & Eccles, M. R. Conjugate for efficient delivery of short interfering RNA (siRNA) into mammalian cells. *FEBS Lett.* **558**, 63–68 (2004).

105. Turner, J. J. *et al.* RNA targeting with peptide conjugates of oligonucleotides, siRNA and PNA. *Blood Cells, Mol. Dis.* **38**, 1–7 (2007).
106. Lee, Y.-J., Erazo-Oliveras, A. & Pellois, J.-P. Delivery of Macromolecules into Live Cells by Simple Co-incubation with a Peptide. *ChemBioChem* **11**, 325–330 (2010).
107. Eguchi, A. *et al.* Efficient siRNA delivery into primary cells by a peptide transduction domain-dsRNA binding domain fusion protein. *Nat. Biotechnol.* **27**, 567–571 (2009).
108. Kim, S. W. *et al.* RNA interference in vitro and in vivo using an arginine peptide/siRNA complex system. *J. Control. Release* **143**, 335–343 (2010).
109. Skotland, T., Iversen, T. G., Torgersen, M. L. & Sandvig, K. Cell-penetrating peptides: possibilities and challenges for drug delivery in vitro and in vivo. *Molecules* **20**, 13313–13323 (2015).
110. Chiu, Y.-L., Ali, A., Chu, C., Cao, H. & Rana, T. M. Visualizing a Correlation between siRNA Localization, Cellular Uptake, and RNAi in Living Cells. *Chem. Biol.* **11**, 1165–1175 (2004).
111. Wang, H. *et al.* Biocompatible, chimeric peptide-condensed supramolecular nanoparticles for tumor cell-specific siRNA delivery and gene silencing. *Chem. Commun.* **50**, 7806–7809 (2014).
112. Ruseska, I. & Zimmer, A. Internalization mechanisms of cell-penetrating peptides. *Beilstein J. Nanotechnol.* **11**, 101–123 (2020).
113. Tünnemann, G. *et al.* Cargo-dependent mode of uptake and bioavailability of TAT-containing proteins and peptides in living cells. *FASEB J. Off. Publ. Fed. Am. Soc. Exp. Biol.* **20**, 1775–1784 (2006).
114. Kosuge, M., Takeuchi, T., Nakase, I., Jones, A. T. & Futaki, S. Cellular internalization and distribution of arginine-rich peptides as a function of extracellular peptide concentration, serum, and plasma membrane associated proteoglycans. *Bioconjug. Chem.* **19**, 656–664 (2008).
115. Boisguérin, P., Konate, K., Josse, E., Vivès, E. & Deshayes, S. Peptide-Based Nanoparticles for Therapeutic Nucleic Acid Delivery. *Biomedicines* vol. 9 (2021).
116. Wender, P. A. *et al.* The design, synthesis, and evaluation of molecules that enable or enhance cellular uptake: peptoid molecular transporters. *Proc. Natl. Acad. Sci. U. S. A.* **97**, 13003–13008 (2000).
117. Derossi, D., Williams, E. J., Green, P. J., Dunican, D. J. & Doherty, P. Stimulation of mitogenesis by a cell-permeable PI 3-kinase binding peptide. *Biochem. Biophys. Res. Commun.* **251**, 148–152 (1998).
118. F, M., S, L., U, L., S, F. & A, G. Mechanisms of cellular uptake of cell-penetrating

peptides. *J. Biophys.* **2011**, (2011).

119. Lundberg, P. & Langel, U. A brief introduction to cell-penetrating peptides. *J. Mol. Recognit.* **16**, 227–233 (2003).
120. Konate, K. *et al.* Peptide-Based Nanoparticles to Rapidly and Efficiently "Wrap 'n Roll" siRNA into Cells. *Bioconjug. Chem.* **30**, 592–603 (2019).
121. Margus, H., Padari, K. & Pooga, M. Insights into cell entry and intracellular trafficking of peptide and protein drugs provided by electron microscopy. *Adv. Drug Deliv. Rev.* **65**, 1031–1038 (2013).
122. Kauffman, K. J. *et al.* Optimization of Lipid Nanoparticle Formulations for mRNA Delivery in Vivo with Fractional Factorial and Definitive Screening Designs. *Nano Lett.* **15**, 7300–7306 (2015).
123. Wadia, J. S., Stan, R. V & Dowdy, S. F. Transducible TAT-HA fusogenic peptide enhances escape of TAT-fusion proteins after lipid raft macropinocytosis. *Nat. Med.* **10**, 310–315 (2004).
124. Kaplan, I. M., Wadia, J. S. & Dowdy, S. F. Cationic TAT peptide transduction domain enters cells by macropinocytosis. *J. Control. release Off. J. Control. Release Soc.* **102**, 247–253 (2005).
125. Richard, J. P. *et al.* Cellular uptake of unconjugated TAT peptide involves clathrin-dependent endocytosis and heparan sulfate receptors. *J. Biol. Chem.* **280**, 15300–15306 (2005).
126. Veldhoen, S., Laufer, S. D., Trampe, A. & Restle, T. Cellular delivery of small interfering RNA by a non-covalently attached cell-penetrating peptide: quantitative analysis of uptake and biological effect. *Nucleic Acids Res.* **34**, 6561–6573 (2006).
127. Trabulo, S., Cardoso, A. L., Mano, M. & De Lima, M. C. P. Cell-Penetrating Peptides-Mechanisms of Cellular Uptake and Generation of Delivery Systems. *Pharmaceuticals (Basel).* **3**, 961–993 (2010).
128. Erazo-Oliveras, A., Muthukrishnan, N., Baker, R., Wang, T.-Y. & Pellois, J.-P. Improving the endosomal escape of cell-penetrating peptides and their cargos: strategies and challenges. *Pharmaceuticals (Basel).* **5**, 1177–1209 (2012).
129. Sonawane, N. D., Szoka, F. C. J. & Verkman, A. S. Chloride accumulation and swelling in endosomes enhances DNA transfer by polyamine-DNA polyplexes. *J. Biol. Chem.* **278**, 44826–44831 (2003).
130. Dowdy, S. F., Setten, R. L., Cui, X.-S. & Jadhav, S. G. Delivery of RNA therapeutics: the great endosomal escape! *Nucleic Acid Ther.* **32**, 361–368 (2022).
131. Du Rietz, H., Hedlund, H., Wilhelmson, S., Nordenfelt, P. & Wittrup, A. Imaging

small molecule-induced endosomal escape of siRNA. *Nat. Commun. 2020 111* **11**, 1–17 (2020).

132. Hou, K. K., Pan, H., Schlesinger, P. H. & Wickline, S. A. A role for peptides in overcoming endosomal entrapment in siRNA delivery - A focus on melittin. *Biotechnol. Adv.* **33**, 931–940 (2015).
133. Lönn, P. *et al.* Enhancing Endosomal Escape for Intracellular Delivery of Macromolecular Biologic Therapeutics. *Sci. Rep.* **6**, (2016).
134. Takayama, K. *et al.* Effect of the attachment of a penetration accelerating sequence and the influence of hydrophobicity on octaarginine-mediated intracellular delivery. *Mol. Pharm.* **9**, 1222–1230 (2012).
135. Chen, L. *et al.* Destabilization of artificial biomembrane induced by the penetration of tryptophan. *Appl. Surf. Sci.* **257**, 5070–5076 (2011).
136. Jerjes, W. *et al.* Photochemical Internalization for Intracellular Drug Delivery. From Basic Mechanisms to Clinical Research. *J. Clin. Med.* **9**, 528 (2020).
137. Ohtsuki, T. *et al.* The molecular mechanism of photochemical internalization of cell penetrating peptide-cargo-photosensitizer conjugates. *Sci. Rep.* **5**, 18577 (2015).
138. Berg, K. & Moan, J. Lysosomes and microtubules as targets for photochemotherapy of cancer. *Photochem. Photobiol.* **65**, 403–409 (1997).
139. Wang, J. T.-W., Berg, K., Høgset, A., Bown, S. G. & MacRobert, A. J. Photophysical and photobiological properties of a sulfonated chlorin photosensitiser TPCS(2a) for photochemical internalisation (PCI). *Photochem. Photobiol. Sci. Off. J. Eur. Photochem. Assoc. Eur. Soc. Photobiol.* **12**, 519–526 (2013).
140. Wang, J. T.-W., Berg, K., Høgset, A., Bown, S. G. & MacRobert, A. J. Photophysical and photobiological properties of a sulfonated chlorin photosensitiser TPCS2a for photochemical internalisation (PCI). *Photochem. Photobiol. Sci.* **12**, 519–526 (2013).
141. Jørgensen, J. A. L., Longva, A. S., Hovig, E. & Bøe, S. L. Evaluation of Biodegradable Peptide Carriers for Light-Directed Targeting. *Nucleic Acid Ther.* **23**, 131–139 (2013).
142. Otterhaug, T. *et al.* Photochemical Internalization Enhanced Vaccination Is Safe, and Gives Promising Cellular Immune Responses to an HPV Peptide-Based Vaccine in a Phase I Clinical Study in Healthy Volunteers. *Front. Immunol.* **11**, (2021).
143. Soe, T. H., Watanabe, K. & Ohtsuki, T. Photoinduced Endosomal Escape Mechanism: A View from Photochemical Internalization Mediated by CPP-Photosensitizer Conjugates. *Molecules* **26**, (2020).
144. Dupont, E., Prochiantz, A. & Joliot, A. Penetratin Story: An Overview BT - Cell-

Penetrating Peptides: Methods and Protocols. in (ed. Langel, Ü.) 29–37 (Springer New York, 2015). doi:10.1007/978-1-4939-2806-4_2.

145. Vercauteren, D. *et al.* The use of inhibitors to study endocytic pathways of gene carriers: optimization and pitfalls. *Mol. Ther.* **18**, 561–569 (2010).
146. Schmidt, N., Mishra, A., Lai, G. H. & Wong, G. C. L. Arginine-rich cell-penetrating peptides. *FEBS Lett.* **584**, 1806–1813 (2010).
147. Gilleron, J. *et al.* Image-based analysis of lipid nanoparticle–mediated siRNA delivery, intracellular trafficking and endosomal escape. *Nat. Biotechnol. 2013 317* **31**, 638–646 (2013).
148. Pei, D. & Buyanova, M. Overcoming Endosomal Entrapment in Drug Delivery. *Bioconjug. Chem.* **30**, 273–283 (2019).
149. Chiu, Y.-L. & Rana, T. M. RNAi in human cells: basic structural and functional features of small interfering RNA. *Mol. Cell* **10**, 549–561 (2002).
150. Yang, B. *et al.* High-throughput screening identifies small molecules that enhance the pharmacological effects of oligonucleotides. *Nucleic Acids Res.* **43**, 1987–1996 (2015).
151. Dowdy, S. F. Overcoming cellular barriers for RNA therapeutics. *Nat. Biotechnol. 2017 353* **35**, 222–229 (2017).
152. Oliveira, S., Fretz, M. M., Høgset, A., Storm, G. & Schiffelers, R. M. Photochemical internalization enhances silencing of epidermal growth factor receptor through improved endosomal escape of siRNA. *Biochim. Biophys. Acta - Biomembr.* **1768**, 1211–1217 (2007).
153. Guo, Y. *et al.* Copackaging photosensitizer and PD-L1 siRNA in a nucleic acid nanogel for synergistic cancer photoimmunotherapy. *Sci. Adv.* **8**, eabn2941 (2024).
154. Roscigno, G. *et al.* Modulating the Crosstalk between the Tumor and the Microenvironment Using SiRNA: A Flexible Strategy for Breast Cancer Treatment. *Cancers (Basel).* **12**, (2020).
155. Wu, S. Y., Lopez-Berestein, G., Calin, G. A. & Sood, A. K. RNAi therapies: drugging the undruggable. *Sci. Transl. Med.* **6**, 240ps7 (2014).
156. Parvani, J. G. & Jackson, M. W. Silencing the roadblocks to effective triple-negative breast cancer treatments by siRNA nanoparticles. *Endocr. Relat. Cancer* **24**, R81–R97 (2017).
157. Jiang, Y., Huo, S., Hardie, J., Liang, X.-J. & Rotello, V. M. Progress and perspective of inorganic nanoparticle-based siRNA delivery systems. *Expert Opin. Drug Deliv.* **13**, 547–559 (2016).
158. Burnett, J. C. & Rossi, J. J. RNA-based therapeutics: current progress and future

prospects. *Chem. Biol.* **19**, 60–71 (2012).

159. Sepp-Lorenzino, L. & Ruddy, M. Challenges and opportunities for local and systemic delivery of siRNA and antisense oligonucleotides. *Clin. Pharmacol. Ther.* **84**, 628–632 (2008).
160. El Dika, I. *et al.* An Open-Label, Multicenter, Phase I, Dose Escalation Study with Phase II Expansion Cohort to Determine the Safety, Pharmacokinetics, and Preliminary Antitumor Activity of Intravenous TKM-080301 in Subjects with Advanced Hepatocellular Carcinoma. *Oncologist* **24**, 747-e218 (2019).
161. Pardi, N., Hogan, M. J., Porter, F. W. & Weissman, D. mRNA vaccines — a new era in vaccinology. *Nat. Rev. Drug Discov.* **17**, 261–279 (2018).
162. He, Q., Gao, H., Tan, D., Zhang, H. & Wang, J.-Z. mRNA cancer vaccines: Advances, trends and challenges. *Acta Pharm. Sin. B* **12**, 2969–2989 (2022).
163. Liu, B., Zhou, H., Tan, L., Siu, K. T. H. & Guan, X.-Y. Exploring treatment options in cancer: tumor treatment strategies. *Signal Transduct. Target. Ther.* **9**, 175 (2024).
164. Miao, L., Zhang, Y. & Huang, L. mRNA vaccine for cancer immunotherapy. *Mol. Cancer* **20**, 41 (2021).
165. Khattak, M. A. *et al.* 663P First-in-human, phase I/II, monotherapy, dose-escalation study of mRNA-4359, an mRNA-encoded PD-L1/IDO1 antigen-specific therapy, in advanced/refractory solid tumors. *Ann. Oncol.* **35**, S521–S522 (2024).
166. Schoenmaker, L. *et al.* mRNA-lipid nanoparticle COVID-19 vaccines: Structure and stability. *Int. J. Pharm.* **601**, 120586 (2021).
167. Lens, S. M. A., Voest, E. E. & Medema, R. H. Shared and separate functions of polo-like kinases and aurora kinases in cancer. *Nat. Rev. Cancer* **10**, 825–841 (2010).
168. Weerdt, B. C. M. van de & Medema, R. H. Polo-Like Kinases: A Team in Control of the Division. *Cell Cycle* **5**, 853–864 (2006).
169. Lowery, D. M., Lim, D. & Yaffe, M. B. Structure and function of Polo-like kinases. *Oncogene* **24**, 248–259 (2005).
170. Liu, Z., Sun, Q. & Wang, X. PLK1, A Potential Target for Cancer Therapy. *Transl. Oncol.* **10**, 22–32 (2017).
171. Tut, T. G. *et al.* Upregulated polo-like kinase 1 expression correlates with inferior survival outcomes in rectal cancer. *PLoS One* **10**, e0129313 (2015).
172. Yim, H. & Erikson, R. L. Plk1-targeted therapies in TP53- or RAS-mutated cancer. *Mutat. Res. Mutat. Res.* **761**, 31–39 (2014).
173. Jimeno, A. *et al.* A fine-needle aspirate–based vulnerability assay identifies polo-like kinase 1 as a mediator of gemcitabine resistance in pancreatic cancer. *Mol. Cancer*

Ther. **9**, 311–318 (2010).

174. Rödel, F. *et al.* Polo-Like Kinase 1 as Predictive Marker and Therapeutic Target for Radiotherapy in Rectal Cancer. *Am. J. Pathol.* **177**, 918–929 (2010).
175. Toyoshima-Morimoto, F., Taniguchi, E. & Nishida, E. Plk1 promotes nuclear translocation of human Cdc25C during prophase. *EMBO Rep.* (2002).
176. Sultan, A. A. *et al.* Disulfonated tetraphenyl chlorin (TPCS2a)-induced photochemical internalisation of bleomycin in patients with solid malignancies: a phase 1, dose-escalation, first-in-man trial. *Lancet Oncol.* **17**, 1217–1229 (2016).
177. Lund, K. *et al.* The novel EpCAM-targeting monoclonal antibody 3–17I linked to saporin is highly cytotoxic after photochemical internalization in breast, pancreas and colon cancer cell lines. *MAbs* **6**, 1038–1050 (2014).
178. Høgset, A. *et al.* Photochemical internalisation in drug and gene delivery. *Adv. Drug Deliv. Rev.* **56**, 95–115 (2004).
179. Jerjes, W. *et al.* Photochemical Internalization for Intracellular Drug Delivery. From Basic Mechanisms to Clinical Research. *J. Clin. Med.* **9**, (2020).
180. Wang, T., Larcher, L. M., Ma, L. & Veedu, R. N. Systematic Screening of Commonly Used Commercial Transfection Reagents towards Efficient Transfection of Single-Stranded Oligonucleotides. *Molecules* **23**, (2018).
181. Berg, K., Dietze, A., Kaalhus, O. & Høgset, A. Site-specific drug delivery by photochemical internalization enhances the antitumor effect of bleomycin. *Clin. cancer Res. an Off. J. Am. Assoc. Cancer Res.* **11**, 8476–8485 (2005).
182. Mang, T. S. Lasers and light sources for PDT: past, present and future. *Photodiagnosis Photodyn. Ther.* **1**, 43–48 (2004).
183. Mallidi, S. *et al.* Beyond the Barriers of Light Penetration: Strategies, Perspectives and Possibilities for Photodynamic Therapy. *Theranostics* **6**, 2458–2487 (2016).
184. Chang, M., Huang, Y.-W., Aronstam, R. S. & Lee, H.-J. Cellular delivery of noncovalently-associated macromolecules by cell-penetrating peptides. *Curr. Pharm. Biotechnol.* **15**, 267–275 (2014).
185. Liu, C., Zhang, L., Liu, H. & Cheng, K. Delivery strategies of the CRISPR-Cas9 gene-editing system for therapeutic applications. *J. Control. release Off. J. Control. Release Soc.* **266**, 17–26 (2017).
186. Ezzat, K. *et al.* PepFect 14, a novel cell-penetrating peptide for oligonucleotide delivery in solution and as solid formulation. *Nucleic Acids Res.* **39**, 5284–5298 (2011).
187. Falato, L., Gestin, M. & Langel, Ü. Cell-Penetrating Peptides Delivering siRNAs: An

Overview. *Methods Mol. Biol.* **2282**, 329–352 (2021).

188. Hoshyar, N., Gray, S., Han, H. & Bao, G. The effect of nanoparticle size on in vivo pharmacokinetics and cellular interaction. *Nanomedicine* **11**, 673–692 (2016).
189. Wisse, E., Jacobs, F., Topal, B., Frederik, P. & De Geest, B. The size of endothelial fenestrae in human liver sinusoids: implications for hepatocyte-directed gene transfer. *Gene Ther.* **15**, 1193–1199 (2008).
190. Qiu, Y. *et al.* Effective mRNA pulmonary delivery by dry powder formulation of PEGylated synthetic KL4 peptide. *J. Control. Release* **314**, 102–115 (2019).
191. Aldrian, G. *et al.* PEGylation rate influences peptide-based nanoparticles mediated siRNA delivery in vitro and in vivo. *J. Control. Release* **256**, 79–91 (2017).
192. Nie, S. Understanding and overcoming major barriers in cancer nanomedicine. *Nanomedicine* **5**, 523–528 (2010).
193. Ye, J. *et al.* CPP-assisted intracellular drug delivery, what is next? *Int. J. Mol. Sci.* **17**, 1892 (2016).
194. Lingasamy, P. & Teesalu, T. Homing peptides for cancer therapy. *Bio-nanomedicine cancer Ther.* 29–48 (2021).
195. Bolhassani, A. Potential efficacy of cell-penetrating peptides for nucleic acid and drug delivery in cancer. *Biochim. Biophys. Acta (BBA)-Reviews Cancer* **1816**, 232–246 (2011).
196. Simberg, D. *et al.* Biomimetic amplification of nanoparticle homing to tumors. *Proc. Natl. Acad. Sci.* **104**, 932–936 (2007).
197. Ekineker, G. *et al.* Phthalocyanine-based mesoporous organosilica nanoparticles: NIR photodynamic efficiency and siRNA photochemical internalization. *Chem. Commun.* **55**, 11619–11622 (2019).
198. Yaghini, E. *et al.* Endolysosomal targeting of a clinical chlorin photosensitiser for light-triggered delivery of nano-sized medicines. *Sci. Rep.* **7**, 6059 (2017).
199. Dąbrowski, J. M. *et al.* Engineering of relevant photodynamic processes through structural modifications of metallotetrapyrrolic photosensitizers. *Coord. Chem. Rev.* **325**, 67–101 (2016).
200. Dondi, R. *et al.* Flexible synthesis of cationic peptide–porphyrin derivatives for light-triggered drug delivery and photodynamic therapy. *Org. Biomol. Chem.* **14**, 11488–11501 (2016).
201. Stranadko, E., Shabarov, V., Riabov, M. & Duvansky, V. Photodynamic therapy in the treatment of esophageal cancer. *Endoscopy* **52**, OP339 (2020).
202. Park, J., Lee, Y.-K., Park, I.-K. & Hwang, S. R. Current Limitations and Recent

Progress in Nanomedicine for Clinically Available Photodynamic Therapy. *Biomedicines* vol. 9 (2021).

203. Allison, R. R. *et al.* Photosensitizers in clinical PDT. *Photodiagnosis Photodyn. Ther.* **1**, 27–42 (2004).
204. Dąbrowski, J. M. & Arnaut, L. G. Photodynamic therapy (PDT) of cancer: from local to systemic treatment. *Photochem. Photobiol. Sci.* **14**, 1765–1780 (2015).
205. Inoue, K. 5-Aminolevulinic acid-mediated photodynamic therapy for bladder cancer. *Int. J. Urol.* **24**, 97–101 (2017).
206. Weng, Y., Xiao, H., Zhang, J., Liang, X.-J. & Huang, Y. RNAi therapeutic and its innovative biotechnological evolution. *Biotechnol. Adv.* **37**, 801–825 (2019).
207. Guo, S., Zhang, M. & Huang, Y. Three 'E' challenges for siRNA drug development. *Trends Mol. Med.* **30**, 13–24 (2024).
208. Nelson, J. *et al.* Impact of mRNA chemistry and manufacturing process on innate immune activation. *Sci. Adv.* **6**, eaaz6893 (2020).
209. Eftekhari, Z. *et al.* Advancements and challenges in mRNA and ribonucleoprotein-based therapies: From delivery systems to clinical applications. *Mol. Ther. Nucleic Acids* **35**, (2024).